UNIVERSITÉ DE STRASBOURG

École doctorale Physique et Chimie-Physique

INSERM Unité 1121 Biomatériaux et Bioingénierie

THÈSE présentée par :

Adrien ROUSSELLE

soutenue le : **09/12/2022**

pour obtenir le grade de : **Docteur de l'université de Strasbourg**

Discipline / Spécialité : **Bio-Ingénierie, Biomatériaux**

Bioimpression de tissus biologiques à partir de microparticules poreuses

THÈSE dirigée par

M. Youri Arntz	**Maitre de conférence** – INSERM UMRS 1121 Biomatériaux et Bioingénierie, *Université de Strasbourg*
M. Dominique VAUTIER	**Ingénieur de Recherche INSERM** – INSERM UMRS 1121 Biomatériaux et Bioingénierie, *Université de Strasbourg*

RAPPORTEURS

Mme. Alem-Marchand Halima	**Professeure des Universités**– CNRS UMR 7198 Institut Jean Lamour, *Université de Lorraine*
M. Catros Sylvain	**Professeur des Universités – Praticien Hospitalier** – Dental School – INSERM UMR 1026 Biotis, *Université de Bordeaux*

MEMBRES INVITES

Mme. Kellenberger Esther	**Professeure des Universités**– Doyen adjoint – Faculté de pharmacie, *Université de Strasbourg*
M. De Oliveira Hugo	**Ingénieur de Recherche INSERM** – INSERM UMR 1026 Biotis, *Université de Bordeaux*

Remerciements

Je voudrais d'abord remercier Pierre Schaaf et Philippe Lavalle de m'avoir accepté dans leur unité de recherche. Je voudrais aussi remercier Philippe Lavalle pour tous ses conseils, encouragements et son soutien pour tous les projets présents et futurs.

Je suis extrêmement reconnaissant à Halima Alem-Marchand et Sylvain Catros d'avoir accepté les rôles de rapporteur.

Je remercie également Esther Kellenberger et Hugo De Oliveira d'avoir accepté de faire partie de ce jury.

Je tiens aussi à remercier particulièrement Hugo De Oliveira et toute l'équipe Inserm 1026 pour tous leurs conseils et leur aide pour la mise en place de la bioimpression dans ce projet.

Table of contents

Abbreviations list

Cells

Blood-derived endothelial colony forming cells	**ECFCs**
Chondrosarcoma cells	**HCS-2/8**
Dental Pulp Stem cells	**DPSCs**
Fibroblast cells	**NIH/3T3**
Human umbilical vein endothelial cells	**HUVEC**
Mesenchymal stem cells	**MSCs**
Murin myoblast cells	**C2C12**
Periodontal Ligament Stem cells	**PDLSc**

Molecules and products

Bovine serum albumin	**BSA**
Collagen	**ColI**
Collagen methacrylate	**ColIMa**
Deionized water	**DW**
Dichloromethane	**DCM**
Dulbecco's modified eagle medium	**DMEM**
Epsilon Poly-lysine	**ε-PL**
Gelatin methacrylate	**GelMa**
Hyaluronic acid	**HA**
Hyaluronic acid methacrylate	**HAMA**
Lithiumphenyl2,4,6trimethylbenzoylphosphinate	**LAP**
Muller-Hinton medium	**MH**
Phosphate buffered saline solution	**PBS**
Poly (D,L-lactide-co-glycolide acid)	**PLGA**
Polyethylene glycol	**PEG**
Polylactic acid	**PLA**
Poly-lysine	**PLL**
Polytetrafluoroethylene	**e-PTFE**
Polyvinyl-alcohol	**PVA**

Material, measurements and other

Biosafety cabinet	**PSM**
Computer-aided design	**CAD**
Congenital diaphragmatic hernia	**CDH**
Laser-assisted bioprinting	**LAB**
Loss modulus	**G"**
Optical density	**DO**
Rotations per minute	**rpm**
Standard Triangle Language	**STL**
Storage modulus	**G'**
Three-dimensional	**3D**

Figures list

Chapter 1

Chapter 2

Chapter 3

Chapter 4

Conclusion

Tables list

Introduction

Three-dimensional (3D) printing applied to cells, also called bioprinting, is an emerging technology for printing complex biological systems that can reproduce patterns similar to native tissues (Santoni, 2022). This is based on the ability of bioprinting to position cells very precisely within a matrix of polymers reproducing the extracellular environment.

Bioprinting has applications in regenerative medicine(Moghaddam *et al.*, 2021), tissue engineering (Marga *et al.*, 2012) (by example with the start-up Poeitis), pharmaceutical research (Peng *et al.*, 2017) (Hagenbuchner, Nothdurfter and Ausserlechner, 2021) and cancer research(Augustine *et al.*, 2021).

The polymer matrix with living cells composes the bioink. This bioink can be printed to form structures with varying degrees of complexity, and thus reproduce architectures, properties and functions of specific tissues. To do so, different bioprinting technologies exist: extrusion printing, inkjet or Inkjet printing, laser-assisted printing and finally stereolithography printing (Hölzl *et al.*, 2016). Each of these technologies has its advantages and limitations (such as printing speed, cost of use, cell viability). However, the most widespread and widely used technology is bioprinting by extrusion or microextrusion, as evidenced by the number of publications, patents and commercially available machines (Santoni, 2022). Extrusion bioprinting is based on the same principle as 3D printing of plastic materials, but instead of plastics, polymers with living cells are printed (Pati *et al.*, 2015). Complex structures can thus be printed layer by layer to get as close as possible to native tissues, as demonstrated by V.M. Gaspar *et al* in their review Advanced Bottom-Up Engineering of Living Architectures(Gaspar *et al.*, 2019).

However, even considering their differences all bioprinting technologies have common limitations (cell density, vascularization etc.) (Sigaux *et al.*, 2019) but in the case of extrusion printing we have identified two particularly unfavorable limitations. Indeed, a common limit to all these technologies is the low cell density of printed structures compared to the cell density of organs. Most human organs have a cell density between 10^9 and 10^{11} cells per mL (McClelland *et al.*, 2012). However, it is very difficult to obtain these concentrations in the laboratory, all the more so for the large volumes

necessary for some experiments. The second limitation, more specific to this technology, is cell viability after printing. Indeed, during the extrusion of the cells, a shearing force is applied on the cells, damaging them. These shear forces considerably decrease cell viability in short- and long-term cultures (Zhao *et al.*, 2015) (Ning, 2020).

To address the issues of bioprinting, most research focuses on improving hydrogels and printing methods (Forget *et al.*, 2017) (Boularaoui, 2020). In this thesis work we have implemented a new method that addresses the issues of cell density and viability after printing for extrusion bioprinting. Indeed, we have produced and adapted “microscaffolds” (or microcarriers) of porous Poly (D,L-lactide-co-glycolide) (PLGA). These microscaffolds have a double objective: to serve as "microcarriers" (or micro-carriers) before printing to increase the cell proliferation surface and increase the cell density more quickly and at a lower financial cost (low quantity of culture medium and less working time). These porous microscaffolds will also serve as mechanical protection for the cells during extrusion. The cells will colonize the porosities of the microscaffolds which will thus absorb the shearing forces and protect the cells during the extrusion printing step.

This thesis work seeks to develop production methods and demonstrate the benefits of using these microscaffolds on different cell types. Different methods of producing and adapting microscaffolds have been developed. Their impact on cell proliferation and viability was assessed. Microscaffolds have also been used to develop organoids, cell structures made in vitro in three dimensions. These printed cell structure have made it possible to study intercellular responses between stem cells and cancer cells.

This manuscript is organized into four chapters.

Chapter 1 will provide a state of the art on bioprinting, the use of PLGA microscaffolds in the medical field and finally the use of porous microscaffolds for bioprinting.

Chapter 2 will be dedicated to the description of cell lines, bioprinting inks, printing parameters and finally microscaffolds used in this thesis.

Chapter 3 will present the results of the production of microscaffolds and their impact on the proliferation, viability and migration of four cell types. It will include an article, titled “Enhancing cell viability, proliferation and migration in 3D printing of organoids with pre-cellularized porous PLGA microscaffolds” published in Bioprinting. This article

will be preceded by an introduction followed by complementary results and perspectives offered by this technology. A general conclusion on the production and contribution of microscaffolds will end this chapter.

Chapter 4 will focus on the results of printing a membrane prototype with muscular cells to fill congenital diaphragmatic hernias. These results will be in the form of a draft article. It will be preceded by an introduction and followed by complementary results, showing the importance of the adaptation of microscaffolds to the cell type. To end this chapter, a conclusion and perspectives on the next steps of the study.

To conclude, this thesis manuscript will end with a “General Conclusion and Perspectives” section. Appendices will be provided to give additional information.

Chapter 1: State of the art

1. BioPrinting

Three-dimensional (3D) bioprinting is an emerging and recent technology. Indeed, in 1988 Klebe (Klebe, 1988) tried to adapt an inkjet HP thermal printing to print collagen. The term organ tissue was only introduced in 1999. Following this, the first bioprinter was developed in 2003 with the modification, by the Boland group, of a commercial thermal Inkjet printer to deposit cells (Wilson and Boland, 2003).

This technology relies on the ability of bioprinting to produce complex structures with living cells whose organization and functionality are similar to those of native tissues. In particular, the objective of bioprinting technologies is to better control the precise positioning of living cells, within a biopolymer-based matrix and in a layer-by-layer structuring, allowing the adjustment of the geometry and maturation of the tissue over time. The first step for the bioprinting process as a whole is the pre-processing with the cell selection, material selection and the design or morphology selection. The second step is the procession with the printing parameters setting, bioprinting and crosslinking. The third step is the post-processing with the cellular maturation, if needed cellular differentiation and cellular tests such as cellular viability and proliferation analyses. The fourth step is the evaluation of the bioprinted product, their structure, morphology and functionality. These steps are described in Figure 1.

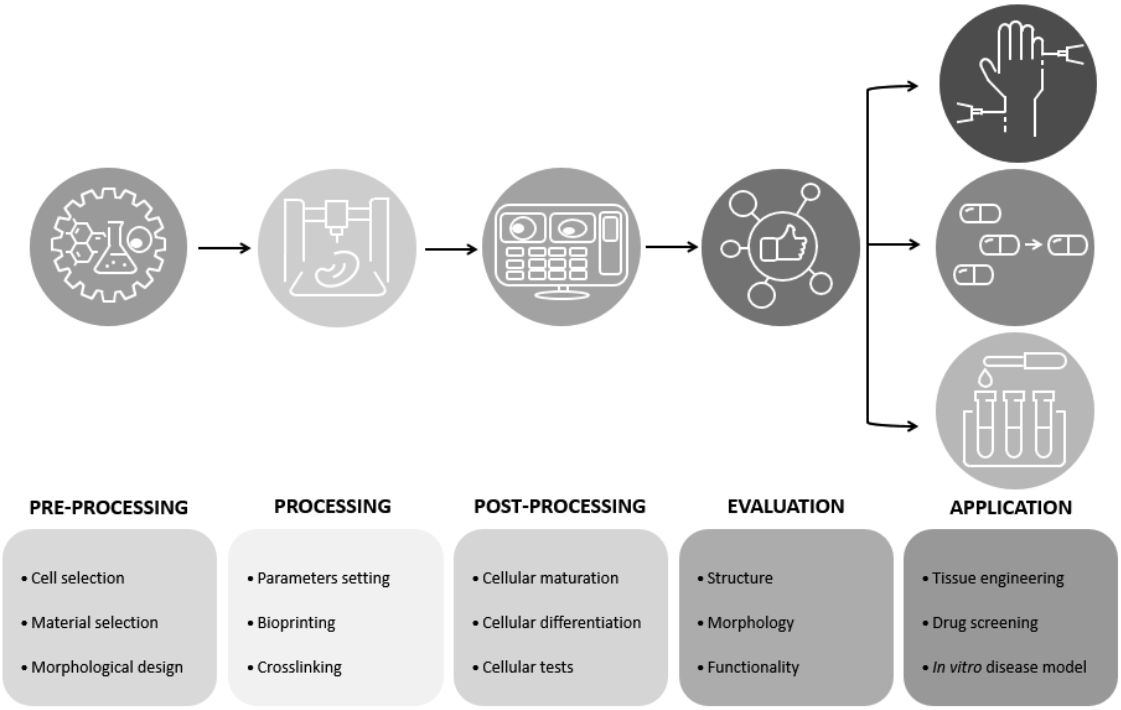

Figure 1 Bioprinting process, evaluation and applications

1.1. Bioprinting methods

According to their mechanisms, bioprinting techniques can be classified into four major groups: **extrusion**-based bioprinting (Figure 2 A), **inkjet** or droplet-based bioprinting (Figure 2 B), **laser-assisted (LAB)** bioprinting (Figure 2 C) and **stereolithography-based** bioprinting (Figure 2 D) (Khoeini *et al.*, 2021).

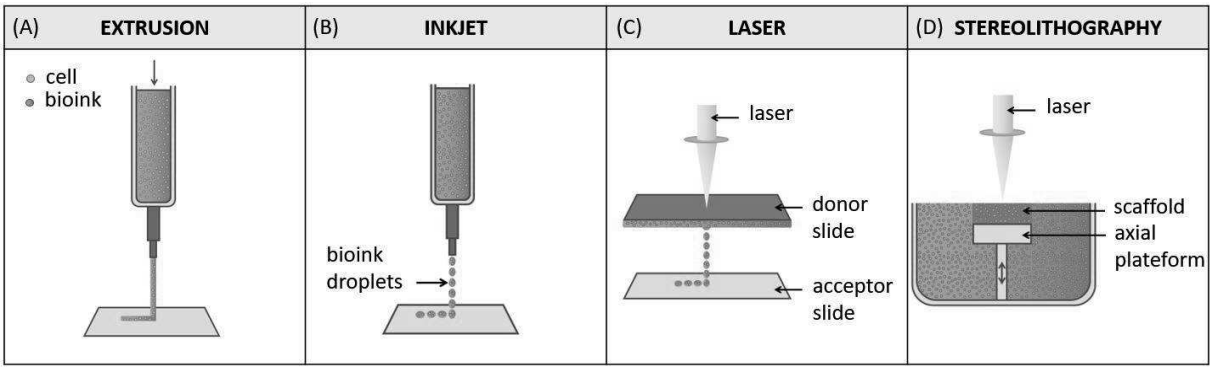

Figure 2 Bioprinting technologies With extrusion bioprinting (A), Inkjet bioprinting (B), Laser-assisted bioprinting (C) and Stereolithography (D)

Here we will define these four groups and their applications. We will then discuss their limitations and new methods to improve these technologies.

- Extrusion-based bioprinting

Extrusion-based bioprinting (Figure 2 A) uses physical force to “push” the bioink into cylindrical filaments by pneumatic, mechanical or by creating a magnetic field-driven micro- extrusion in a computer-controlled process (Figure 3) (Smith *et al.*, 2004) (Ozbolat and Hospodiuk, 2016).

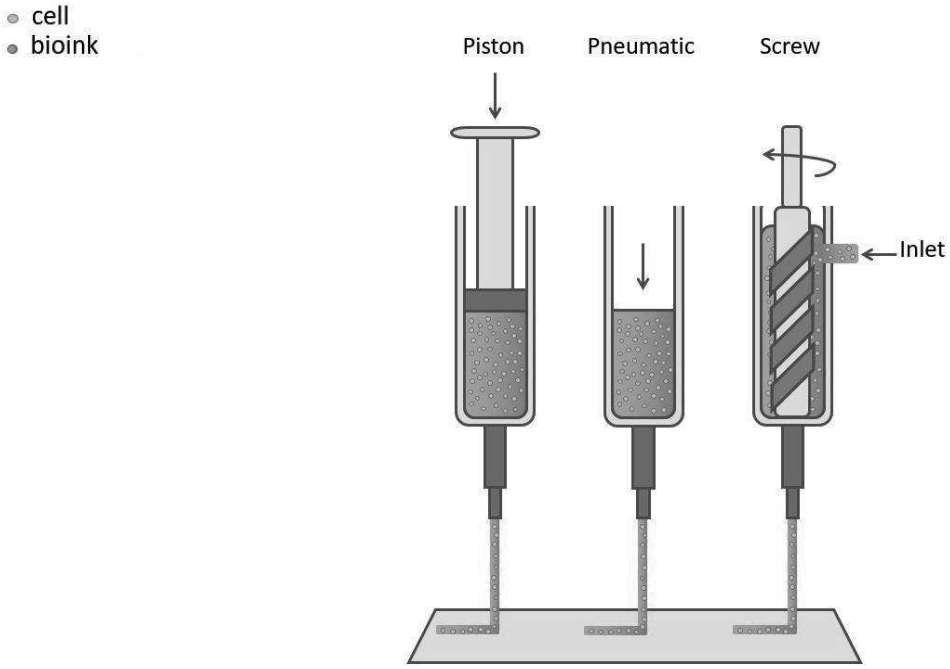

Figure 3 Extrusion bioprinting

This is the most widely used technique due to its ease and cost effectiveness. This method has one of the highest cell density possible in bioprinting with a fast printing speed. It also allows printing different materials at the same time with different cell types, which facilitates the printing of complex cellular structures such as vascularized bone like structures (Leucht, 2020) or cardiac like tissues (Lee *et al.*, 2019). This technique also has the advantage of being user-friendly, which contributes to its popularity. It should be noted that the forces used during the extrusion of the bioink with cells induce a shear stress on the cells. This shear stress can cause damages on the cell membranes, rendering them inactive or inducing apoptosis (Boularaoui, 2020; Ning, 2020) (Figure 4). This is one of the two major specific drawbacks of extrusion

bioprinting, the viability of extruded cells is low compared to other methods. The second specific drawback is the resolution of the printed constructs, which depends on the nozzle used, the thinner the nozzle, the higher the shear stress (Blaeser *et al.*, 2016). The shear stress of bioinks can be decreased by crosslinking the bioink during extrusion. Indeed, printing a bioink with a low viscosity reduces the shear stress during the extrusion, while reticulating it during the extrusion allows the bioink to have the mechanical strength to be printed into 3D structures. It has been done by the team of Cathal D.O'Connell *et al* (O'Connell *et al.*, 2020): they developed a method to decrease shear stress while maintaining high mechanical force to print complex structures that do not collapse on themselves. This last point is a recuring problem for extrusion bioprinting where the viscosity of the bioink has to be considered to keep a low shear stress but mechanical force sufficient to have self-supporting constructs. The needles used for extrusion bioprinting have an important role on the resolution of the printed structure but also on the cell viability. Indeed, Li *et al* (Li *et al.*, 2011) demonstrated that cell damage using a tapered needle is lower than using a cylindrical needle. Likewise, smaller diameter for the needle will have a stronger negative effect on the cell viability.

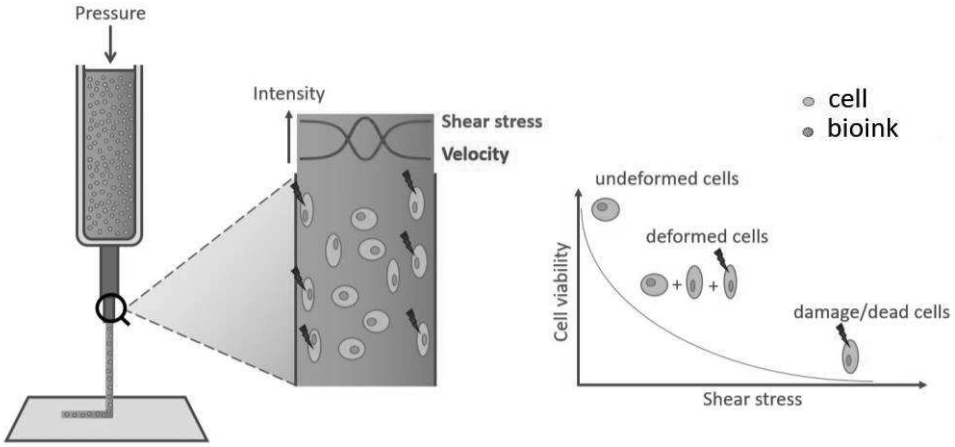

Figure 4 Shear stress during extrusion bioprinting

There are many derivations of extrusion bioprinting that reduce the limitations of this technology. For example, extrusion bioprinting in support media or gel baths (Bhattacharjee *et al.*, 2015) (Highley, Rodell and Burdick, 2015) is an emerging technology where the deposition of the bioink is done in support media (McCormack *et al.*, 2020) (Figure 5). This technology is also named FRESH bioprinting for Freeform

reversible embedding of suspended hydrogels. This helps in the structuration of the 3D structure and enables the use of inks with very low viscosities thus decreasing the shear stress and increasing cell viability with an increased resolution. Indeed, the team of Lee *et al* (Lee *et al.*, 2019) bioprinted, into suspended hydrogels with a high resolution (20µm filament), components of the human heart and even capillaries. With this new method presented in their work they were able to print patient specific anatomical structures and perusable vasculature and micro-vascularization.

Another modification of extrusion bioprinting is the coaxial extrusion bioprinting, where several materials are printed at same time, from the same nozzle or different nozzles. This has been used to induce the reticulation of the bioink (Ma *et al.*, 2022) or to print different bioinks with different cell types. In their work Gao *et al* (Gao *et al.*, 2015), used coaxial extrusion bioprinting to create a hollow structure inside the bioprinted structure for the exchange of nutriments, to reproduce blood vessels.

Finally, extrusion bioprinting can be combined with imaging technology to observe directly the bioprinted constructs in real time. Indeed, the team of Brassard *et al* (Brassard *et al.*, 2021) use a microscope above the printing stage to precisely control the bioprinting position to print small structures such as capillaries.

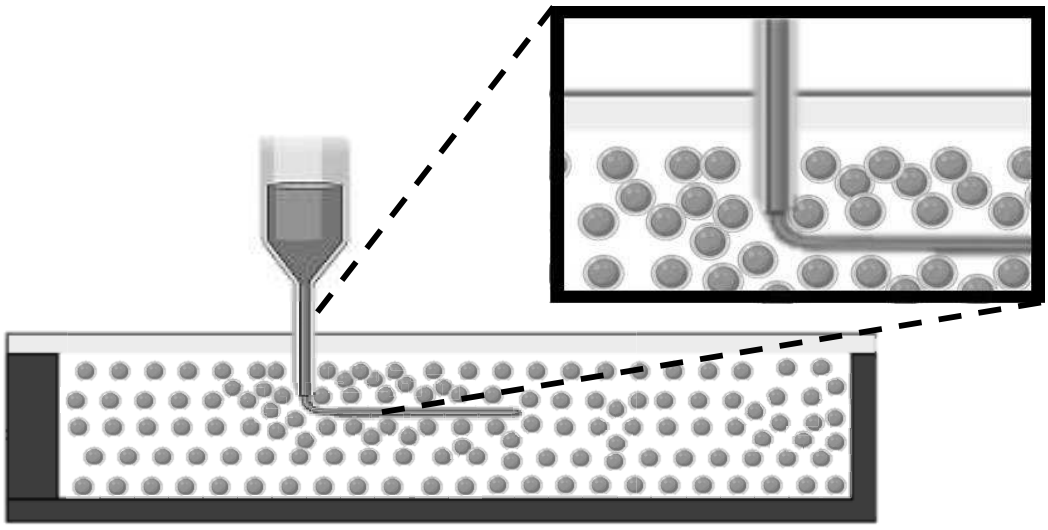

Figure 5 Extrusion bioprinting in a suspension bath

(Adapted from the work of Lee et al (Lee et al.*, 2019))*

- Inkjet bioprinting

Inkjet bioprinting (Figure 2 B) is defined as the printing of very small volumes (up to 100 pico liters) of a viscous bioink (droplets) onto a substrate. This method uses various energy sources such as piezoelectric, acoustic or thermal (Gudapati, Dey and Ozbolat, 2016) (Li *et al.*, 2020). Inkjet bioprinting of live cells was first proposed by Wilson and Boland in 2003 (Wilson and Boland, 2003) and done for the first time, with bacterial cells, by Xu *et al* (Xu *et al.*, 2004). The droplets are deposited on receptive surfaces and assembled into complex structures layer by layer (Figure 1.6). The gap between two droplets should be considered and the stability of the construct should be taken into account.

When using a thermal energy source, a micro-resitor heats up between 200-3000°C evaporating the surrounding bioink, and generating a vapor bubble that expand rapidly to expel bioink droplets (Miri *et al.*, 2019) (Figure 6 A). The short-term heating does not affect cell viability, indeed, according to Martin *et al* (Martin, Hoath and Hutchings, 2008) the cells are heated for only 2µs with a small temperature rise of 4 to 10°C. For acoustic or piezoelectric energy source (Figure 6 B), the bioink is extruded from the cartridge using actuators when a pulse is applied. This technique is defined by a high printing speed, with very good resolution (50–300µm), low cost, the ability to print different materials at the same time and good viability (higher than 80-95%) (Saunders and Derby, 2014) (Martin, Hoath and Hutchings, 2008). The limitations of this technique are the use of low viscosity inks, the difficulty of use, frequent clogging and the low density of cells (to avoid too much viscosity that would render the formation of droplets impossible). The team of Annalisa Tirella *et al* (Tirella *et al.*, 2011) also demonstrated the importance of the stiffness of the deposition surface which can induce cell damage. The substrate stiffness tested were 5kPa, 5MPa and 5GPa and demonstrated an important negative impact of the highest stiffness on the cell viability at 4 hours.

Inkjet bioprinting has been applied to several applications such as tissue engineering, cell micropatterning, *in vivo* cell printing, gene expression modification and drug development (Li *et al.*, 2020; Kumar, Ebbens and Zhao, 2021). For example, Christensen et al (Christensen *et al.*, 2015) inkjet bioprinted cell structures to mimic blood vessels, by printing precise tubular structures. Furthermore, the inket technology can be used to formulate drugs, as was done by Melendez et al (Meléndez *et al.*, 2008).

To resume, inkjet bioprinting has great performances but should not be considered for printing “large” constructs with high cell density, indeed, the fabrication speed is lower than extrusion bioprinting.

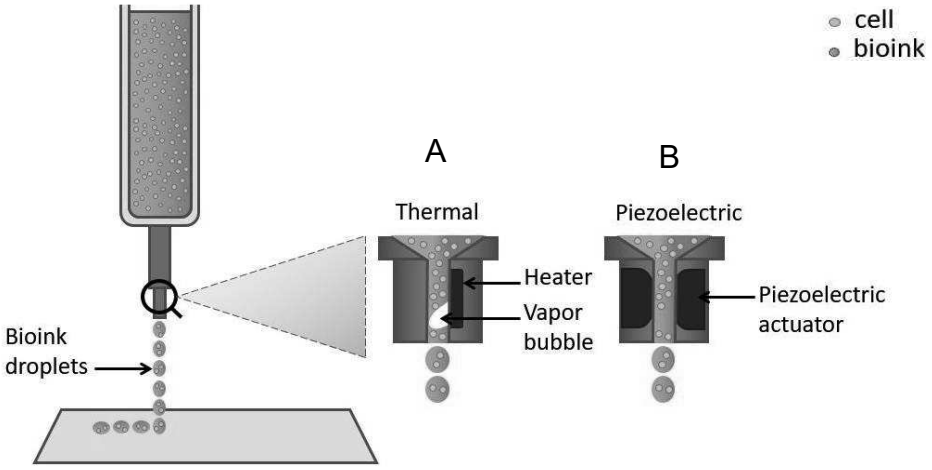

Figure 6 Inkjet bioprinting

With a focus on the two main technologies by thermal (A) and piezoelectric (B) energy source

- Laser-assisted bioprinting

Laser-assisted bioprinting (Figure 2 C) uses laser energy to precisely fabricate tissue constructs by selectively patterning hydrogels. This method does not use a nozzle but a donor slide composed of a slide of a light absorbent material (often metal), a coating of bioink and a transparent material. A laser pulse is absorbed on the donor slide which leads to the generation of a high-pressure bubble. The bubble expands and deposits bioink droplets onto the receptive surface (glass slide) (Dou *et al.*, 2021). This is a non-contact technique which limits the risks of contamination. It also decreases the forces applied to the cells, allowing a high viability rate around 85% (Hopp, 2012). The cell viability is high but can be reduced by thermal damage and mechanical stress of the bioprinting (Karakaidos *et al.*, 2022) . The laser energy used for the bioprinting process can also affect the cell viability. Indeed, S. Cartos *et al* showed that increasing the laser energy has a negative effect on cell viability. They also demonstrated that other parameters such as ink viscosity and thickness have an effect on cell viability, with an

increase in thickness having a benefic effect on cell viability (Catros *et al.*, 2011). LAB also allows the generation of high resolution droplets (10-100µm) with high cell density (Karakaidos *et al.*, 2022). LAB allows a smaller cell density than other bioprinting methods such as extrusion but can be as high as 10^8 cells/mL in microscale organization (Guillotin *et al.*, 2010). But, as with inkjet the range of viscosity is reduced for the printing process, the limitations for the assembly of 3D constructs with droplets remain the same as for inkjet bioprinting. This method is also more expensive than others and is more complex to set up.

LAB has application in bone, skin, cornea among others in tissue engineering. Indeed, Sorkio et al (Sorkio *et al.*, 2018) used laser assisted bioprinting to print structures mimicking corneal tissues. Human embryonic stem cells with adipose tissue derived stem cells were printed with a bioink composed of laminin and collagen to print the stromal constructs. The printed cells demonstrated a good viability after printing and expressed key proteins. It can also bioprint organoids and cell aggregates in very specific applications (Ventura, 2021).

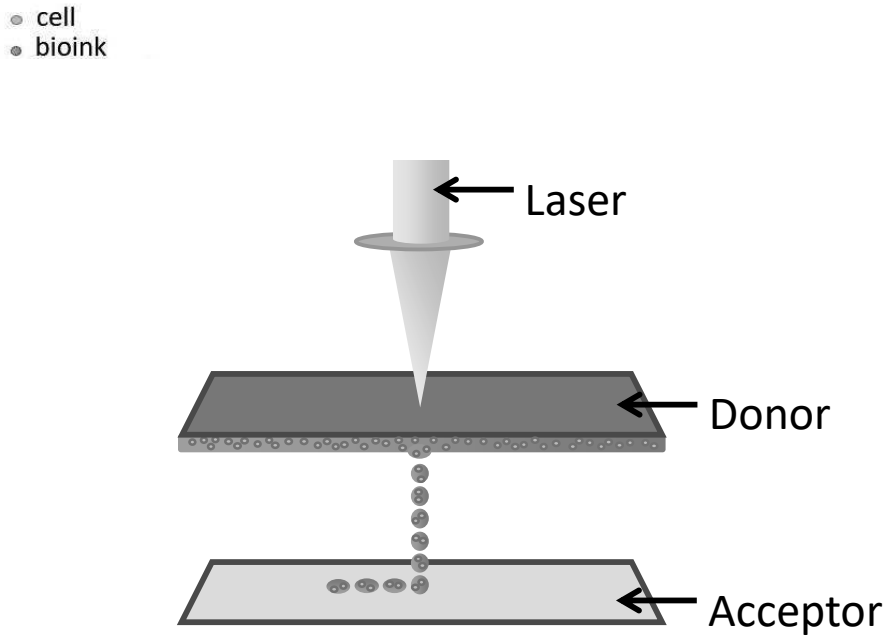

Figure 7 Laser-assisted bioprinting

- Stereolithography-based bioprinting

Stereolithography-based bioprinting (Figure 2 D) is based on the polymerizing of photosensitive biomaterials to create complex structures. This technique requires a vat of photosensitive biomaterials with encapsulated cells. A laser beam selectively polymerizes sections of the bioink to create a complex structure (Derakhshanfar *et al.*, 2018). This technique allows to build structures with a resolution of 50-100µm (Gauvin *et al.*, 2012). The printing platform only needs to move in the Z direction, simplifying the use of this technology. No forces are applied to the cells during printing, only polymerizing light, thus, the viability rate is over 85% (Wang *et al.*, 2015). But the use of UV light which can damage the cells as well as the limited choice of photosensitive biopolymers for the precursor bioinks and the use of photo-initiators, most often cytotoxic, are major limitations for the use of this bioprinting technique. This is way, visible light is studied to polymerize the bioinks, without damaging the cells (Lin *et al.*, 2017) (Z. Wang *et al.*, 2018). Blue light, near the UV light (405nm) can be used instead of the toxic 365nm. Another limitation is the possibility to print only one material at the time and the use a vat of biomaterial. All these limitations restrict the range of stereolithographic bioprinting which is not often used with cells inside the bioink. It is preferred to print very complex structures compared to extrusion or droplet based bioprinting.

Contrary to other bioprinting methods, stereolithography is used to construct cell-less scaffolds with a good resolution to be seeded after printing. Indeed, Gauvin *et al* printed complex scaffolds to mimic the microarchitecture of tissue with gelatin methacrylate (GelMa) hydrogel. Theses microscaffolds were then seeded with human endothelia cells to obtain a high cell density and adhesion (Gauvin *et al.*, 2012).

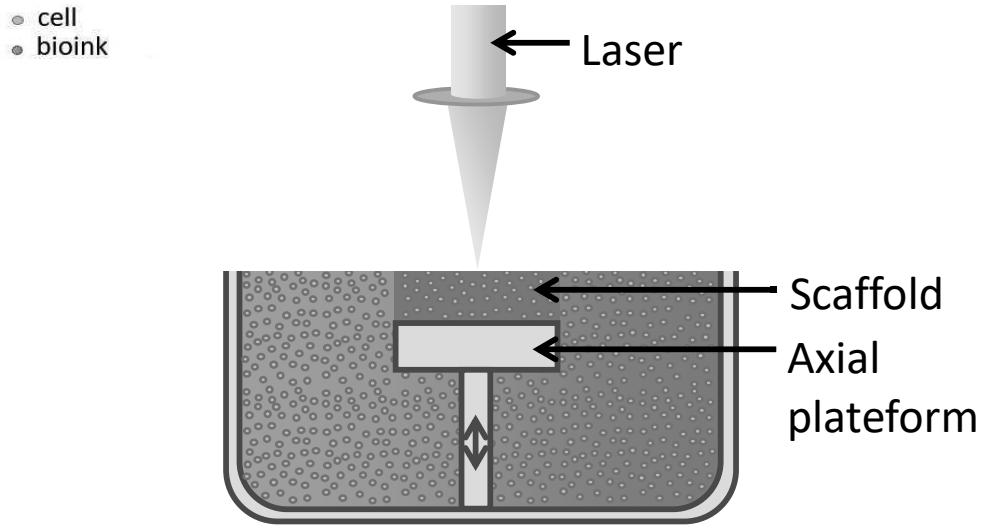

Figure 8 Stereolithography schematic

1.2. Limits of bioprinting

Like any new technology, bioprinting has disadvantages that further limit its development and application in certain areas. Here we will present general limitations of bioprinting. The limits of each technology have already been presented in the previous section.

- Cell density

The first limitation of bioprinting is the amount of cells needed to print a cellular structure. Indeed, if we want to reproduce a tissue or an organ, it is necessary to get as close as possible to the density found *in vivo* which is between $10^9 \text{and } 10^{11}$cells per mL (McClelland *et al.*, 2012). However, it is very difficult today to produce so many cells. It would take considerable time, many resources (human and material) and it would have a significant cost. Therefore, it is necessary to find a solution to increase the number of cells available before printing. It is possible to culture with microcarriers, which increases cell proliferation by increasing the proliferation surface before printing. R. Levato's team produced Polylactic acid (PLA) microcarriers and cultured them with mesenchymal cells before printing them. This made it possible to obtain a faster proliferation of cells before printing and after printing to obtain a higher cell density than without microcarriers (Levato *et al.*, 2014) (Figure 9). The study also demonstrated the

importance of the inoculation step, indeed, when mixing separately the cells and the microcarriers in the bioink, the cells were observed in the first steps of adhesion after 4h (Figure 9 A). Whereas when pre-seeding the cells on the microcarriers before mixing in the bioinks, the cells were found adhered and expressing organized actin fibers (Figure 9 B).

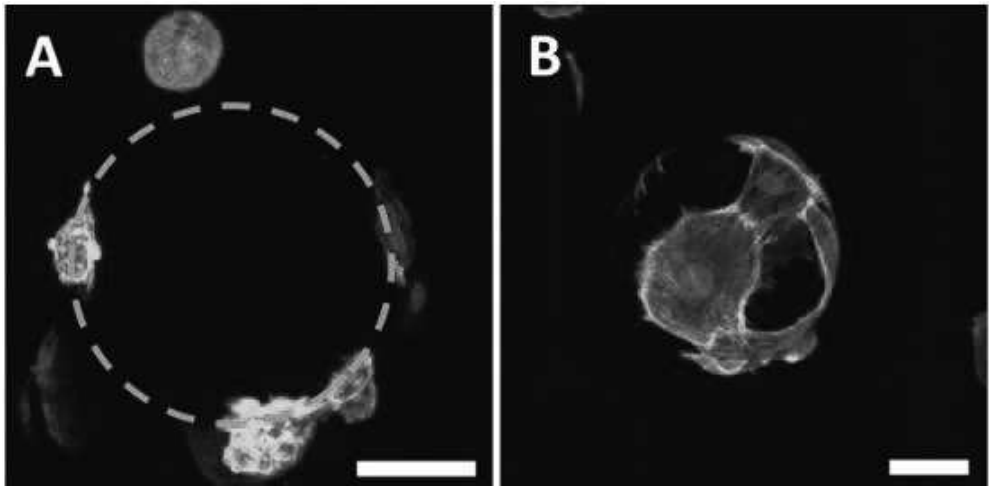

Figure 9 Cell laden microcarriers

Adapted from R. Levato *et al* (Levato *et al.*, 2014) *scale bar 40µm*

- Cell viability

Cell viability is an extremely important parameter that goes hand in hand with cell density. Different printing techniques will have different effects on cell viability. Indeed, some techniques will have a high cell viability (greater than 85%) but a low cell density, others will have a high cell density but will apply a shear stress on the cells at the time of printing which will induce damage and increased cell death.

Inkjet and extrusion techniques have indeed a higher cell density but during the printing phase apply a high shear stress on the cells. Cell viability can therefore be greatly reduced during the extrusion phase. This is because extrusion methods use constant pressure to dispense the bio-ink from the print nozzle as a continuous filament, which generates shear stresses that can damage the cell membrane and ultimately cause cell death. Indeed, according to the review by Boularaoui *et al* (Boularaoui, 2020) damage to cells and more particularly to the cell membrane is proportional to the shear stress applied. It starts at no damage when there is no stress to 100% damage at high stress. The shear stress is directly related to the parameters of extrusion pressure,

diameter of the printing nozzle and the viscosity of the bioink (Blaeser *et al.*, 2016) (Ning, 2020).

The viscosity of hydrogels has a determining role for the shear stress applied to the cells in a complex structure. The team of Zhao *et al* (Zhao *et al.*, 2015) demonstrated a proportional decrease in cell survival when increasing the viscosity of a bioink composed of gelatin and alginate.

The optimization of the bioprinting process is necessary to obtain the best possible viability. The team of Ouyang *et al* (Ouyang *et al.*, 2015) obtained a cell viability as low as 55.52 ± 2.37% after bioprinting. After optimization of the diameter of the printing nozzles, the temperature in the cartridge and the printing chamber, the bioprinting process showed a viability of 90.84 ± 1.02%.

- Vascularization

Vascularization is one of the essential points in the bioprinting of tissues and organs because the viable maturation of printed tissues and organs depends on their vascularization (Sigaux *et al.*, 2019). Indeed, the vascular system on any organ has the role of exchanging nutrients, gases and removing waste (Leucht, 2020). During longer term maturation, cell viability may also be decreased by cell asphyxiation. Indeed, if the bioprinted construction is too large a size without vascularization, then the nutrients, oxygen and waste will have difficulty in crossing all the reticulated gel and will cause increased mortality in this zone (Chen *et al.*, 2021).

Thus, to survive and proliferate a cell must be less than 100-200µm from a source of nutrients and waste exchanges (Carmeliet and Jain, 2000; Rouwkema, Rivron and van Blitterswijk, 2008). This limits the size of the constructions to less than 1mm without vascularization. This also poses a limitation for the implantation of printed tissues *in vivo* because the neovascularization is too reduced to support the new implanted tissue. The vascular supply must be present at the time of implantation (Clark, 1939).

It also depends on the bioink used, the rate of crosslinking and the cell density. This is why all bioprinting methods need vascularization methods. Different approaches are used depending on the desired application, the tissue being constructed and the bioprinting method.

It is possible to use so-called sacrificial cell-free printing gels to form "channels" in a printed structure (Datta, 2017) (Miri *et al.*, 2019). Indeed, when printing a complex structure, it is possible to use a sacrificial ink in the construction, which will be removed during the maturation phase to leave a space where the culture medium can infiltrate in order to exchange nutrients and wastes. Inks that can be used as sacrificial inks are inks that can be easily removed without damaging the construction as a whole. For example, Pluronic F127® (Shamma *et al.*, 2022) can be printed at room temperature and then removed by lowering the temperature of the construction and rinsing it with sterile Phosphate buffered saline PBS.

The impression of cells that can differentiate into blood vessels (Novosel, 2011; Leucht, 2020). The team of Chen *et al* (Chen *et al.*, 2012) demonstrated in their work that it was possible to bioprint in GelMa hydrogels of blood-derived endothelial colony-forming cells ECFCs and mesenchymal stem cells MSCs that would allow the development of blood vessels inside the bioprinted construct. When the bioprinted constructs were implanted *in vivo,* blood vessels with erythrocytes from the graft developed and connections with blood vessels of the host developed. The team of Lise De Moor (De Moor *et al.*, 2018) also developed a method of bioprinting vascularized spheroids with Human umbilical vein endothelial cells (HUVEC) that spontaneously formed a capillary-like network.

It is also possible to use coaxial bioprinting, and to print a hallow structure. This was done by Gao *et al* (Gao *et al.*, 2015) who printed a double layer construct tube with alginate hydrogel to permit the exchange of nutriments (Figure 10). Indeed, the team of Gao *et al* printed $CaCl_2$ with the inner nozzle printed alginate with the outer part of the coaxial nozzle (Figure 10 A). The $CaCl_2$ solution diffused and reticulated the alginate solution creating a hollow tube (Figure 1.10 B). Finally, the most outer solution of alginate was not reticulated (due to the diffusion of the $CaCl_2$ solution) to adhere to the next printed layer (Figure 10 C) before being immerged into a bath of $CaCl_2$ to complete the reticulation of the construction.

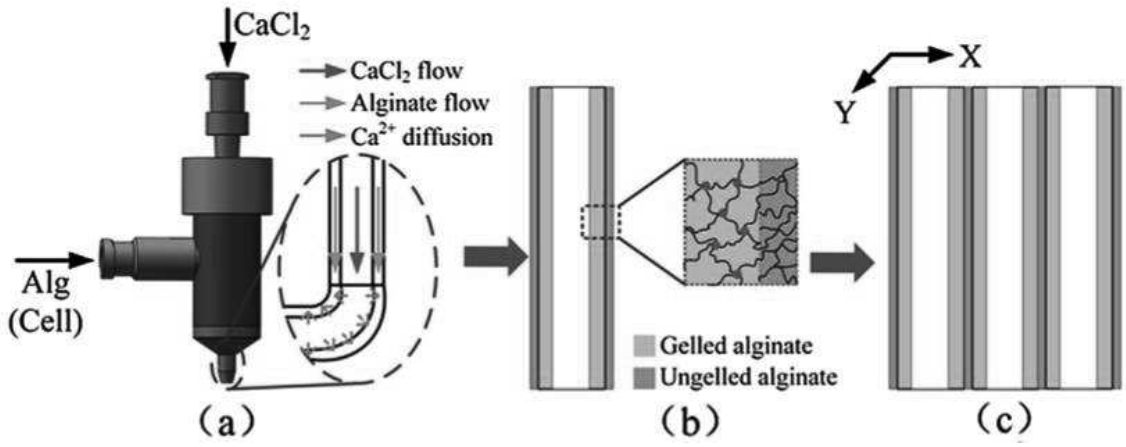

Figure 10 Coaxial bioprinting to produce hallow tubes

Adapted from Gao *et al* (Gao *et al.*, 2015)

- Microbial contaminations

Two main sources of contamination can be identified. The first comes from printed objects and the ink itself, which represents a rich environment enable the proliferation of microorganisms over longer study times. The second comes from the printing device itself, which is often bulky and not compatible with printing under a biosafety cabinet (PSM), therefore generally not allowing work under a sterile atmosphere (Muthukrishnan, 2021).

The norm is to use antibiotics or antifungals in culture media, but we have been observing, for years, an increase in antibiotic resistance (Tenover and McGowan, 1996). Antibiotics in the culture medium may not prevent or limit the proliferation of pathogens protected by the bioink and the construction because of the limitation of exchanges with the culture medium in the printed constructs. This is one of the reasons why 3D bioprinting is starting to study and develop antibiotic-free antibacterial bio-inks (Muthukrishnan, 2021).

In this light, the use of bioink components with antimicrobial properties seems promising to limit microbial infections. However, intrinsic modifications of the bioink can decrease its biocompatibility or its physico-chemical characteristics (O'Connell *et al.*, 2019). For example, the biocompatibility of the bioink can be reduced by the addition of toxic antibacterial functions, as shown by the addition of quaternary ammonium

functional groups (Yue *et al.*, 2015) or the addition of silver nanoparticles (Wu and Hong, 2019).

- No bioprinting gold standard

Finally, regardless of the technologies used, each bioprinting laboratory has its own printing methods, bioprinting inks and printing parameters. *De facto*, the reproducibility of work and the standardization of bioprinting in a major issue. There are four main families of bioprinting technology, with particularities for each of them, a very large number of printing inks with very varied compositions and finally all the printing parameters (Correia Carreira, Begum and Perriman, 2020). It is therefore extremely difficult to reproduce the work of another group without using the exact same conditions, inks and parameters according to N. Sigaux *et al* (Sigaux *et al.*, 2019).

- Choice bioprinting technology

The choice of printing technique will therefore be based on a compromise of all the elements mentioned above to obtain the desired results for the intended application. For example, if a high cell density is sought, the choice will be preferentially oriented towards extrusion bioprinting, while the LAB or stereolithography will be favored to obtain the best resolution.

- Ethics of bioprinting

The ethical aspect of a technology is an often overlooked aspect of research. Being a relatively new technology, and very future looking, bioprinting involves many ethical and regulatory questions (Vijayavenkataraman, Lu and Fuh, 2016; Patuzzo *et al.*, 2017).

The first ethical question is: should we simply repair and replace or should we enhance the human body? Indeed, with bioprinting it would be possible, in the future, to replace organs with better functioning organs, enhancing the human body.

The second ethical consideration we can have is the source of the cells used for research. Indeed, the use of human embryonic stem cells is questioned and legally controlled (Lo and Parham, 2009).

The third ethical question that can be asked is the price and access to bioprinted organs in a free market society. Indeed, there is a risk that organs would be only

available to the rich. But it would help to develop and make organs available in the future. It could also help in the problematic of finding organs in dead donor (consent) and in live donors (motivation of donating tissues), reducing the waiting list.

Finally, bioprinting could enable the reduction or even elimination of the need to involve tissue or animal experiments in scientific research (Patuzzo *et al.*, 2017).

1.3. Applications of bioprinting

Bioprinting finds applications in many fields, which we briefly discuss here.
3D printing is already used to assist with surgeries or to reproduce human models with anatomical dimensions from medical images (Pugliese *et al.*, 2018). In surgery, these models make it possible to produce exact models of intervention areas and therefore allow greater preparation of the medical team. This has already been used in neurological and spinal surgery (Waran *et al.*, 2014).
In tissue engineering, native tissues could be produced with allogenic cells from the patient to make allografts. Synthetic bioprinted skin has already been commercialized by the French start-up *Poietis*. Several research teams are developing bio-printed artificial skin that matures faster than skin produced by traditional tissue engineering such as the team of Pourchet *et al* (Pourchet *et al.*, 2017).

Bioprinting can also be used in pharmaceutical development and research of new drug molecules. Indeed, the selection and validation of new drug molecules takes on average ten years and between 314 million and 2.1 billion with a median of 1.3 billion dollars. These estimations are for the marketing of a single drug (Van Norman, 2016; Wouters, McKee and Luyten, 2020). This high cost and very long time to bring a new drug to market is largely explained by the study designs used, which are expensive and use sub-optimal models. Indeed, the first selection of the molecules of interest is done on 2D cell models and animal models. Many molecules of interest are selected because they work in these model but will have a lesser effect in human clinical studies and in 3D models (Kuriakose *et al.*, 2019; Dhamecha *et al.*, 2020). These inappropriate models allow the selection of molecules that will not have an effect in vivo involving unnecessary costly and long studies. With more suitable bioprinted models (X. Wang *et al.*, 2018), the number of studies would be greatly reduced and the time and cost to bring a new product to market molecule would be greatly reduced. In a 2020 study, the team of S. Han *et al* (Han *et al.*, 2020) demonstrated the greater action, on a certain

type of tumor, of a combination of anti-tumor molecules and of a molecule inhibiting the development of blood vessels than the anti-tumor molecule conventionally used. This study demonstrated the interest of a bio-printed model to test new therapies with a model closer to the human model.

This drug selection is even more important and specific in the case of cancer drugs and personalized medicine. Indeed, clinical studies can be biased in the choice of patient cohorts and each disease/cancer is unique and will respond differently to drug molecules. With bioprinting, *in vitro* models of the tumor microenvironment are extremely close to *in vivo*. In a 2019 study, Ellen Langer *et al* (Langer *et al.*, 2019) bioprinted different cell types derived from patient cells to form a tumoroid that was able to self-organize, produce extracellular matrix and respond to external stimuli. This study has shown that it is possible to extract cells from a patient to bioprint them in a specific configuration and reproduce a diseased organ or tissue. This could make it possible to select the most suitable molecule to treat a type of disease with specific characteristics or to treat a person in a specific way. In a recent study, Erick Breathwaite *et al* (Breathwaite *et al.*, 2020) bioprinted a bone model and demonstrated their model was more sensitive and biologically relevant as a drug screening model than traditional 2D *in vitro* testing models. Therefore, bioprinting could allow to select and test more specifically new molecules, but also molecules that have been rejected.

Bioprinting also opens new perspectives to understand the mechanisms of complex biological processes with new and more accurate models (Daly *et al.*, 2021). With various bioprinting technologies it is possible to print complex structures to observe cell-cell interaction in completely controllable environments from the cell types, cell matrix and external stimuli. But it is very difficult to reproduce exactly the biochemical, structural and biophysical properties of a native tissue, so most often simplified versions are bioprinted.

1.4. Summary

The four bioprinting methods discussed above have their own perks and drawbacks, recapped in Table1. Among these methods, the one that is the most employed bioprinting technique is extrusion bioprinting for technical and financial reasons. It also the fastest and can use the highest cell density of all bioprinting methods.

TABLE 1.1 SUMMARY OF ADVANTAGES AND LIMITATIONS OF EACH BIOPRINTING METHOD

Method	*Advantages*	*Limitations*
Inkjet bioprinting	-Compatible with live and non-living materials -Speed of printing -High-cell viability -High resolution	-Clogging of nozzle -Low cell density -Shear-stress -High-viscosity bioinks -Low mechanical strength
Extrusion bioprinting	-Cell density -Speed of printing -Cost effective -High versatility (multi materials) -Ease of use	-Shear-stress inducing low cell viability -Low resolution
Laser based bioprinting	-Speed of printing -High cell viability (>85%) -High variability of printing inks	-Low fabrication speed -Low cell density -High cost
Stereolithography	-High cell viability (>90%) -High resolution of printing -No need for X-Y movement	-Large amount of bioink -Low cell density UV light reticulation -Lack of multi-material bioprinting

2. Bioprinting bioinks

Bioinks are generally classified into two categories, scaffold based and scaffold free. The most common category is the scaffold based bioink, where cells are loaded into hydrogels or similar materials and printed into 3D structures (Figure 11). At the contrary, cells are printed without any external biomaterial for the scaffold free bioink, mimicking embryonic development (Hospodiuk *et al.*, 2017). In this work, we have chosen to focus solely on scaffold based bioinks.

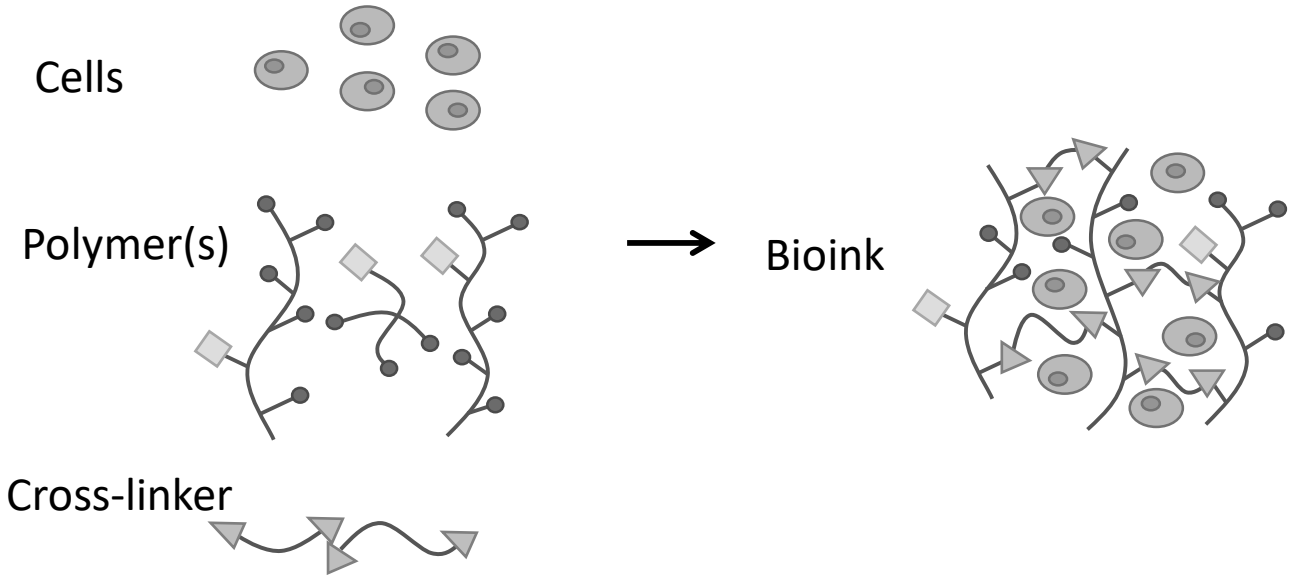

Figure 11 Bioink formulation

In example the red circles represent amines, blue squares methacrylate groups and the yellow triangles the cross-linker (adapted from (Rutz, Lewis and Shah, 2017))

2.1. Hydrogels and soft materials for bioprinting

The bioink is a necessary and essential component that combines living cells with hydrogels or soft materials that will be printed. The choice of the bioink components is essential for their physical properties. They must promote the printability of the bioink, allow gelation (physical or chemical) and be biodegradable.

Important features of the ideal bioink material for any application are biocompatibility, printability (shear thinning ability), high mechanical integrity and stability, insolubility in cell culture medium, *in vitro* or *in vivo* biodegradability at a rate appropriate to the regenerating tissue and the ability to promote cell adhesion (He *et al.*, 2016). After printing, constructs need to maintain the designed shape and structural strength and integrity, maintain 3D architecture for a defined period of time *in vitro*, and easily maintain cells within the construction and degrade over time *in vivo*.

According to C. A. DeForest and K. S. Anseth (DeForest and Anseth, 2012) cells will thrive best in an aqueous environment, in which their migration and matrix deposition is not hindered by a dense polymer network. Unfortunately, hydrogels with a low

polymer network will lack mechanical strength and the ability to maintain their printed shape, resulting in a low shape-fidelity (Malda *et al.*, 2013). Thus, most bioprinted hydrogels are done so with some amount of polymer network which impacts the overall viability rate of cells. It is then important to balance between shape fidelity and cell viability to obtain the ideal bioink.

Hydrogels are a class of crosslinked polymeric substances capable of retaining large quantities of water. They are wildly used in tissue engineering and cell-laden hydrogels allow cell proliferation and growth, and facilitate formation of tissue. These materials can absorb up to 1,000 times their initial weight in aqueous medium without dissolving (Ahmed, 2015), making them ideal for cell encapsulation. Furthermore, hydrogels are very permeable to oxygen, nutrients and other water-soluble compounds, rendering them very attractive materials for bioengineering (Thomas *et al.*, 2009; Zhu and Marchant, 2011) and tissue engineering.

Hydrogels used in tissue engineering can be classified into two groups: naturally-derived hydrogels such as gelatin, fibrin, collagen, chitosan, alginate and synthetically-derived hydrogels such as Pluronic® or polyethylene glycol (PEG) (Malda *et al.*, 2013).

- Natural based hydrogels

Natural based hydrogels can be classified according to their extraction origin. Hydrogels such as collagen, fibrin, and gelatin can be extracted from vertebrates and thus possess signaling molecules inherent to cell adhesion whereas hydrogels like alginate and agarose are extracted from other living organisms such as algae or sea weeds that do not possess these signaling molecules (Lee and Mooney, 2012; Gasperini, Mano and Reis, 2014). Considering their origin, some of these compounds are able to mimic the native tissue environment as they possess several essential features of the native extracellular matrix (ECM) components (Tibbitt and Anseth, 2009).

In this work we used alginate, gelatin, collagen and hyaluronic acid, so we will focus on these natural components.

Alginate is one of the most used hydrogel in bioprinting because it is a biocompatible and inexpensive material. It is a polysaccharide composed of alternating β-D-

mannuronate and its C-5 epimer α-L-guluronate units (Jungst *et al.*, 2016). Ionic reticulation is usually used by reticulating in solution of calcium chloride ($CaCl_2$) or calcium sulphate. Divalent calcium ions form a bridge, due to the attraction of negatively charged carboxylic acid groups between two close alginate chains (Lai *et al.*, 2016). However, despite the intrinsic properties of alginate that make it a good candidate for hydrogel bioprinting, it was shown that due to its hydrophilic nature proteins are minimally adsorbed thus decreasing cell attachment (Rowley, Madlambayan and Mooney, 1999). Therefore, chemical modifications are often required to promote cellular adhesion and survival. The concentration of alginate determines the viscosity of the solution and the crosslinking time. It is also possible to work with a semi-crosslinked solution by mixing with a low concentration of $CaCl_2$ (Hazur *et al.*, 2020) before printing.

Gelatin is a water-soluble protein, a denatured form of collagen. Gelatin is a base component in many hydrogels for biopritning such as, gelatin/alginate, gelatin/chitosan, gelatin/hyaluronic acid, gelatin/fibrinogen, gelatin/alginate/fibrinogen, and gelatin/alginate/fibrinogen/hyaluronic acid (Wang *et al.*, 2017). The combinations are numerous and have very interesting characteristics, such as excellent biocompatibilities, rapid biodegradability, good cell migration, proliferation and non-immunogenicity (Wang *et al.*, 2017). Gelatin can easily form a gel by thermally inducing crosslinking and reversing at 37°C. All these properties make gelatin based hydrogels and methacrylate gelatin (GelMa) (see Figure 12) some of the most used hydrogel in bioprinting (Liu *et al.*, 2017) .

Another protein extensively used in bioprinting is collagen, which is one of the most important proteins in mammals, composing almost 25% of the protein mass. It is also a highly conserved protein cross-species inducing minimal immunological proteins and has a helical structured (Ferreira *et al.*, 2012). It facilitates cell adhesion and growth through abundant cell-binding domains (Gullberg and Lundgren-Åkerlund, 2002). However, its use is usually coupled with another component. Indeed, it remains in a liquid state at low temperatures and forms fibrous structures with higher temperatures. The gelation time of collagen alone is too long for regular bioprinting, taking up to half an hour at 37°C. This slow reticulation makes it difficult to build complex 3D structures. The low mechanical properties of collagen induce a need to use of other hydrogels or

the chemical modification of collagen such as methacrylation to increase the speed of reticulation. Indeed, D. Wallace *et al* (Wallace, 2003) and C. Helary *et al* (Helary *et al.*, 2010) presented collagen hydrogels as having poor mechanical properties such as poor mechanical stability and durability. Thus, collagen hydrogels needed to be modified to present interesting uses in tissue engineering.

Hyaluronic acid is a major component of the extracellular matrix of cartilage. It is a non-sulfated linear glycosaminoglycan. It is comprised of repeated disaccharide units of D-glucuronic acid and N-acetyl-D-glucosamine fragments linked by alternating β-1,4 and β-1,3 glycosidic bonds (Zhong *et al.*, 1994) . It has excellent biocompatibility and ability to form hydrogels of different mechanical forces. However, similarly to collagen, hyaluronic acid has a slow gelation rate and poor mechanical properties. Nevertheless, its intrinsic proprerties such as controllable architecture and degradation make it a perfect candidate mixed with other components for bioprinting hydrogels to improve its reticulation. Indeed, hyaluronic acid is important in cell migration (Baier *et al.*, 2007), has very few cross species variations and excellent biocompatibility (Baier Leach *et al.*, 2003).

Chitosan is a natural polymer used for the fabrication of bioinks (Vanaei *et al.*, 2021). Chitosan is biocompatible and has antimicrobial capabilities, however, hydrogels of chitosan have low gelation rates. This is why chitosan is most often used in combination with other. Indeed, chitosan has been used with alginate for neural tissue (Gu *et al.*, 2016) and with collagen in tissue engineering (Suo *et al.*, 2021)

Silk and fibrin are also natural components used to produce hydrogels. Fibrin is a protein derived from fibrogen and silk a natural fiber protein produced by weaver spider and some insects. Both have a high biocompatibility.

- Synthetic based Hydrogels

As discussed, natural based hydrogels generally have poor mechanical properties but contain important bioactive molecules, while their synthetic counterparts have adaptable mechanical properties but lack bioactive molecules for cell adhesion or migration (Zhu and Marchant, 2011).Contrary to natural polymers, synthetic polymers do not possess favorable intrinsic properties to cell culture. However, synthetic

polymers can be adapted to the bioprinting process to improve their biocompatibility and increase cell viability, migration and proliferation by adding RGD elements (cell-binding sites) by example. They can also be enhanced to improve their structural and mechanical proprieties with rapid gelation and better shear thinning proprieties for bioprinting. Synthetic polymers have a better 3D structure but are often less biocompatible and lack bioactive components. Indeed, the primary advantage of synthetic bioinks over naturally derived sources is the ability to manipulate their chemical and physical properties as necessary. The molecular weight, functional groups, crosslinking rates, and other mechanical properties of the components of synthetic bioinks can be adapted for a specific bioprinting method. The main disadvantage in using synthetic bioinks is the lack of signals for cellular interactions. Synthetic bioinks do not typically contain natural cellular attachment sites and do not effectively mimic the environment of a biological ECM (Bishop *et al.*, 2017).

Pluronic® F-127 (mainly used as sacrificial ink) and Poly(ethylene glycol) are two of the mainly used synthetic polymers.

So-called "sacrificial" inks, most often based on polymers of non-natural origin, can be used as a support or sacrificial ink intended to be eliminated during the maturation of the print (Aydin, Kucuk and Kenar, 2020).

PLGA can also be used as a synthetic polymer. Indeed, PLGA could be directly bioprinted with embedded living cells (and other biological elements) as demonstrated by the study of E. Naseri *et al* (Naseri *et al.*, 2020) by printing PLGA at low temperatures.

- Commercial bioinks

There are numerous commercial bio-inks available on the market for numerous applications. The most used components for commercial bioinks are alginate, gelatin and gelatin methacrylate (Tarassoli *et al.*, 2021) supplemented with other components.

In the Table 2, we present some examples of ready to use bioinks offered by well-established bioprinting private companies.

TABLE 2.2 LIST OF COMMERCIAL BIOINKS AND THEIR COMPOSITION

	Ready to use bioinks	Gelatin based	Collagen based	Alginate based	Hyaluronic acid based	PEDFA based	Other
CellInk	22	8	4	3	2	5	1
Innoregen	6	5	1	/	/	/	/
Brinter	6	1	2	1	1	/	1
Bio-inx	4	1	1	/	/	/	2
Allevi	2	/	2	/	/	/	/

The most used bioprinting method is still extrusion bioprinting, which explains why most available commercial bioinks are produced for extrusion bioprinting. These industrial bioinks were developed to enable having the same conditions and printing conditions for precise cell types. However, it is interesting to note even with all these advantages, many laboratories will still work with their own lab-made bioinks.

2.2. Crosslinking of bioinks

Crosslinking is an important process after bioprinting, it allows the reticulations of printed hydrogels, either by extrusion/laser or inkjet bioprinting. There are different reticulation methods that can be classified into different groups: mechanical ionic, hydrophobic and hydrogen bonding interactions, stereo-complexation, self-assembly of peptides or amphiphilic polymers into micellar structures are some of the well-established mechanisms which are known to drive physical crosslinking of hydrogels (Jungst *et al.*, 2016).

- Chemical crosslinking

Chemical reticulation provides mechanically better stability compared to physical reticulation discussed previously (Jungst *et al.*, 2016) It is characterized by covalent bindings between polymer chains. Chemical crosslinking requires external crosslinker which can result in cytotoxicity (Hennink and van Nostrum, 2012).The concentration of reticulation agent will determine the degree of reticulation, which will result in a hydrogel with a higher mechanical propriety. The photo-initiated radical polymerization of methacrylate groups (Fig 1.12) is a very suitable method for to control the crosslinking in time and space as shown by B.D Fairbanks *et al* (Fairbanks *et al.*, 2009) where monomers undergo curing to form a crosslinked polymetric network when exposed to UV light (Decker, 2002) . Hydrogels need to be modified with functional

groups such as methacrylate to undergo photopolymerization. A photo-initiator is also needed for the photopolymerization. Irgacure or Lithium phenyl-2,4,6-trimethylbenzoylphosphinate (LAP) are some of the most widely used photo-initiator in bioprinting community (Fairbanks *et al.*, 2009) Y. Yan *et al* in their work describe the methacrylation of gelatin and the reticulation process with LAP and blue light 405nm, less toxic for cells than UV light (365 nm) (Yan *et al.*, 2022)

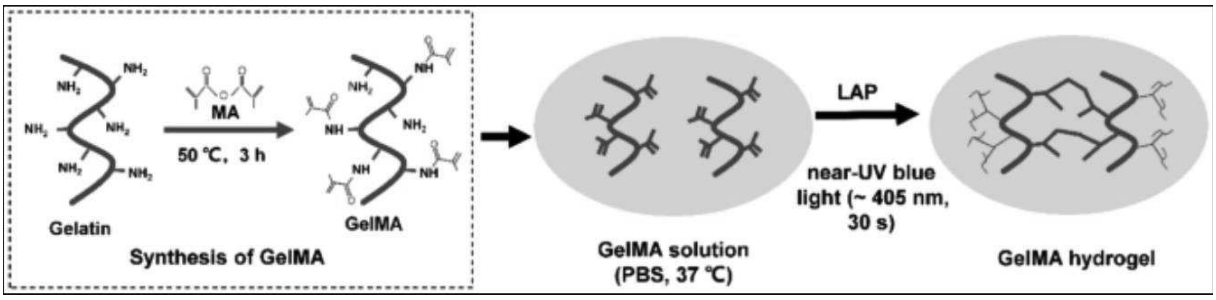

Figure 12 Methacrylation of Gelatin methacrylate and reticulation by blue light (taken from Y. Yan et al.(Yan et al.*, 2022) 2021)*

But these photo-initiators can be cytotoxic, even at low concentrations as well as the UV light radiation. To counter this, it is possible to leach the photo-initiator from the hydrogel after reticulation (Arcaute, Mann and Wicker, 2006) and to switch from UV light to visible light. Indeed, it is possible to use LAP with a radiation at 405 nm (blue light) which is non-cytotoxic whereas Irgacure requires UV light. It is also possible to use very low concentrations of (<0.1%) photo-initiator (0.1% or lower) as in done in Oliveira *et al* (Oliveira *et al.*, 2021) and recommended by Fedorovich *et al.*, 2009 (Fedorovich *et al.*, 2009).

- Physical crosslinking

A growing interest in the bioprinting community is to be able to crosslink the bioink without adding an external agent.

Physical crosslinking such as ionic bonding, hydrogen bridges or hydrophobic interactions, which are often temperature dependent (Oryan *et al.*, 2018), are the three most commonly used physical crosslinks in hydrogels for bioprinting.

- Enzymatic crosslinking

A lesser commonly used way of crosslinking hydrogels is to employ enzymatic reactions. The most usual is to take advantage of the reaction of fibrin with thrombin the two main precursors of blood clotting (Benedikt *et al.*, 2000; Scheraga, 2004). Indeed, with its cytocompatibility and cell adhesion properties, fibrin is a widely used bioink in bioprinting (Lee *et al.*, 2010; Ehsan *et al.*, 2014; Shpichka *et al.*, 2020).

2.3. Characterization of bioinks

To mechanically characterize bioinks, before and after crosslinking, application of rheometer is the most popular method. Doing so, the yield stress (minimum force required for the bio-ink to begin to start flowing), the storage modulus (G'), the loss modulus (G") and the viscosity can be determined. Parameters G’ and G’’ are particularly interesting to analyze. As described in the review “Printability and cell viability in extrusion-based bioprinting from experimental, computational, and machine learning views” by A. Malekpour (Malekpour and Chen, 2022), the loss tangent (G’’/G’) which makes the bioink behave more like a solid or a liquid is an important parameter, allowing to characterize a bioink. Indeed, a high loss tangent shows that the bioink has a very fluid behavior, therefore will extrude easily but will lack mechanical strength. Whereas, a low loss tangent shows that the bioink has an almost solid behavior, a high stiffness and shear stress, allowing a good mechanical strength but requires more pressure to be extruded. Nevertheless, viscosity is the most important parameter for the rheological characterization of the hydrogel (*Essentials of 3D Biofabrication and Translation*, 2015).

- Viscosity

The viscosity of a fluid is the resistance of the fluid to flow when stress is applied. The importance of viscosity during bioprinting has been raised in particular by Chimene *et al* work (Chimene, Kaunas and Gaharwar, 2020). They showed high viscosity will helped maintain a structure after printing for extrusion bioprinting but increased the shear stress thus decreasing the cell viability. High viscosity also impedes the surface tension necessary for droplet formation in inkjet bioprinting. The viscosity of a polymer and more particularly of a hydrogel is mainly determined by the polymer concentration and its molecular weight. The printing fidelity and shape retention depends on the viscosity of the hydrogel used. It has been showed by Celikkin *et al* (Celikkin *et al.*,

2018) that a lower concentration of polymers promotes more cell proliferation and cell migration but has lower mechanical proprieties. Polymers with high molecular weights are then more attractive in hydrogels, offering higher viscosities with low polymer concentrations. Such polymers are found in natural derived polymers such as collagen and hyaluronic acid (Malda *et al.*, 2013).

- Shear thinning

Shear thinning refers to the non-newtonian behavior in which the viscosity decreases as the shear rate increases.

In the shear thinning phase after extrusion bioprinting, the viscosity of the bioink decreases with the increasing shear stress rate, which is suitable for further extrusion, the formation of uniform filaments and increased cell survival during extrusion. Holzl *et al* (Hölzl *et al.*, 2016) claimed that one of the key characteristics of a bioink in the extrusion phase is shear-thinning, which minimizes shear stress. If the viscosity changes little with the shear force or if the yield stress is high, the hydrogel is not suitable for extrusion bioprinting.

- Yield stress

The yield stress is the minimum force that changes the proprieties of the deformation of a materiel from elastic to plastic deformation. If this yield stress is too high, it will be impossible or very hard to apply enough force for the material to form a printable filament without applying a very high shear stress to the cells during extrusion bioprinting (Mouser *et al.*, 2016).

2.4. Bioink requirements and limits

Bioink requirements are highly dependent on the printing technique.

Indeed, for **extrusion bioprinting** hydrogels used fall into the category of non-newtonian fluids, where viscosity is strongly dependent on shear rate (Jungst *et al.*, 2016). Hydrogels with shear thinning and thixotropic behavior (a viscosity that decreases when stress is applied) are also well suited. For shear thinning hydrogels, during the extrusion or phase creating the shear thinning, the shear forces will align the polymer chains, rendering them extrudable. The phenomena of thixotropy, which is time dependent, enables a stable form for a material at rest, and exhibit low viscosity

for the bioink when inside the printing nozzle during extrusion and still be able to regain its stability after extrusion.

The limits of viscosity for extrusion bioprinting ranges from 30 mPa/s to 60×10^7MPa/s according to Mandrycky *et al* (Mandrycky *et al.*, 2016). The adding of cells can impact the viscosity of cells. Ouyang *et al* (Ouyang *et al.*, 2020) showed that bellow 2×10^6 cells/mL there is no significant difference in bioink viscosity. One of the main limitations of hydrogels for extrusion bioprinting is their non-supporting characteristics. Indeed, according to D. Chimene *et al* (Chimene et al. - 2020) conventional hydrogel bioinks are mechanically weak and require reinforcement. As showed previously, the viscosity of the bioink affect cell viability (Zhao *et al.*, 2015). Cell viability decrease with the increase of bioink viscosity.

For **inkjet**, the bioink usually has a low cell concentration (<10^6 cells/mL) and low viscosity so that it can flow easily through the tube system and nozzle without clogging (Hölzl *et al.*, 2016). These bioinks should possess rheopectic properties, where rheopectic materials have a time-dependent non-Newtonian behavior implying an increase in viscosity as shear stress is applied, triggering droplet formation. The surface tension of the bioink is a very important parameter on which the final result depends. The viscosities supported and used in inkjet bioprintning are between 3.5 and 12 mPa/s (Mandrycky *et al.*, 2016). As seen before, an important cell density will increase the viscosity of the bioinks, thus limiting the cell concentration of inkjet bioinks. In addition, the droplets should solidify immediately after landing on the receptive surface to be able to form complex 3D structures. Finally, the droplets need the have a fast gelation when landing on the substrate.

Laser based or cell transfer techniques consists of transferring the bioink from a reservoir to a suitable surface by the formation of laser-induced jet, with viscosity in general ranges from 1 to 300 mPa/s (Mandrycky *et al.*, 2016). The bioink should have a viscosity high enough to stay in the cartridge before printing and be able to transfer thermal energy into kinetic energy.

In **stereolithography** bioprinting a laser is used to polymerize a photocurable bioink material in a vat. The bioink thus needs to be a photolymerizable hydrogel, which limits the choices of material and should be further reinforced with photo-initiators (but at a

low concentration because are often toxic) and light absorbers to initiate photopolymerization and enable fabrication of complex 3D structures (Hospodiuk *et al.*, 2017). Important requirements of these bioinks are stability over time and high-mechanical strength as well as the ability to keep cells uniformly distributed in the non-reticulated bioink solution, are other important requirements of bioinks used with this technology.

For all bioprinted products, the degradation is an important parameter, depending on the materials used for the bioinks and the maturation environment. The degradation of the bioinks should release only non-toxic components for biocompatibility. Finally, the degradation rate should be slow enough for the cell to have time to maturate but fast enough to not “trap” the cells after the maturation. Wu *et al* (Wu *et al.*, 2016) implemented a new bioink with controllable degradation to improve the alginate bioink applications. Indeed, in this study the limitation of the degradation of alginate was put in light, reducing the maturation and proliferation of cells in these bioinks. With their novel method, the degradation rate is controlled thus increasing the proliferation of the studied cells.

3. Cell aggregates

The terms of spheroid and organoid have been used indifferently to name one or the other in literature. And indeed, these two biological constructions have overlapping applications and origins, but can be differentiated by their cellular source, method of production and complexity. Bioprinting cellular aggregates enables the research on already formed cellular structures and increases the cellular density of bioprinted constructions.

3.1. Spheroid

A spheroid is a 3D aggregate of cells that allows the study of tissues and micro-tumors on a smaller scale. These aggregates are self-organizing 3D structures of 500 µm in cross-section that are generally spherical in shape and have a size limitation due to the diffusion of nutrients, gases and signals (Hayden and Harbell, 2021). Scaffold free

methods are the most common and used methods as they are easy to set up, inexpensive and fast. The spheroid architecture is considered more relevant to study cell-cell interaction and cell matrix interaction than 2D cultures. Thus, spheroids have been used in numerous applications ranging from the production of tumorous cells models to drug screening (Santi *et al.*, 2020) or tumor cells models and cell interaction (Kunz-Schughart *et al.*, 2001; Jiang *et al.*, 2005).

Cells for spheroids can have multiple origins and are not limited, they can come from cell lines, primary cells or even cells from tumor tissues, where they will be enriched with cancer cells (Raghavan *et al.*, 2017; Tomás-Bort *et al.*, 2020).

Spheroids can be fabricated by three main methods. The first and historic method is the suspended drop method. In this method, a plate containing drops of cells and medium is inverted and cells aggregate spontaneously at the bottom of the drops (Harrison, 1906; Timmins and Nielsen, 2007), as shown in Figure 13. The size of the spheroids can be controlled with the concentration of cells in the droplet. This method is very simple to set up but the monitoring of the development of the spheroid is difficult. Indeed, due to the configuration, visualization of cells by microscopy for example can be tricky.

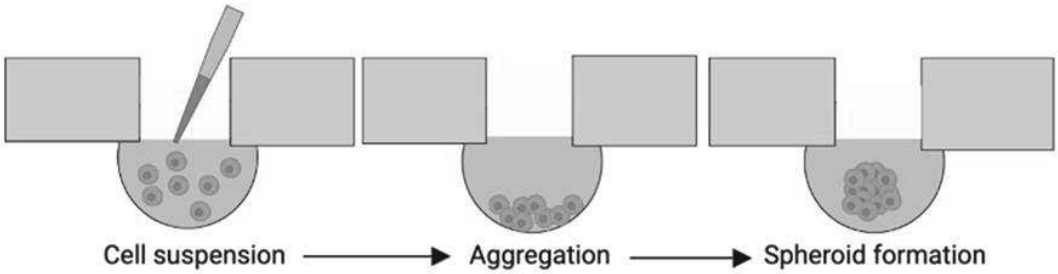

Figure 13 Spheroid formation by drop method

(adapted from Chew et al(Chew et al.*, 2020))*

A second method is to use spinner flasks with or without scaffolds, where the cells will aggregate under the agitation (Sutherland, 1971). Indeed, under the agitation the cells will aggregate together rather than on the surface of the flask, creating a spheroid. Thirdly, cells can form spheroids when cultured with non-adherent substrates, causing them to aggregate into spheroids. For example, this method is used in the static overlay technique where cells cannot adhere on the surface and aggregate (J M Yuhas, 1977).

More recently, this method was used for the technique of non-adherent micro-patterned surfaces, where a flow of cell medium traps cells inside micro-patterns in the surface, aggregating the cells into spheroids (Rivron *et al.*, 2009). A gentle rocking of the surface can help produce aggregates faster. The main issue with this method is the lack of control over the size and shape of the produced spheroids(Costa *et al.*, 2018).

Except for the newest methods (Vinci *et al.*, 2012; Fennema *et al.*, 2013), spheroid reproducibility is very difficult to achieve and is one of the major limitations of spheroid production with the size limitation. But there are other problems, such as the difficulties in imaging these cells aggregate or the lack of control of cell positioning with multicellular spheroids.

To address some of these issues, microscaffolds can be used in the fabrication process of the spheroids. In some cases, these spheroids are considered as micro-tissues rather than spheroid (Jiang *et al.*, 2005).

Bioprinting could also be used with spheroid formation to improve both technologies. Indeed, it is possible to print either individual cells or cell aggregates inside the bioink to obtain dense cellular constructs. This new emerging technology is named either spheroid assembly, cell spheroid bioprinting or even bio-assembly. This is not only limited to spheroids but also organoids (Moldovan, Hibino and Nakayama, 2017).

Compared to organoids, spheroids are simpler 3D models but are very easy to fabricate and can mimic several aspects of tumors or other cellular constructions.

3.2. Organoid

The term organoid appears for the first time in 1946 with Smith and Cochrae and means “to resembled an organ”. Today, organoids are more often considered 3D self-organizing constructions of cells closely resemble and mimic the original tissue from which they are derived, both histologically and genetically (Gunti *et al.*, 2021). The source of cells for organoid production is more limited than for spheroids. Indeed, the source of cells are pluripotent stem cells (embryonic stem cells or induced pluripotent stem cells) and organ specific adult stem cells (Dutta, Heo and Clevers, 2017).These constructions are self-organizing 3D cellular structures, but instead of one cell adhering to another, the cells differentiate in response to physical or chemical signals.

Organoids can be fabricated by employing growth factors on the different stem cells described earlier. The cells will differentiate and auto organize into small scale structures mimicking organs or tissues. It is also possible to use the 3D growth environment of the cells to guide the organoid formation in concert with growth factors. Indeed, the team of Gjorevski *et al* (Gjorevski *et al.*, 2022) developed intestinal crypt like structures in specific 3D environment to better control their formation and reproducibility. Usually matrigel is used to support the development of complex organoids as a basal support. Matrigel is an extracted reconstructed basement membrane from the Engelbreth-Holm-Swarm (EHS) mouse sarcoma. Matrigel is composed of 60% laminin and 30% collagen IV (Corning). But due to the complexity and poor definition of matrigel, studies are looking into replacing matrigel to better control the signal of differentiation received by the cells (Kozlowski, Crook and Ku, 2021).

Organoid of varied organs have been developed, organoids of colon, stomach, ovaries, pancreas, prostate, lung, liver (Dutta, Heo and Clevers, 2017) and intestine as shown in Figure 14.

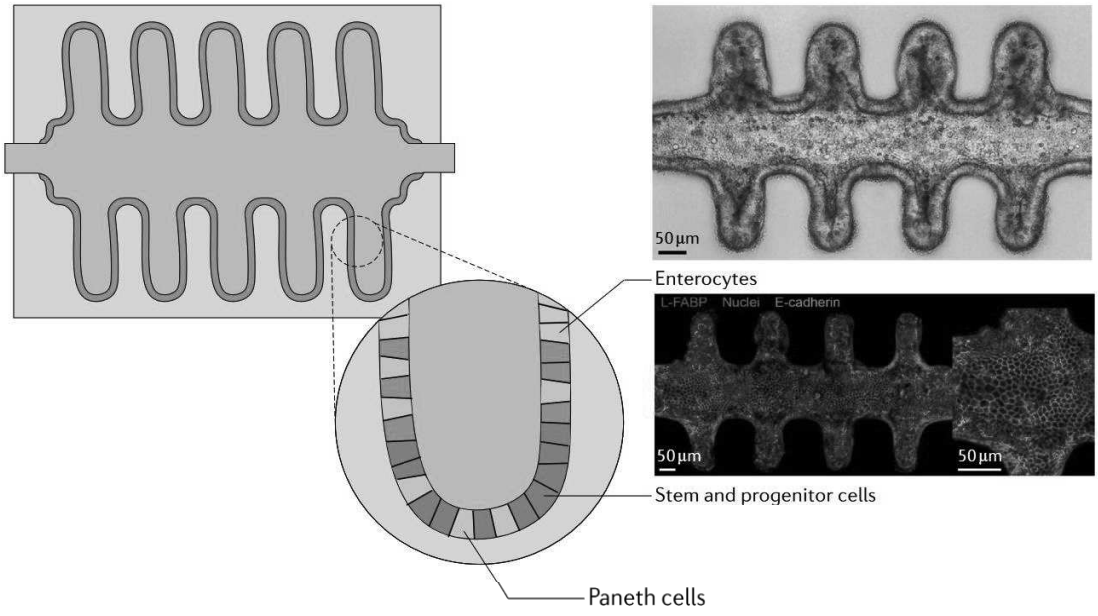

Figure 14 Intestine crypt organoid

(adapted from Hofer et al (Hofer and Lutolf, 2021))

Organoids can be used to model diseases such as inflammatory bowel disease and cystic fibrosis among others, allowing to better understand them and develop personalized drugs by using patient derived cells (Dutta, Heo and Clevers, 2017). Another possible use of organoids is to model infectious diseases. Indeed, organoids have been used to model infections by the Zika virus (Garcez *et al.*, 2016; Wells *et al.*, 2016) or bacterial infections (Bartfeld and Clevers, 2015). These models could be used for clinical approaches for new treatments. A special case is made for tumor organoids, also called tumoroids (Xu *et al.*, 2018). Tumorous cells, derived from the patient can be cultured, in spinning flasks or non-adherent plates.

To help with the complexity and variability of natural matrices, PLGA scaffolds as well as derivate as polyethylene glycol (PEG) were developed to support organoid cultures with hydrogels (Kaur *et al.*, 2021).

An important limitation of organoid or spheroid production is the reproducibility and heterogeneity (Hofer and Lutolf, 2021). While, the environment and chemicals in the model can be controlled, the precise localization of cells cannot. This is why organoids and spheroids can also be produced by bioprinting into compatible bioinks where the localization, layers and morphology of cells and structure can be precisely controlled.

3.3. Bioprinting of cellular aggregates

The development of complex cellular models by 3D bioprinting could be useful to better mimic *in vivo* environments and study intercellular responses. The advantage of printing a multi-culture is that the 3D location of cells can be precisely chosen to mimic the *in vivo* model. Moreover, organoids and cell aggregates have a size limitation without a vascular system. Indeed, as previously discussed in 1.3 Limits of bioprinting, the size limit a non-vascular system is of 400 µm. Bioprinting cell aggregates with a vascular system could remedy this size limit. Finally, bioprinting can be applied to precisely control the bioink components with ECM components and organize them into defined spatial positions.

This spatial position of ECM components has been achieved by bioprinted by the team Yi *et al* to induce an oxygen gradient to recapitulate the structure and biochemical and

biophysical proprieties of an *in vivo* tumor (Yi *et al.*, 2019). This model was used to determine the best therapeutic drug combination with the bioprinting of patient derived cells. The team of X. Cao *et al* (Cao *et al.*, 2019) also controlled the environment of a tumoroid by bioprinting. X. Cao *et al* designed a coaxial bioprinting to construct a tumoroid with hollow vessels, modeling blood and lymphatic vessels and integrated with a gelatin bioink breast cancer cells to form a tumoroid containing both blood vessels and lymphatic vessels. This allow a better modeling of the complex micro-tumor environment.

Bioprinting cell aggregates can also help to reduce important limitations of bioprinting such as vascularization. Indeed, the team of De Moor *et al* (De Moor *et al.*, 2018) bioprinted spheroids of endothelial cells to create a vascular network.

Extrusion bioprinting is the most used bioprinting method but also a common method used to bioprint organoids (Ren *et al.*, 2021). The team of Bertassoni *et al* (Bertassoni *et al.*, 2014) bioprinted blocks of loaded GelMa bioinks to bioprint organoids and cellular aggregates. The bioprinted constructs maintained cellular activity over time.

4. Microscaffolds for bioprinting

Microscaffolds are three-dimensional matrix providing mechanical support for cell adhesion, proliferation and cell survival (Loh and Choong, 2013). To our knowledge mere two studies combined microscaffolds with bioprinting. This combination was also hypothesized in the work of Ibrahim T.Ozbolat (Ozbolat, 2017). The first study by Levato *et al* produced PLA microcarriers (or microscaffolds) to increase the cellular density before printing (Levato *et al.*, 2014). The cell laden microcarriers were then bioprinted into complex structures with a high density and viability. The second study attempted to bioprint porous PLGA microscaffolds by extrusion bioprinting to enhance cellular viability, without success due to clogging of the printing nozzle (Tan *et al.*, 2016) . Nevertheless, the combination of microscaffold technology with bioprinting opens new pathways to improve extrusion bioprinting. Indeed, these porous microscaffolds can serve as a proliferation surface for the cells before and after bioprinting and also serve as a mechanical protection for the cells against shear forces during the physical extrusion action of bioprinting.

Both applications using microscaffolds for bioprinting used PLGA or PLA, two similar polymers. We chose to focus our study on PLGA microscaffolds as this polymer used in many biomedical applications due to its highly versatile, stable, biocompatible and degradability proprieties (Danhier *et al.*, 2012).

4.1. Poly(DL-lactic acid-co-glycolic acid)

As previously noted, PLGA is a biodegradable polymer which degrades into two non-harmful monomers (Elmowafy, Tiboni and Soliman, 2019). This polymer is formed by monomers of glycolic and lactic acid assembled to form a linear aliphatic polyester (Figure 15).

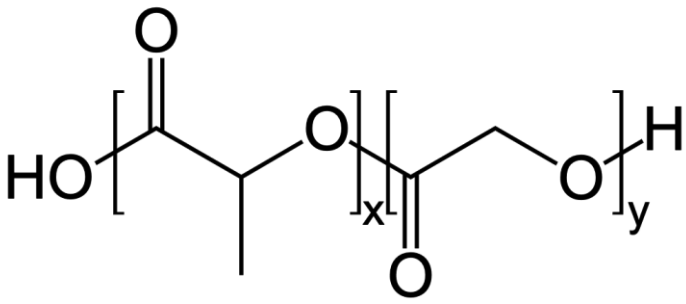

Figure 15 Poly Lactic co-Glycolic Acid (PLGA)

Where x equals the number of lactic acid units and y equals the number of glycolic acid units (credits Fvasconcellos)

PLGA typically has a glass transition temperature between 40 and 60 °C depending on the ratio of lactic and glycolic acid. Indeed, PLGA are identified according to this ratio, a PLGA 75:25 is composed of 75% of lactic acid and 25% of glyclic acid. The properties of PLGA change according to the ratio. Some of these properties were tested by Soon Eon Bae *et al* (Bae *et al.*, 2009). The team found that as the proportion of lactic acid increases, the polymer becomes mechanically stiffer when the proportion of lactic acid increases.

- **PLGA degradation**

The degradation of PLGA leads to metabolite monomers, lactic acid and glycolic acid (Figure 16). Lactide and glycolic are endogenous and easily metabolized by the body via the Krebs cycle. Minimal toxicity is associated with the use of PLGA in the human body (Kumari, Yadav and Yadav, 2010)

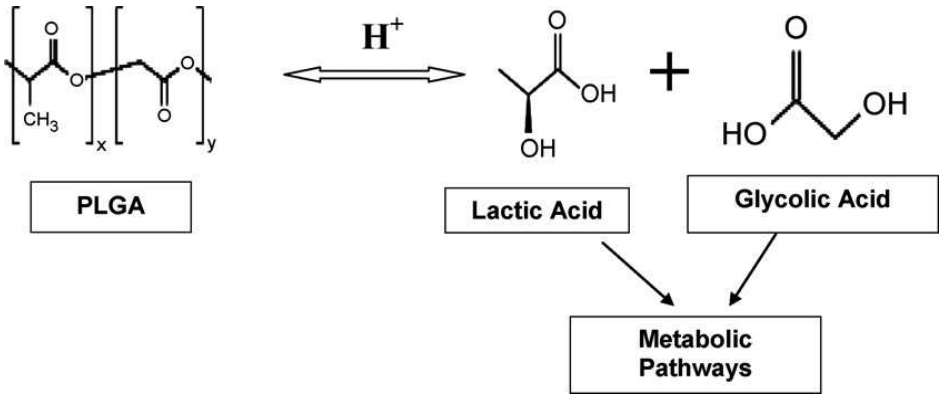

Figure 16 Degradation of PLGA into Lactic acid and glycolic acid monomers Taken (Kumari, Yadav and Yadav, 2010)

The polymer degrades by hydrolysis of the ester bond, a process that is enzymatically catalyzed (Dunne, Corrigan and Ramtoola, 2000). Polymer properties such as molecular weight also control the degradation rate. The degradation time can vary from several months to several years, depending on the copolymer ratio.

It is also possible to verify the degradation of PLGA in solution or in medium. Indeed, Yoon JJ *et al* (Yoon and Park, 2001) tested the degradation time of PLGA in a PBS solution and found that the PLGA particles will present mophology changes, swelling, when degradating. The pH of the medium can be tested and recorded during the experiments because there is a release of acid when PLGA particles are degraded, thus inducing an acidification of the media around the particles (Fu *et al.*, 2000). This acidification of the medium is an indicator of the degradation rate of the particles.

The degradation products of PLGA have also been shown to accelerate the degradation of PLGA. Thus it is possible to accelerate the degradation by adding the products of degradation or remove them to slow down the degradation over time.

The size and shape of the PLGA have an effect on the degradation time. Indeed, large particles (>50 µm) appear to degrade faster (Dunne, Corrigan and Ramtoola, 2000). The degradation products formed in the small particles can diffuse faster while they remain longer in the larger particle, catalyzing the degradation of the remaining particle (Dunne, Corrigan and Ramtoola, 2000). Having pores within the particles can also impact the degradation rate. Indeed, with the pores, the degradation products can more easily escape from the particle and *in fine* diminish the degradation rate.

It is also possible to accelerate the rate of degradation by increasing the temperature of the medium (Dunne, Corrigan and Ramtoola, 2000).The *in vivo* environment can have an important impact on the degradation compared to *in vitro*. Indeed, inflammation can occur naturally when PLGA is introduced into the body. An increase in temperatures of one or up to three degrees is possible.

The density of the particles is an important parameter for the degradation rate of said particles. To density can be determined by the following equation (Smith *et al.*, 2019):

$$\frac{\text{number of particles}}{\text{g}} = \frac{6 \times 10^{12}}{\rho \pi d3}$$

Where ρ is the particle density in $\frac{\text{g}}{cm^3}$ and d is the size of the particles in μm.

4.2. PLGA applications

PLGA is used in biomedical applications to deliver specific drugs or biological agents in the body (Kumari, Yadav and Yadav, 2010). Indeed, one of the most important and most documented uses of PLGA is as a drug delivery agent. PLGA drug carriers allow the controlled drug release over long periods of time with a single injection (Makadia and Siegel, 2011) (Ford Versypt, Pack and Braatz, 2013).

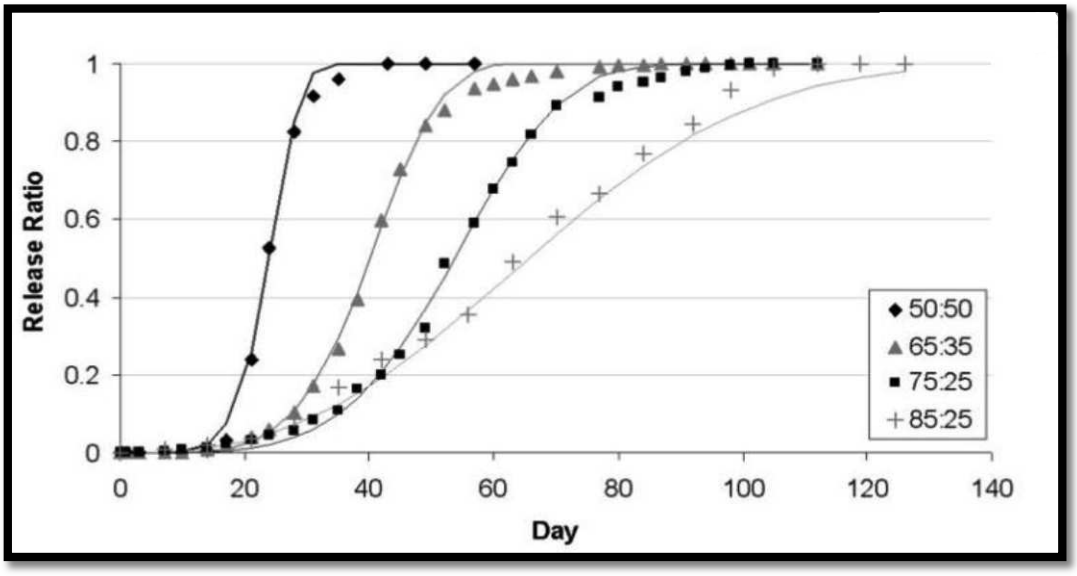

Figure 17 Release profile in time for PLGA 50:50, 65:35, 75:25, 85:25

Taken from Hirenkumar K. Makadia et al (Makadia and Siegel, 2011)

The release of the carried drug depends on the degradation of the PLGA. There are two phenomena in the drug release. The PLGA degradation and the PLGA erosion. As we can see with the results of drug release *in vivo* (Figure 17), there is an initial burst of drug release, related to the drug type, the drug concentration and the polymer hydrophobicity. The moment of this burst will also depend principally on the molecular ratio of the PLGA used. In the second phase of the drug release, there is a slower release from the degradation of the polymer bulk. Monomeric products are released in the medium, creating an escape route for the drug.

Rohiverth Guarecuco *et al* (Guarecuco *et al.*, 2018), used the drug release PLGA particles as vaccine carriers. Indeed, a problem with vaccination comes from the need of a second or third injection, sometimes months after the first one. With the use of PLGA particles, a first burst of vaccination agents was spontaneously released in the media and a second burst and third burst were released after a few months. Thus abolishing the need for further injections.

The second use for PLGA is as biological agents. Indeed, PLGA is biocompatible and has been used for cell expansion (Qutachi *et al.*, 2014, 2018) and in *in vivo* applications for cell replacement or therapy such as building of organoids (Langer *et al.*, 2019).

The required diameter of PLGA particles will be of at least of 50µm with a pore size of at least 20µm, to permit the circulation of nutriments (Choi *et al.*, 2010). PLGA particles can be used as scaffolds to form organoids and cell platforms to assess the response of engineered 3D tissues versus 2D tissues *in vitro* (X. Wang *et al.*, 2018; Kuriakose *et al.*, 2019; Dhamecha *et al.*, 2020)(Langer *et al.*, 2019).

Indeed, Kuriakose *et al* tested six cancer drugs in a 2D monolayer of A549 lung tumor cells compared with a tested 3D configuration of A549 lung tumor cells within PLGA particles. They found that the drugs induced more cell death in the 2D configuration than 3D (Kuriakose *et al.*, 2019). Lung cancer cells cultured on porous PLGA particles showed higher drug resistance compared to 2D models at the same concentration of cancer drugs. This shows that cells respond differently depending on their special

arrangement. Disease models were produced with microporous particles of PLGA used as scaffolds for different type of cells, forming the tissue and the extracellular matrices to better understand natural phenomena and find new therapeutic treatments (Reid *et al.*, 2019). Finally, PLGA particles can also be used to directly treat diseases such as strokes, inducing the repair of the neural tissue, increasing the proliferation and transport of neural cells (Bible *et al.*, 2009).

However, D. Smith *et al* (Smith *et al.*, 2019), showed that negatively charged PLGA particles (measured by zeta potential), although unfavorable for cell adhesion, does not completely prevent it. To increase cell adhesion on PLGA particles, the surfaces can be functionalized by extracellular matrix adhesion proteins such as collagen, fibronectin or laminin (Kuriakose *et al.*, 2019) and also with PLL (Smith *et al.*, 2019) or amine groups (Chung *et al.*, 2008). Indeed, the team of H. Tan *et al* (Tan *et al.*, 2009) demonstrated that RDG modified PLGA/gelatin micro-particles has a better chondrocyte adhesion, proliferation and viability rate than PLGA/gelatin micro-particles

The shape of the particles is also important for cell proliferation before injection and after injection in tissues for cell distribution. Indeed, Jin-Wook Yoo *et al* (Yoo, Doshi and Mitragotri, 2010) have tested PLGA particles with either a spherical or ellipsoidal shape. The spherical shaped PLGA particle allows a better cell proliferation before injection and a faster endocytosis.

4.3. Production of PLGA microscaffolds

A wide range of protocols are mentioned in the literature for the production of PLGA (Makadia and Siegel, 2011)(Qutachi *et al.*, 2014)(Choi *et al.*, 2010). Various parameters such as PLGA concentration, solvent concentration, surfactant concentration, emulsions speed can be modified to obtain particles with specific shapes, sizes and pores diameters. The ideal pore size depends on the uses of the particles. For drug delivery the pore size has to be small (below 0,1 µm) or absent whereas for cell proliferation and adhesion the pore size must be large enough to allow cell adhesion and nutriment flow (Choi *et al.*, 2010).

As previously noted, non-porous particles are ideal for drug delivery, as the lack of porosities prevents the liberation of drugs before a specific time or reaching the targeted tissue. These particles are typically less than 50 µm in diameter, allowing faster particle degradation and drug release (Dunne, Corrigan and Ramtoola, 2000).

Teams like Daniel Smith *et al* (Smith *et al.*, 2019) and Ki Woo Chun *et al* (Chun *et al.*, 2004) have produced non-porous particles for various biomedical applications. They used single and double emulsion process.

According to Tan *et al* (Tan *et al.*, 2016), the pores of the particles used as scaffolds for mammalian cells cover an minimal optimal size ranging from 0,1-20 µm. Indeed, cell infiltration would be impossible with too small pores but submicron pores facilitate nutrient/gas/detritus exchanges. Sung-Wook Choi also showed that pore size under 20 µm have a negative effect on the long term (longer than 7 days) for cell proliferation. Indeed, pore sizes smaller 20 µm can be obtruded very fast by the extra-cellular matrix synthesized by developing cells. However, small pore size may be an advantage as long as the culture time is short (less than 7 days)(Choi *et al.*, 2010). Aneetta E. Kuriakose *et al* (Kuriakose *et al.*, 2019) also demonstrated that a minimum size of pore for cell proliferation is of 20 µm.

Different protocols can be used to produce particles with similar results. Indeed, the team of Chung *et al* (Chung *et al.*, 2008) use a gas production method to obtain very of porous particles of 175µm. The team of Smith *et al* (Smith *et al.*, 2019) used a double emulsion microfluidic method to obtain highly porous particles with a mean diameter of 260µm. Finally, the team of Kuriakose et al used a double emulsion method to obtain particles up to 42µm (Kuriakose *et al.*, 2019).

In this first chapter, we have seen the different existing bioprinting technologies, their advantages and limitations, their applications and the selected bioinks. On this basis, we determined that extrusion bioprinting was the most suitable technology for our studies. For this reason, we focused on two of the main limitations of this technology: the cell density necessary and available at the time of printing and the low cell viability after printing. This low viability is due to the shear forces exerted by the bioink during the extrusion phase. To overcome these two limitations, we hypothesized that the use of porous spherical structures, like cell microcarriers of PLGA, can increase the proliferation surface before the printing process and mechanically protect the cells from shear forces, increasing cell viability.

5. Aim of the thesis

With the conclusions of the last chapter, we have chosen, in this thesis work, to develop porous microparticles of PLGA to overcome the limitations of extrusion bioprinting. Non-porous microcarriers have already been studied in order to increase cell proliferation with bioprinting, and have demonstrated convincing but limited results (Levato *et al.*, 2014). The addition of high porosity and coatings increases the attractiveness of the microparticles or microscaffolds for the cells to adhere to the surface and the interior of the microscaffolds. These microscaffolds colonized by the cells can then serve as “microcarriers” for the cells during bioprinting. Indeed, our hypothesis is that the cells that have colonized the interior and the surface of the microscaffolds will be protected from shear forces. Finally, the bioprinted microscaffolds can serve as scaffolds for the cells in the bioink, and serve as a platform for cell development over time. To this end, in this work, we first produced reproducible and reliable microscaffolds of PLGA with coatings from ECM constituents adapted to the cellular model selected. We then tested the efficiency of these microscaffolds on different cell types on their proliferation before printing and their viability after printing. Additionally, the impact of microscaffolds after printing on biological processes such as cell migration was studied. This work is presented in chapter 3: “Enhancing cell survival in 3D printing of organoids using innovative bioinks loaded with pre-cellularized porous microscaffolds. »

Based on our results from chapter 3 and on our microscaffolds, we set up a project with a biomedical application in partnership with Doctor Isabelle Talon. The objective of this partnership is to develop implants that reproduce the diaphragm in order to treat diaphragmatic hernia. Indeed, today there is a lack of implants to regenerate the diaphragm and the bioprinting of muscle cells on suitable membranes can respond to this lack. This is why we bioprinted, with our microscaffolds, muscle cells on BSA membranes produced by the Albupad group. We then observed the effects of our microscaffolds adapted to muscle cells and to this application on cell proliferation and viability.

Chapter 2: Materiel and Methods

1. Cell lines used and their characteristics

In this thesis work we studied the effects of bioprinting with the microscaffolds on a variety of cells to demonstrate the beneficial effects on these cells. Each cell line is described and their culture method is explained.

1.1. Dental Pulp Stem Cells (DPSCs)

DPSCs are human dental pulps stem cells isolated in accordance with French legislation (informed patient consents, Institutional Review Board approval of the protocol used: C17-78, DC-2018-3353). DPSCs were extracted from human teeth at the dental clinic of the Hopital Civil of Strasbourg (for phenotypic characterization see Ehlinger *et al* (Ehlinger *et al.*, 2021)). They were used at passages 2-6. The cells were cultured in minimal essential medium (MEM) Alpha Gibco supplemented with 10% fetal bovine serum (FBS) (Dutscher S1810-50) and 100 units/mL penicillin, 100 mg/mL streptomycin (Dutscher, L0022-100) in an incubator at 37°C and 5% CO_2. Cells cultured until 90% of confluence were removed with trypsine (Dutscher, L0615-500) and either used for experimentation or subcultured with a ratio of $5x10^4$ cells per 75 cm_2 flask. DPSCs in passage number 2 to 6 were used for all the experiments with similar results.

DPSCs cells are adult organ specific stem cells which have the ability to differentiate into adipocytes, neural-like cells but also into cells with similar characteristics than mesoderm and endosteum cells (Jeong *et al.*, 2020). DPSCs have been used for the formation of dental organoids by the team of Sang Yum Jeong *et al*. They demonstrated, after maturation and differentiation, mineralization and odontoblasts differentiation in the produced organoid.

1.2. Periodontal Ligament Stem Cells (PDLSc)

PDLSc are human periodontal ligament stem cells isolated in accordance with French legislation (informed patient consents, Institutional Review Board approval of the protocol used: C17-78, DC-2018-3353). PDLSc were extracted from human teeth in the dental clinic of the Hopital Civil of Strasbourg. They were used at passages 2-6. The cells were cultured in MEM Alpha Gibco supplemented with 10% FBS (Fetal bovine serum, Dutscher S1810-50) and 100 units/mL penicillin, 100 mg/mL

streptomycin (Dutscher, L0022-100) in an incubator at 37°C and 5% CO_2. Cells cultured until 90% of confluence were removed with trypsine (Dutscher, L0615-500) and either used for experimentation or subcultured with a ratio of $5x10^4$ cells per 75 cm^2 flask.

1.3. Chondrosarcoma cells (HCS-2/8)

HCS-2/8 cells are a clonal cell line with cartilage phenotype established from a human chondrosarcoma from Takigawa *et al* (Takigawa *et al.*, 1989). They were used at passages 10-28. Cells were cultured in Alpha MEM Eagle supplemented with 20% FBS and 100 units/mL penicillin, 100 mg/mL streptomycin in an incubator at 37°C and 5% CO^2. Cells cultured until 90% of confluence were removed with trypsine (Dutscher, L0615-500) and used for experimentation.

1.4. Fibroblast cells (NIH/3T3)

NIH/3T3 are fibroblast cells originated from NIH Swiss fetal mouse were purchased from ATCC (CRL-1658TM). The cells were cultured in high glucose Dulbecco's modified eagle medium (DMEM) supplemented with 10% FBS and 100 units/mL penicillin, 100 mg/mL streptomycin in an incubator at 37°C and 5% CO2. Cells cultured until 80% of confluence were removed with trypsine (Dutscher, L0615-500) and used for experimentation. The cells were used at passages 10-28.

1.5. Murin myoblast cells C2C12

C2C12 is a murrin myoblast cell line that is a subclone (produced by H. Blau, *et al*) of the mouse myoblast cell line established by D. Yaffe and O. Saxel) that were purchased from ATCC (CRL-1772). They were used at passages 8-25. The cells were cultured in high glucose DMEM and supplemented with 20% and 100 units/mL of penicillin, 100 mg/mL streptomycin in an incubator at 37°C and 5% CO_2. Cells cultured until 70% of confluence were removed with trypsin (Dutscher, L0615-500) and used for experimentation.

1.6. Human myoblasts cells

Human myoblasts were used at passages 8-25. The cells were cultured in high glucose DMEM and supplemented with 20% and 100 units/mL of penicillin, 100 mg/mL streptomycin in an incubator at 37°C and 5% CO2. Cells cultured until 60% of

confluence were removed with trypsin (Dutscher, L0615-500) combined with scraping with a cell scrapper and used for experimentation.

2. Bioink

2.1. Bioink composition

The first bioink used in this work, that we named CollHama is composed of 0.2% collagen methacrylate (CollMA) and 1% hyaluronic acid methacrylate (HAMA). Due to its low polymer concentration, the shear stress of this ink during printing is low, but its mechanical strength is also low. In this work we named it CollHama.

The second bioink used in this study is named CollHaGel and is composed of 0.2% collagen methacrylate and 1% hyaluronic acid methacrylate with 5% gelatin. This bio-ink is composed of products of natural origin with sacrificial gelatin serving as an additional support. Gelatin increases viscosity of the ink during printing and promotes crosslinking depending on temperature. Gelatin allows the first of two reticulations with a first induced by cold and the second by UV cross-linking. The gelatin is then removed by successive rinsing with culture medium at 37°C. The shearing stress of this ink is slightly higher than the CollHama ink but thanks to its double reticulation, its mechanical strength, during printing is better. In fact, the first reticulation by temperature is instantaneous, which makes it possible to have mechanical strength as soon as printing. Gelatin was included in the formulation as a bioprinting adjuvant, as it added a structural and reticulation component during printing. After printing, and following UV reticulation, the gelatin was removed with successive baths of heated cell medium (37°C), which allows to leach the gelatin without losing cells or structural integrity, as previously shown by *L. Ouyang et al* (Ouyang *et al.*, 2020) (Figure 18). Indeed, in their work Ouyang *et al* used gelatin to induce a first gelation of the ink by cooling the printing bed followed by a UV crosslinking and finally a leaching of the gelatin with successive medium baths. It is also possible that the gelatin "leaching" makes the structures more porous thus increasing the exchanges between the structure and the culture medium.

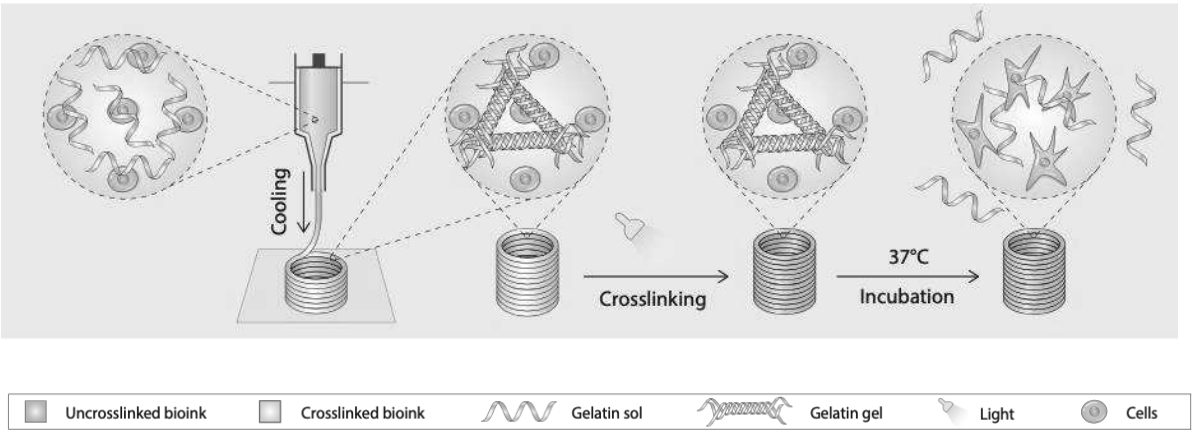

Figure 18 Gelatin as mechanical support for bioprinting before leaching

Adapted from Ouyang *et al* (Ouyang *et al.*, 2020)

For these two inks, we chose to work with hyaluronic acid, already widely used in bioprinting (Clark *et al*; 2019). This allows to have a structuring of the imprint but used alone has a low attraction for cells and allows low proliferation. Therefore, we added collagen here, which unlike hyaluronic acid does not allow structuring but promotes cell proliferation and viability.

2.2. Bioink production

The first hydrogel CollHama, was prepared by diluting 2% (w/v) HAMA in cell medium and mixing with 0.6% (w/v) stock CollMa. The solution was then neutralized with NaOH 0.1M and the photoinitiator, lithium phenyl-2,4,6-trimethylbenzoylphosphinate (LAP), was added for a final concentration of 0.1% (w/v) (Fairbanks *et al.*, 2009). The volume was adjusted with cell medium (Oliveira *et al.*, 2021).

The second hydrogel, was prepared by mixing a 10% (w/v) gelatin solution, 4% (w/v) HAMA solution, 0.6% (w/v) neutralized CollMa solution and the photoinitiator LAP (final 0.1% (w/v)) to the aforementioned final concentrations, and by adjusting the final volume using cell medium.

2.3. Reticulation

In this work, we chose UV light as the main reticulation method for all our bioinks. We worked with UV light of 365 nm and tested the viability of our cells in each case. As a

second reticulation method, we chose temperature reticulations for the CollHamaGel bioink.

3. Printing parameters

The printing parameters are the settings used to properly produce complex 3D structures. They depend on the bioprinter used and the bioink printed. Only a very specific range of parameters will result in viable bioprinted structures.

In this work, we used two different bioprinters: The BioBot Basic (from Advanced solution) which is an extrusion printer with polar coordinates. This printer can print up to 5 different materials at the same time and is controlled either directly with G-Code or by the company's software with STL (Standard Triangle Language) models.

We also used the BioX (from CellInk) which is also an extrusion and droplet printer (using for both cases extrusion heads). This printer can print up to 3 materials with 3 printing heads that can be modified for other applications (UV reticulation, camera, plastic 3D printing etc.)

We looked at five important printing parameters which should be adjusted before each new printing experiment, namely the speed, the pressure, the cartridge temperature, the bed temperature and the printing design.

3.1. The printing speed

The printing speed is a very important parameter because it will determine the printing time and, with the printing pressure, the size and shape of the printed filaments. The speed and the pressure have an intimate relationship. Indeed, a simple test can determine the best printing speed for a given printing pressure. By printing the same shape with the same pressure and changing the printing speed in a certain range (± 5 mm/s), it is possible to find the best printing speed.

For both BioBot and BioX bioprinters, and for both CollHama CollHamaGel bioinks, the printing ranged from 10 to 12mm/s.

3.2. The printing pressure

The printing pressure can be considered as the most important parameter for the viability of the printed cells. Indeed, the higher the printing pressure, the faster the bioink will be extruded and the higher the shear stress. With a higher shear stress, the viability rate of cells is impacted and decreased(Boularaoui, 2020). It is therefore very important to find the right balance between pressure, viability and time of printing.

For the BioBot printer with the CollHama bioink and CollHamaGel bioink the printing speed ranged from 0.7 to 2.5kPa. For the BioX printer with the CollHama bioink and CollHamaGel bioink the printing speed ranged from 70 to 103kPa.

3.3. The cartridge temperature

The cartridge temperature is the internal temperature of the bioink and the printhead. Most hydrogels used in bioprinting have an inversed relation between viscosity and temperature. Indeed, in most cases the higher the temperature, the lower the viscosity. Thus heating the bioink right before printing decreases the shear stress and allows to maintain cells in good temperature conditions.

The Biotbot does not have a temperature controlled cartridge. Therefore, before each printing the syringes were heated at 37°C for 15 minutes and used for a maximum of 10 minutes. With the BioX the cartridges were heated at 30°C for all bioinks.

3.4. The bed temperature

Some printers have a controllable bed temperature, either for crosslinking or keepings cells at the right temperature.

For the BioX we choose to work with a bed at 10°C to reticulate the gelatin contained in the CollHamaGel bioink. In other cases, we kept the bed at room temperature (23-25°C). This setup was not performed with the Biobot since it does not have the bed temperature control option.

3.5. Printing design

For the print design, a computer-aided design (CAD) software was used to produce STL files who are 3D models that are going to be printed. They are made from scratch or modified by the users. Most recent bioprints, such as the BioX have a user friendly

software to help produce of modify STL files. Otherwise CAD software such as Blender, Scli3r, Creo or FreeCAD can be used to produce the STL files (Junk and Kuen, 2016). For the BioBot we chose to work either with Scli3r or a homemade slicer, to transform our files are transformed into G-code, the code used to control the printer. A slicer will "slice" the 3D file to create the coordinates of the printed construct and send it to the printer. It is also possible to write the G-code from scratch to control precisely what will be printed, how and when. But this is a very tedious are difficult (at least I thought so when doing it) process, prone to errors.

4. PLGA microscaffolds

In this thesis, we studied and produced microscaffolds of PLGA 50/50 (P2191), PLGA 75/25 and Resomer® 50/50. Resomer has exactly the same composition as PLGA 50/50 but with a different production method. All PLGA and Resomer were purchased from Sigma and are acid terminated. All the microscaffolds produced had a goal size of 80µm ± 20µm.

4.1. Microscaffolds production

For the PLGA 50/50 production the protocol used is the following. First, a 2% (w/v) PLGA solution in DCM was produced. For this, PVA was dissolved in distilled water to form a 0.3% (w/v) solution. A 10% (w/v) gelatin solution was then produced by dissolving gelatin with the newly formed PVA solution. The first emulsion was created by mixing the PLGA solution with a 10% (v/v) of the solution of gelatin/PVA for 3 minutes at 3000 rotations per minute (rpm). This formulation was then poured into an ice-cold solution of excess of PVA 0.3% (w/v) (hardening bath) to form the second emulsion. The suspension of microscaffolds was then steered at 200 rpm overnight to allow DCM evaporation. The next morning, the suspension was heated to 50°C for 30 minutes and then washed with deionized water (DW) to remove all gelatin from the microscaffolds. The formed microscaffolds were then washed with DW and lyophilized for 24 hours.

After lyophilization, the particles were etched in a solution of 70% (v/v) EtOH and 30% (v/v) 0.25 M NaOH. The absolute ethanol solution partially dissolved PLGA to increase the porosity of the microscaffolds and the NaOH improved the wettability (Qutachi *et*

al., 2014). The microscaffolds were agitated for 3 minutes in the etching solution before being washed three times with distilled water.

The protocol production for microscaffolds of Resomer PLGA 50/50 is identical in every point.

The production of microscaffolds of PLGA 75/25 has never been as successful in terms of size and porosity as with PLGA 50/50. We were able to produce microscaffolds of the right size but the size distribution of the microscaffolds was too large compared to PLGA 50/50. The intersect properties of PLGA 75/25 are very interesting but not necessary for the work of this thesis. Indeed, the degradation rate of PLGA 50/50 and 75/25 are different, thus the ratio can be used to slow or accelerate the degradation of the produced microscaffolds.

We quantified the size of the scaffolds and porosity by SEM imaging using a FEI Quanta FEG 250 microscope (FEI Company, Eindhoven, The Netherlands) with an accelerating voltage of 2 kV or optical imaging (with the Keyance) after each production.

4.2. Degradation of microscaffolds

The degradation of PLGA microscaffolds depends on the molecular ratio, the size of the microscaffolds used, their porosity and the acidity of the medium. According to the literature and information of the PLGA and Resomer used in this work, the degradation time is expected to be more than 3 months, longer than all our experiments. To check that our microscaffolds do not degrade during our experiments, we immerged microscaffolds in cell medium and checked the pH every week during four weeks. After this time, we found no change in pH. Since if the degradation had been degraded, the pH of the medium would have decreased, this means that our microscaffolds were not significantly degraded after one month of immersion. However, the pH constancy we observed does not mean that the surface of our microscaffolds is not degraded.

4.3. Coatings

Coatings have been developed to improve the attraction of PLGA microscaffolds to cells. Three coatings were tested and used in this work.

The first coating is a coating of collagen type 1-4 from rat's tail. The protocol used is the following. First, PLGA microscaffolds were filtered with a 140 µm nylon filter (Sigma) and then immersed in 6% (v/v) hexanediamine in 1-propanol, with agitation for 10 minutes. The PLGA microscaffolds were then washed with DW three times and immersed in a 1% (v/v) glutaraldehyde solution for 4 hours. At the same time, a 0.5% (w/v) solution of collagen in 3% (v/v) acetic acid was prepared. The microscaffolds were then again washed three times with DW and immersed into the collagen solution for 24 hours at 4°C (Dhamecha *et al.*, 2020).

The second coating is a PLL coating. The PLGA microscaffolds were filtered using a 140 µm nylon mesh (Sigma) and immersed in a 0.25 M NaOH solution at room temperature for 30 minutes under agitation. PLGA microscaffolds were then washed three times with DW and immersed for 24 hours in a 1 mg/mL PLL solution with 0.25mM NaCL at 4°C overnight.

The third coating is a coating of ε-PL. This coating was performed in the same conditions as in PLL coating, but instead of 1 mg/mL PLL solution we used 1 mg/mL ε-PL.

4.4. Cell agitation culture

Cells were put in contact with the microscaffolds before printing in bioreactors with a gentle agitation of 50 rpm during 3 hours in incubators at 37 °C and 5% CO2. After 3 hours, the agitation was stopped and the bioreactors left in the incubator for 48 hours or 72 hours depending on the cell type studied. The cellularized microscaffolds were then added to the bioink and printed. Cells alone were also cultured into bioreactors in the same conditions to compare the effect of microscaffolds.

4.5. Antimicrobial microscaffolds

Nanoparticle formulation was based on the protocols of Yang *et al* (Yang *et al.*, 2017). Briefly, 50mg of PLGA was dissolved in 3mL of dichloromethane (DCM). 10 mL of 2% polyvinyl-alcohol (PVA) in water was added and the sample was sonicated at puissance 8 (arbitrary measure), 20% active cycles for 5 minutes to create an emulsion. This emulsion was stirred at 1000 rpm overnight to evaporate DCM. Suspension was centrifuge at 13 200 rpm and wash three times with miliQ water at 37°C. The formed nanoparticles were then coated with the antimicrobial ε-PL.

The ε-PL coating is identical to the PLL coating described earlier.

Specific methods can be found in their relative works and chapters.

Chapter 3: Extrusion bioprinting with porous PLGA microscaffolds

1. Introduction

In 2002, Landers *et al* adapted the new rapid prototyping technology, a continuous 3D dispensing of liquids and pastes, to print for the first time hydrogel (Landers *et al.*, 2002). This lead to extrusion bioprinting and was commercialized as “3D-Bioplotter. Over the 20 years since these results, extrusion bioprinting was developed and incorporated living cells inside the hydrogels and became the most used bioprinting technology used today. The technology is still based on the same principle. A force will “push” a bioink containing living cells to form a 3D structure. Compared to other bioprinting technologies such as inkjet, laser based bioprinting and stereo lithography, extrusion bioprinting is easy to use, can print high viscosity bioinks and important cell densities (>10^8cells by militer and cell aggregates) (Heinrich *et al.*, 2019).

However, while being the most common bioprinting technology it has its limitations. Indeed, while it is possible to print with the highest cell densities compared to other bioprinting technologies, obtaining the same cell density than *in vivo* organs remains an unresolved challenge (McClelland *et al.*, 2012). Furthermore, due to the shear stress applied during the extrusion phase, an increased in cell damage and a decrease in cell viability is induced (Mandrycky *et al.*, 2016).

To remedy to these two problems, we developed porous biodegradable PLGA microscaffolds. They act as microcarriers before bioprinting to increase the proliferation surface of the cells, thus, increasing the cell proliferation. During the extrusion process, the microscaffolds protect the cell from the shear stress. In our work we developed a new protocol of production of porous microscaffolds and studied the effects of our microscaffolds on cell proliferation and cell viability before and after bioprinting. We also studied the action of the microscaffolds on more complex cellular structures by monitoring the cell migration.

Briefly, our results showed an increase in cellular metabolic activity before printing when cells are cultured with our microscaffolds. We also demonstrate an increase in cell viability (up to 10%) when bioprinting our cells with coated microscaffolds. Finally, we demonstrated an increase in cell migration when bioprinting complex multi-cellular structures with our microscaffolds compared to cells alone. These results are presented in the following article, published in Bioprinting. In addition, complementary results to those presented in this article are presented in the “Supplementary section”.

2. Article: “Enhancing cell survival in 3D printing of organoids using innovative bioinks loaded with pre-cellularized porous microscaffolds”

Bioprinting 28 (2022) e00247

Contents lists available at ScienceDirect

Bioprinting

journal homepage: www.sciencedirect.com/journal/bioprinting

Enhancing cell survival in 3D printing of organoids using innovative bioinks loaded with pre-cellularized porous microscaffolds

Adrien Rousselle [a,b], Arielle Ferrandon [a,b], Eric Mathieu [a,b], Julien Godet [c], Vincent Ball [a,b], Leo Comperat [d,e], Hugo Oliveira [d,e], Philippe Lavalle [a,b], Dominique Vautier [a,b,*,1], Youri Arntz [a,b,1]

[a] Inserm UMR_S1121, Centre de Recherche en Biomédecine de Strasbourg, 67000, Strasbourg, France
[b] Université de Strasbourg, Faculté de Chirurgie Dentaire, 67000, Strasbourg, France
[c] Public Health Department, Strasbourg University Hospital, Strasbourg, France
[d] University of Bordeaux, Tissue Bioengineering, U1026, F-33076, Bordeaux, France
[e] Inserm U1026, Tissue Bioengineering, ART BioPrint, F-33076, Bordeaux, France

ARTICLE INFO

Keywords:
Microscaffolds
Bioink
Bioprinting
Organoids
DPSCs
HCS-2/8

ABSTRACT

Extrusion bioprinting is a relevant 3D technology to create biological systems in regenerative medicine, pharmaceutical development and cancer research. Bioink is the necessary component to incorporate the cells that will be printed by extrusion bioprinting. However, bioinks and extrusion printing can generate shear stresses mechanically unfavorable for cell survival. We thus developed a bioink, based on methacrylated collagen and hyaluronic acid, in combination with porous poly(D,L-lactic-co-glycolic acid) solid microscaffolds to protect cells against mechanical stress during extrusion printing. We found that porosities of the microscaffolds allowed human chondosarcoma cells to colonize the structure. Moreover, metabolic activity of these chondrosarcoma cells, fibroblast cells, and dental pulp stem cells (DPSCs) incorporated within bioink (before printing) increased 4-fold in presence of a polylysine- or collagen-coated microscaffolds compared with those cultured without microscaffolds. Their survival increased by 10% either by hand deposition or by bioprinting extrusion (bioprinter BioBot®Basic) compared to cells in bioink without microscaffolds. In addition to the mechanoshield properties provided by microscaffolds, they allow the migration of DPSCs stem cells towards HCS-2/8 cancer cells after 7 days of co-culture in an organoid created by bioprinting extrusion while without microscaffolds the cells aggregated and remained static.

1. Introduction

Three-dimensional (3D) bioprinting is an emergent technology to elaborate complex biological systems in regenerative medicine [1], tissue engineering [2], pharmaceutical development [3,4] and cancer research [5]. This relies on the ability of bioprinting to attain complex constructs that are similar in organization and functionality to native tissues. Particularly, the goal of bioprinting technology is to better control the precise positioning of living cells, within a biopolymer-based matrix and in a layer-by-layer structuration, allowing to adjust the geometry and maturation of the tissue over time. Different technologies of bioprinting are available, such as inkjet, laser-assisted and extrusion bioprinting [6].

Ink is the necessary component to associate with living cells to create the bioink that will be printed by extrusion bioprinting [7]. However, bioinks used for extrusion bioprinting are most frequently composed by non self-supporting soft hydrogels, that tend to collapse [8] and thus unfavorable to support in cell adhesion and maturation processes. In addition, extrusion methods use constant pneumatic pressure to distribute the bioink from the printing nozzle as a continuous filament [9] generating shear stresses, that may lead to cell membrane damage and ultimately cell death [10,11]. Previous work showed that the most significant cellular damage due to shear stress occurs within 6 h of printing [12].

To solve these difficulties, our goal is to design a bioink that offers support for cell adhesion and cell protection against mechanical stress

* Corresponding author. Inserm UMR_S1121, Centre de Recherche en Biomédecine de Strasbourg, 67000, Strasbourg, France.
E-mail address: vautier@unistra.fr (D. Vautier).
[1] VD and YA contributed equally to this work.

https://doi.org/10.1016/j.bprint.2022.e00247
Received 29 June 2022; Received in revised form 15 September 2022; Accepted 30 September 2022
Available online 12 October 2022

during extrusion bioprinting. Here, we develop a bio-ink in combination with solid microscaffolds. This bioink based on methacrylated collagen and hyaluronic acid without microscaffolds has been previously used in Oliveira et al., 2021 to successfully print dorsal root ganglia sensory neurons [13].

Hydrogel bioinks can be engineered to incorporate solid microscaffolds, such as fiber-like structures with microscale porosity, facilitating cell function and movement [14,15]. Furthermore, it was shown that ability for cellular infiltration and speed migration depend on the physical properties and microstructure of the hydrogel [16]. Tor and co-worker recently showed that cell-laden microspheres incorporated in bioink hand deposited increased its compressive strength compared to that without microsphere [17]. However, cell-laden microscaffolds incorporated in bioink have not yet been used to construct multi-cellular complexes and controlled bioprinted architecture, precisely the aim of this work.

The choice of the constituents of the bioink is essential for their physical properties [18]. They must support bioink printability [19], enable gelation (physical or chemical) and be biodegradable [20]. According to these criteria, type I collagen and hyaluronic acid, natural components of the extracellular matrix, are used in the composition of our bioinks [21]. We used photo initiated radical polymerization of (meth)acrylate groups grafted on hyaluronic acid or type 1 collagen, a very appropriate method for controlled cross-linking in time and space.

In this work, we developed a method to produce porous PLGA (poly (D,L-lactic-co-glycolic acid) microscaffolds with a simple double emulsion. Microscaffolds were coated with PLL (poly-L-lysine) or collagen I to enhance cell adhesion on their surface. Thus, these microscaffolds could act as micro-carriers, allowing their pre-cellularization in 3D microenvironment to allow cell proliferation before printing and to improve cell viability during the printing process and during the maturation steps.

We first determined whether microscaffolds could protect human chondrosarcoma cells (HCS-2/8 cells), mouse fibroblast cells (NIH 3T3 cells) or human dental pulp stem cells (DPSCs) incorporated in the bioink, hand deposited or bioprinted by extrusion. Secondly, we created an organoid composed of a co-culture system based on HCS-2/8 cells and DPSCs-laden microscaffolds incorporated in bioink. 3D structures were printed by extrusion and the two cellular models contained in microcarriers were co-cultured for 7 days. Then, we determined whether DPSCs and HCS-2/8 cells were able to physically interact in these organoids.

2. Materials and methods

2.1. PLGA microscaffolds synthesis

Poly (D,L-lactide-co-glycolide) PLGA (lactide-glycolide ratio of 50-50, ref P2191), Mowiol®, PVA (Polyvinyl alcohol, ref 81383), DCM (Dichloromethane, ref 270997) Bovine skin gelatin (ref G9391) were purchased from Sigma Aldrich. The porous PLGA microscaffolds were prepared following a double emulsion technique using gelatin as porogen [22]. Briefly, 0.2 g of PLGA were dissolved in 10 mL of DCM to form a 2% (w/v) PLGA solution. PVA was dissolved in distilled water to form a 0.3% (w/v) solution. A 10% (w/v) gelatin solution was then produced by dissolving the gelatin with the newly formed PVA solution. The first emulsion was created by mixing the PLGA solution with 1 mL of a solution of 10% gelatin/PVA for 3 min at 3000 rpm. This formulation was then poured into an ice-cold solution of 120 mL of PVA 0.3% (w/v) (hardening bath) to form the second emulsion. The suspension of microscaffolds was then steered overnight to allow DCM evaporation. The next morning, the suspension was heated to 50° for 30 min and then washed with DW to leach all the gelatin from the microscaffolds. The formed microscaffolds were then washed with DW and lyophilized for 24 h.

2.2. Surface treatment and coating of microscaffolds

The newly formed microscaffolds were first treated with an etching solution [23]. This solution was composed of 70% (v/v) absolute ethanol and 30% (v/v) of 0.25 M NaOH. The absolute ethanol solution partially dissolved PLGA to augment the porosity of the microscaffolds and the NaOH improved the wettability [23]. The microscaffolds were then immersed into excess etching solution, under agitation at 300 rpm for 3 min, before being washed three times with distilled water. Additional surface coatings were also tested, namely: collagen (type 1 collagen from rat tail tendon (ref 11179179001) purchased from Sigma Aldrich) and PLL (PLKB250, MW 52000, Alamanda polymers).

For collagen coating, PLGA microscaffolds were filtered with a 140 µm nylon filter (Sigma) and then immersed in 6% (v/v) hexanediamine in 1-propanol, with weak agitation for 10 min. The PLGA microscaffolds were then washed with DW three times and immersed in a 1% (w/v) glutaraldehyde solution for 4 h. At the same time a solution of collagen 0.5% (w/v) in 3% (v/v) acetic acid was prepared. The microscaffolds were then again washed three times with DW and immersed into the collagen solution for 24 h at 4 °C [24].

For PLL coating, the PLGA microscaffolds were filtered using a 140 µm nylon mesh (Sigma) and immersed in a 0.25 M NaOH solution at room temperature for 30 min under agitation. PLGA microscaffolds were then washed three times with DW and immersed for 24 h in a 1 mg/mL PLL solution at 4 °C overnight. After etching and/or coating, the microscaffolds were washed with DW and lyophilized for further uses and stocked at 4 °C.

2.3. Cell preparation and culture

DPSCs (human dental pulps stem cells) were isolated in accordance with French legislation (informed patient consents, Institutional Review Board approval of the protocol used: C17-78, DC-2018-3353). DPSCs were extracted from human teeth in the dental clinic of the "Hopital Civil" of Strasbourg (for phenotypic characterization see Ref. [25]). They were used at passages 2–6. The cells were cultured in MEM Alpha Gibco supplemented with 10% FBS (Fetal bovine serum, Dutscher S1810-50) and 100 units/mL penicillin, 100 mg/mL streptomycin (Dutscher, L0022-100) in an incubator at 37 °C and 5% CO2. Cells were cultured until 90% of confluence was obtained and were detached with trypsine (Dutscher, L0615-500) and either used for experimentation or subcultured with a ratio of 5×10^4 cells per 75 cm^2 flask. DPSCs in passage number 3 to 6 were used for all the experiments with similar results.

HCS-2/8 cells are a clonal cell line with cartilage phenotype established from a human chondrosarcoma from Takigawa et al. [26]. They were used at passages 10–28. Cells were cultured in Alpha MEM Eagle supplemented with 20% (v/v) FBS and 100 units/mL penicillin, 100 mg/mL streptomycin in an incubator at 37 °C and 5% CO2. Cells cultured until 90% of confluence were detached with trypsine (Dutscher, L0615-500) and used for experimentation.

NIH 3T3 (Fibroblast cells originated from fetal Mouse Swiss NIH) were purchased from ATCC (CRL-1658TM). The cells were cultured in DMEM high glucose supplemented with 10% (v/v) FBS and 100 units/mL penicillin, 100 mg/mL streptomycin in an incubator at 37 °C and 5% CO2. Cells cultured until 80% of confluence were detached with trypsine (Dutscher, L0615-500) and used for experimentation. The cells were used between passages 10–28.

2.4. SEM characterization

The size and porosity of PLGA particles was evaluated using SEM (Scanning Electron Microscopy). Briefly, samples were dropped off on stubs with carbon discs (Oxford Instruments, Gometz la Ville, France) and sputter coated with gold palladium using a HUMMER JR sputter coater device (Technics, Union City, CA, USA). SEM was performed

using a FEI Quanta FEG 250 microscope (FEI Company, Eindhoven, The Netherlands) with an accelerating voltage of 2 kV. A sample of at least 300 different microscaffolds was selected randomly for each specimen. The measurements were done directly with the SEM's software. The statistical analysis was done using Sigma plot software.

2.5. Cell expansion using microscaffolds

Before printing, the cells were cultured into bioreactors with or without microscaffolds to augment the number of cells available for the printing process. Microscaffolds of PLGA uncoated and coated were used at a concentration of 10 mg of microscaffolds for 1 mL of cell medium, with an addition of 5×10^5, 5×10^5 and 2.5×10^5 cells/mL for respectively HCS-2/8, NIH 3T3 and DPSCs. The cell culture was done in sterile 50 mL bioreactor tubes (Tubespin® Bioreaktor 50). The protocol for the 3D culture of cells with microscaffolds was adapted from D. Smith [27]. To insure the adhesion of cells on our microscaffolds the manipulation was done as follows: Cells were detached from the cell culture flask with a trypsin treatment, re-suspended into cell medium and counted with a Neubauer chamber to be seeded at the concentrations mentioned above according to the cell model used. The UV lamp used was a BioGlow® lamp of 6 W used at 3 cm of the particles and with a wavelength of 365 nm. The cells were then seeded into the bioreactors with or without the sterile microscaffolds. To ensure the contact between cells and microscaffolds, a gentle agitation of 50 rpm during 3 h was performed in the incubators (37 °C and 5% CO_2). After 3 h, the agitation was stopped and the bioreactors left in the incubator for 48 h.

2.6. Bioinks preparation

Methacrylated type I collagen (CollMA) and methacrylated hyaluronic acid (HAMA) were produced as previously described [13]. Briefly, type I collagen from bovine skin (6 mg/mL, Sigma-Aldrich) was adjusted to pH 10 using 2 N NaOH. Methacrylic anhydride, molar ratio of 5:1 (with respect to number of lysine amine groups in collagen), was added drop-wise and left to react for 4 h. Then the solution was extensively dialyzed (12–14 kDa, Sigma-Aldrich) against mQ water and then freeze-dried. CollMA stock solution was prepared at 6 mg/mL in 0.02 M acetic acid and stored at 4 °C until further use. Methacrylation degree was determined using the TNBS (Tri-nitro benzene sulfonic acid) assay. For the methacrylation of hyaluronic acid, 1 g of hyaluronic acid (Streptococcus Equi - 1.5–1.8 $\times$ 10 E^6 Da, Sigma-Aldrich, France) was dissolved in 75 mL of mQ grade water. Then, 50 mL of dimethylformamide (Sigma-Aldrich, France) were added and the pH adjusted to 8 using NaOH 1 M. Next, 1.12 mL of methacrylic anhydride (Sigma-Aldrich) was added to the solution, the pH adjusted to 8 and the solution was left under constant stirring overnight at room temperature. 50 mL of NaCl 5 M was added and the volume of the solution was adjusted to 500 mL with mQ grade water. Following extensive dialysis (12–14 kDa, Sigma-Aldrich) the obtained solution was freeze-dried and the polymer recovered. HAMA stock solution was prepared by dissolving the polymer at 2% (w/v) in DMEM HG (Gibco) and stored at 4 °C until further use. Methacrylation degree was determined using nuclear magnetic resonance (NMR).

The first hydrogel used in this study, named CollHama, was a composite of Hyaluronic acid methacrylate (HAMA) 1% (w/v) and collagen methacrylate (CollMA) 0.2% (w/v), prepared by diluting HAMA 2% (w/v) in cell medium and mixing with 0.6% (w/v) stock CollMa. The solution was then neutralized with NaOH 0.1 M and the photoinitiator, lithium phenyl-2,4,6-trimethylbenzoylphosphinate (LAP), was added for a final concentration of 0.1% (w/v) [28]. The volume was adjusted with cell medium [13].

The second hydrogel, named CollHAMAGel, was composed of: CollMA 0.2% (w/v), HAMA 2% (w/v) and Gelatin 5% (w/v). This hydrogel was prepared by mixing a 10% (w/v) gelatin solution, a 4% (w/v) HAMA solution, a 0.6% (w/v) neutralized CollMa solution and the photoinitiator LAP (final 0.1% (w/v)) to the aforementioned final concentrations, and by adjusting the final volume using cell medium. Gelatin was included in the formulation as a bioprinting adjuvant, as it added a structural component during printing. After printing, and following UV reticulation, the gelatin was removed with successive baths of heated cell medium (37 °C), enabling to leach the gelatin without losing cells or structural integrity, as previously shown by L. Ouyang et al. 2020 [29]. For sake of clarity, and following widely accepted nomenclature, hydrogels without cells are designated as biomaterial inks, and the ones including live cells are designated as bioinks. To form the bioinks, the bioreactors used to culture the cells with or without micro-microscaffolds were centrifuged and the supernatant was gently removed. The hydrogels were added to the cellularized micro-scaffold homogenized and printed right after.

2.7. Rheological characterization

The viscoelastic properties of the developed biomaterial inks were examined using a Kinexus Ultra rheometer (Malvern, Great Britain), using a cone and plate geometry. A frequency sweep and time sweep analyses were performed at 25 °C to provide the frequency-dependent and time-dependent storage (G') and loss (G") modulus. The frequency range was set from 0.01 Hz to 20 Hz. For the time sweep analysis, the frequency was set at 1 Hz with a runtime of 30 min, with a measure each 15 s. For both analysis, a constant shear strain of 0.1% was applied. We found that the storage modulus at 10 htz of the hydrogel CollHAMAGel increase 4 times after 3 min ink reticulation (by UV irradiation, SI Table 1). These results are in accordance with those previously described by Oliveira et al. [13].

2.8. Cell metabolic activity evaluation

The metabolic activity of the different cell types was measured when cells were cultured in cell medium with or without the microscaffolds. This metabolic activity was evaluated using a resazurin-based solution [30]. Briefly, the cells are seeded at the density corresponding to those initially used for the 2D culture: 5×10^5 cells/mL for HCS-2/8 and NIH 3T3, and 2.5×10^5 cells/mL for the DPSCs with the appropriate culture medium. 4 conditions were tested for each cell type: cells alone (abbreviated cell), cells with PLGA microscaffolds (abbreviated PLGA), cells with PLGA PLL-coated microscaffolds (abbreviated PLGA-PLL) and cells with PLGA collagen-coated microscaffolds (abbreviated PLGA-Coll), at a concentration of 10 mg/mL of microscaffolds. 6 mL of cell medium with resazurin (10% (v/v)) was added to each well and the bioreactors were incubated at 37 °C for 2 h. Subsequently, 300 µL of supernatant was transferred to dark 96 wells and fluorescence was measured (excitation 640 nm, emission 690 nm, SAFAS, Xenius XC, Safas Monaco). Such measurements were done at T0h, T48h, and T72h. The metabolic activity was calculated with the difference between the measurement and a blank composed of cell medium with 10% resazurin.

2.9. Apoptotic, necrotic, viable cells assay

Cell viability percentage, after printing, was determined using the PromoKine Apoptotic/Necrotic/Healthy Cells Detection Kit. Briefly, Cells were wased twice with 1X binding buffer. Samples were incubated with the staining solution (5 µl of FITC-Annexin V: green for apoptotic cells, 5 µl of Ethidium Homodimer III: red for dead cells and 5 µl of Hoechst 33342: blue for viable cells to 100 µl 1X binding buffer) for 15 min at room temperature, protected from light. Cells were then washed with 1X binding buffer 1–2 times. Cells were covered with 1X binding buffer and observe fluorescence using FITC, Texas Red and DAPI filter sets. Stained cells were then analyzed using a Zeiss LSM 510 confocal microscope equipped with a x20/0.40na objective. Five images by sample were taken. Using the software ImageJ 1.53c (http://rsb.info.nih.gov/ij/), the images were analyzed to determine the percentage of

viable cells compared to apoptotic or necrotic cells. To do so, the total number of blue cells (live) per image were counted, compared to green and red cells (apoptotic and necrotic cells).

2.10. Hand deposition by mean of micropipette

The aim of this step was to select the best culture conditions prior to the use of the extrusion bioprinter. Four conditions of cell culture were tested. The first condition considered the cells cultured alone; the second condition was cell culture with PLGA porous microscaffolds; the third condition with PLGA microscaffolds coated with PLL; and the last condition with PLGA microscaffolds coated with collagen.

2.11. Extrusion bioprinting

The 3D printer used for this study was a pneumatic extrusion based 3D bioprinter BioBot®Basic (Advanced Solutions, Louisville, USA). The bioinks were loaded into a 10 cc syringe (Advanced Solutions), and 18G (0.8 mm diameter) conical tips (FTM Technologies, Nanterre, France) were used during the printing process. The geometry and the printing path was created either using TSIM (Tissue Structure Information Modeling, Advanced Solutions), or by directly sending the G-Code into the 3D Printer by the means of the Pronterface software (open-source software, licensed under the GNU General Public License, version 3). The G-Code was either hand-written, or generated using a custom Slicer developed in collaboration with the Télécom Physique Strasbourg (TPS) school of Strasbourg, France. The aim of this software was to generate the most biologically compatible trajectories in terms of pressure use, *i.e.* the most continuous printing possible for a type of ink with the least number of pressurizations possible to minimize the shear stress applied to cells. The printing parameters were set within a range of 0.9–1.2 psi, with a displacement speed of 250–300 mm/min. After printing, the printed structures were cross-linked using 365 nm UV light with an intensity of 6 W, for a duration of 2 or 3 min. The only bioink used in this section was based on the biomaterial ink CollGelHama. After reticulation, the constructs were washed 3 times with cell medium at 37 °C as to leach out all the gelatin from the construct.

2.12. 3D co-culture organoid printing

HCS-2/8 cells and DPSCs cells were used for the co-culture printing experiments and cultured with Alpha MEM Eagle cell culture supplemented with 20% (v/v) FBS and 1% Pen/Strep. Both cell types were fluorescently labeled before the agitation culture. DPSCs and HCS-2/8 cells were labeled using the PKH26 green fluorescent cell linker and PKH26 red fluorescent cell linker (Sigma, St. Louis, MO), respectively, according to the manufacturer's instructions and observed by Confocal laser scanning microscopy (CLSM) with a Zeiss LSM 710 microscope, using a x 20/0.40 Neofluar Zeiss objective.

Cells were prepared separately, in two different bioreactors and printed with two different syringes. For each cell type, two conditions were tested: firstly, cells were seeded and cultured on PLGA collagen-coated microscaffolds, secondly, as a control, cells were cultured alone in bioreactors. The printing models were prepared before the printing process with the printing conditions adjusted during the process if needed (printing pressure and printing height). The printed structure is shaped like a spiral. It was constituted of an outer layer of stem cells (DPSCs) and a central region of cancerous cells (HSC-2/8 cells). The geometry used to study the interaction between cancer cells and stem cells consisted on a closed cylinder, formed by three layers. The first layer encapsulated stem cells, the second layer considered a central region with cancer cells and an external region with stem cells, and finally the third layer integrated stem cells. With this composition of cancerous and stem cells, we could qualify this structure as an organoid. The development of the spiral structure architecture was performed using Pluronic® F-127 [31,32] as a model ink to optimize the G code with the parameters previously mentioned. The repeatability of the printed products of the BioBot printer was tested with the Pluronic® F127. All printings of the co-cultures were performed using directly G-Code sent to the BioBot with the help of the Pronterface software.

After printing, the printed structures were cross-linked using 365 nm UV light, for a duration of 2 or 3 min. The bioink used for co-cultures was CollHAMAGel. As before, after reticulation, the constructs were rinsed 3 times with cell medium at 37 °C.

Cell migration and development, at 1 day to 7 days after printing, the co-culture samples (organoid), were analyzed using confocal microscopy. Since the printed cells were labeled with two different markers, it was possible to track their location in the construct. Using a confocal microscope, Z-stacks of the organoid were obtained. A Z-stack is a set of confocal images taken where the x- and y-axes remain the same but the distance to the objective (z-axis) is different for each image. When imaging the organoid of DPSCs and HCS 2/8, we positioned ourselves between the first and second layer of the construct.

2.13. 3D image construction with imaris

Z-stacks images of the printed organoids were treated and analyzed with the Imaris software. A surface was created on each cell to determine its position. Each cell position was then calculated with the software to measure the cell migration in time.

2.14. Statistical analysis

The number of living cells, quantified as the fraction of living cells over the total number of cells, was modelled using a Poisson regression for count data with offset to compare model rates instead of counts. The use of offsets was justified because initial populations (total number of cells) were different across conditions. The tested conditions (cell types, printing mode, time, …) were added as independent variables in the model and their multiplicative effects on cell viability were estimated by exponentiating their coefficient. Confidence intervals (95% CI) and p-values testing the hypothesis that the multiplicative effect is equal to one 1 were reported. 95% CI excluding the value of 1 and p-values < 0.05 were considered as significant. Cell metabolic activity were compared using one-way non-parametric ANOVA (Kruskal-Wallis). Post-hoc pairwise Dunn tests were used with Bonferroni multiple-comparison correction to compare conditions to reference. All analyses were performed in R version 4.0.3. The abbreviated notations of the microscaffolds, ink and bioink used in this work are summarized in Table 1.

Table 1
Micro-scaffolds, ink, bioink and notations used in this work.

Micro-scaffolds (cultured in bioreactor)	Notation
Cells alone[a]	Cells
PLGA micro-scaffolds + cells	PLGA
PLGA micro-scaffolds coated with PLL + cells	PLGA-PLL
PLGA micro-scaffolds coated with collagen + cells	PLGA-Coll
Ink	**Notation**
Methacrylated type I collagen	CollMA
Methacrylated hyaluronic acid	HAMA
Methacrylated type I collagen + hyaluronic acid	CollHAMA
Methacrylated type I collagen + hyaluronic acid + gelatine	CollHAMAGel
Ink + cells	**Notation**
Methacrylated type I collagen + hyaluronic acid + cells	Bioink hd (by hand deposition)
Methacrylated type I collagen + hyaluronic acid + gelatine + cells	Bioink bb (by BioBot)

[a] Cells used in this work: NIH 3T3, HCS-2/8 or DPSCs.

3. Results

3.1. Design of porous PLGA microscaffolds with optimal size for cell culture

The main goal of the work was to design microscaffolds able to achieve three physical parameters such as i) offering to the cells an effective surface to enable cell adhesion and proliferation, ii) having a size compatible with that of the printer nozzle diameter to prevent clogging during printing and iii) providing a porosity permitting cells entering the microscaffolds (see Fig. 1). The porous PLGA microscaffolds were prepared following a double emulsion technique using gelatin as porogen (see Materials and methods § 2.1.). Additional surface coatings with collagen type I or PLL were tested. SEM image analysis showed microscaffolds with an average size of 102.8 µm ± 15.8 µm (Fig. 2A). These particle sizes are both optimal for cell culture and for printing because they will not seal the printing tips. 95% of the microscaffolds have size higher than 58 µm and 78.3% of them have a size between 58 µm and 142 µm (Fig. 2B). Moreover, we monitored that 91% of pores which have a size superior to 8 µm (Fig. 2C). SEM and confocal images of HCS-2/8 cells-laden micro-scaffolfds, cultured in bioreactor 3 h under agitation and 48 h without agitation, showed cells penetrating within porosities of the microscaffold surface (Fig. 2D–F). These results suggested that the porosities are sufficiently high in dimension to allow cells to colonize the microscaffolds, this meets the 3rd point of our goals. Our microscaffolds have thus an optimal size and porosity for cell culture.

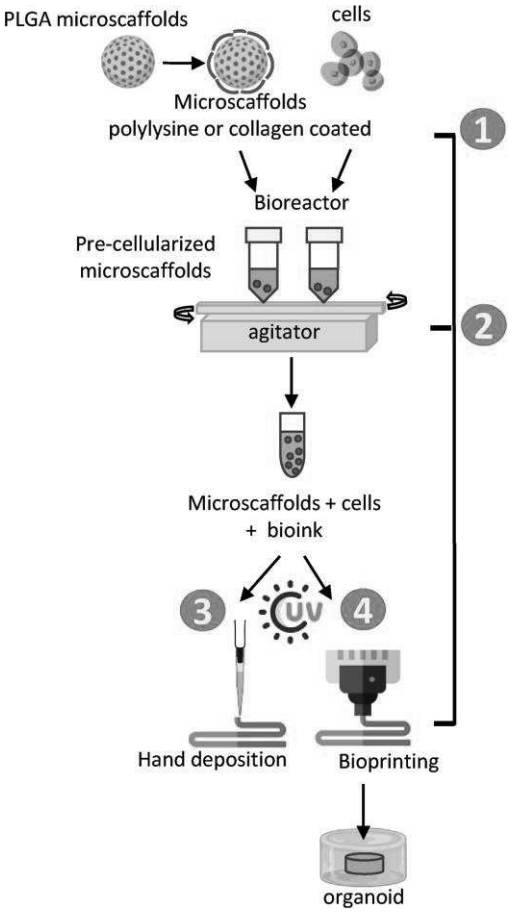

Fig. 1. Cartoon showing the steps of the bioprinting process. (1) Design of the microscaffolds, cells used: NIH 3T3, HCS 2/8 or DPSCs (2) Pre-cellularization of the microscaffolds cultured in bioreactor 3 h under agitation and 48 h without agitation in the appropriate culture medium, (3) Hand deposition by means of a micropipette of cell-laden PLGA microscaffolds in bioink cross-linked by 3 min UV, (4) Bioprinting of organoid with co-culture of DPSCs and HSC- 2/8 cells (bioink cross-linked by 3 min UV). The numbers 1 to 4 corresponding to the steps of the bioprinting process are reported in the concerned next figures.

3.2. Microscaffolds enhance cells metabolic activity

We demonstrate that our microscaffolds have optimal size for cell culture. We then evaluate whether these porous microscaffolds could promote metabolic activity of NIH 3T3 fibroblast cells, HCS-2/8 chondrosarcoma cells and DPSCs stem cells. The cell activity of NIH 3T3 cells cultured for 72 h with PLL-coated microscaffolds was 2.0-fold higher than that of NIH 3T3 cells cultured without microscaffolds (Fig. 3A). For HCS-2/8 cells cultured 48 h with PLL-coated microscaffolds, we observed 2.0-fold higher activity than HCS-2/8 cells cultured without microscaffolds (Fig. 3A). Interestingly, for DPSCs cultured 48 h and 72 h with collagen-coated microscaffolds, cell activity was respectively 2.22 and 3.7-fold higher compared to DPCSs cultured without microscaffolds. DPSCs can grow faster and reach a higher concentration due to the microscaffolds providing a larger surface area available for cell culture (Fig. 3A). Of note, the cell activity of NIH 3T3 and HCS-2/8 cells cultured for 48 h with PLL-coated microscaffolds was respectively 4.5 and 2.4-fold higher than that of cells cultured with microscaffolds without coating. Cell activity of DPSCs cells cultured for 72 h with collagen-coated microscaffolds was 3-fold higher than that of cells cultured with microscaffolds without coating (Fig. 3A).

In summary, there is an increase in cell activity for HCS-2/8 cells, NIH 3T3 cells and DPSCs cells when they are cultured in the presence of microscaffolds compared to those cultured without microscaffolds. Cell activity is further enhanced when microscaffolds are coated either with PLL or collagen as compared to cells cultured with microscaffold without coating.

3.3. Cell-laden microscaffolds incorporated in bioink enhance cell viability after hand deposition

Having established that coated microscaffolds allow cell adhesion and enhanced cell activity of HCS-2/8 cells, NIH 3T3 cells and DPSCs, we next determined if they were able to maintain cells viability after incorporation into the bioink and extrusion process. Pre-cellularized microscaffolds were incorporated into the bioink^{hd} (Table 1) and extruded by hand deposition (by means of a micropipette).

First, by confocal microscopy, we showed that DPSCs cultured 24 h in bioink without microscaffodds were structured in aggregates (SI Fig. 1A). Inversely, DPSCs cultured 24 h in bioink with collagen coated-microscaffolds were uniformly localized on the surface of the microscaffolds and around the microscaffolds (SI Fig. 1B).

The control condition was the bioink^{hd} with cells, without microscaffold, and hand deposited with same geometry. After hand deposition, the bioink^{hd} with free cells or with pre-cellularized microscaffolds, was cross-linked by UV for 1, 3 or 5 min (to find minimal UV exposition duration for cell survival [33] preserving bioink mechanical stability). The hand deposited structures were cultivated for 24 h at 37 °C and 5% CO_2. Cell viability was evaluated by a live/dead assay to determine whether or not the cells survived the potentially harmful effects of UV and printing stress. A cross-linking time of 1 min generated insufficient mechanical stability, showing dissolution of the hand deposited

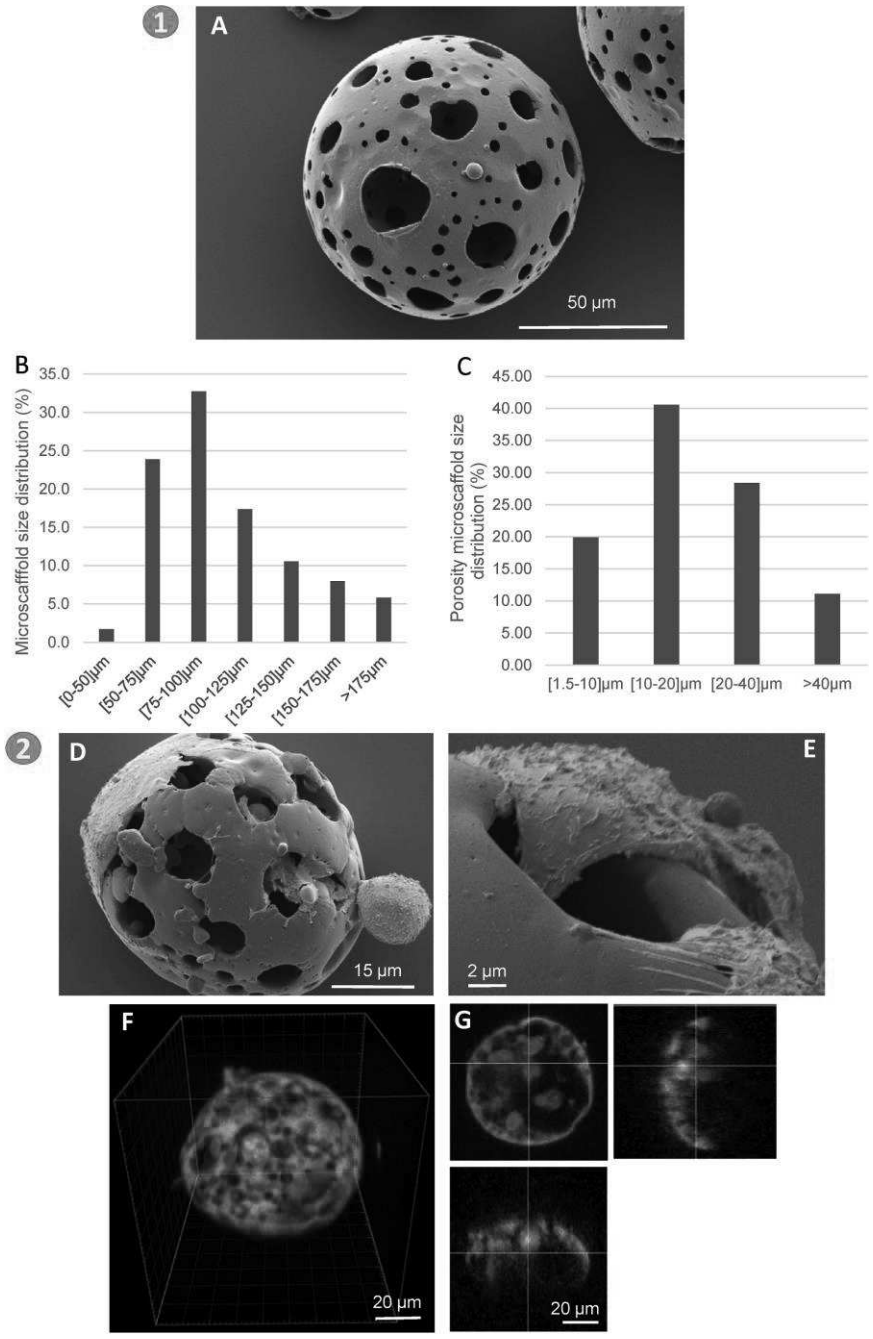

(caption on next page)

Fig. 2. Porous PLGA microscaffolds provide an adhesion surface for cells. A) Representative SEM images of PLGA micro-scaffold, showing micro-porosity, B) PLGA microscaffolds size distribution C) Porosity size distribution at the PLGA microscaffolds surface, D) Representative SEM images of HCS-2/8 cells (in blue) seeded on PLGA microscaffolds at a density of 5×10^5 cells mL^{-1} and cultured for 3 h under agitation and 48 h in culture medium E) Enlargement of a porosity in which a HCS-2/8 cell (in blue) is infiltrated. F) Representative confocal images of HCS-2/8 cells at a density of 5×10^5 cells mL^{-1} and cultured for 3 h under agitation and 48 h in culture medium (in blue) seeded on PLGA microscaffolds (in green, autofluorescence). G) Enlargement of a vertical section confocal image of a porosity in which HCS-2/8 cells (in blue) are infiltrated. (For interpretation of the references to colour in this figure legend, the reader is referred to the Web version of this article.)

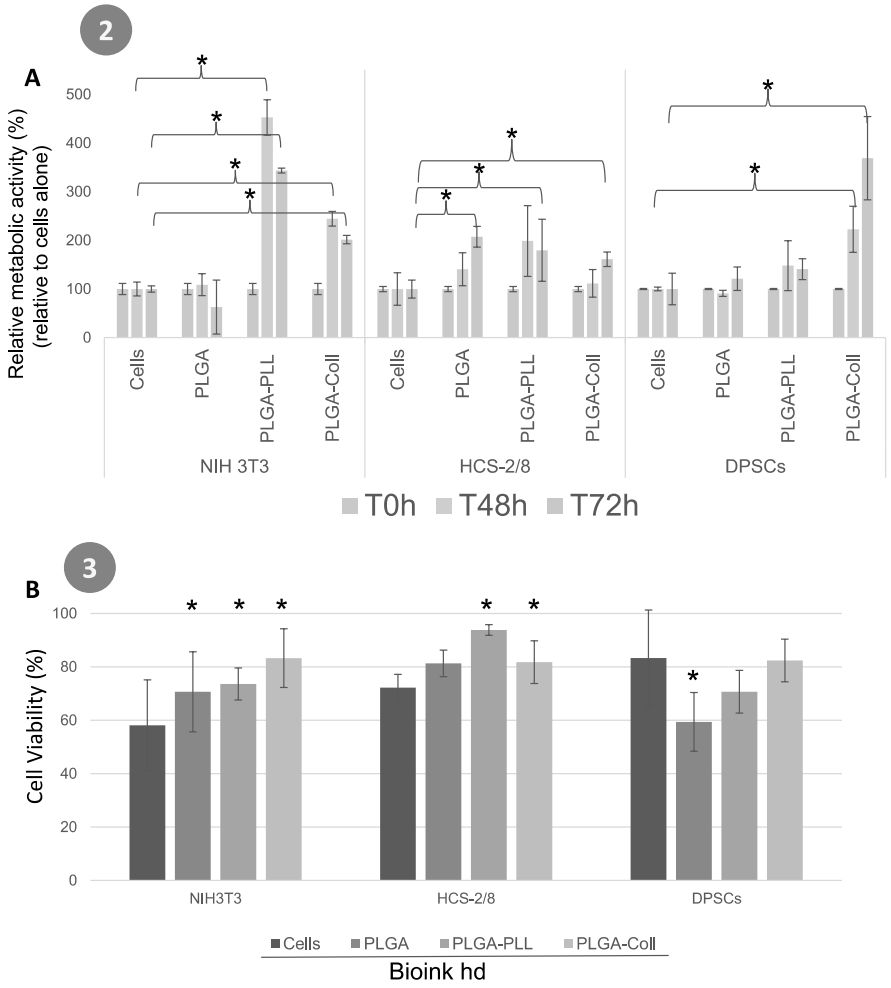

Fig. 3. Cell proliferations on the microscaffolds coated with PLL or Collagen. A) Proliferation of NIH 3T3, HCS-2/8 and DPSCs was monitored after 48 h and 72 h of culture by resazurin measurements using alamar blue assay. 100% corresponds to the proliferation of cells alone for each time. Results are means of two independent experiments. B) Percentage of surviving NIH 3T3, HCS-2/8 and DPSCs in bioink hand deposited with 3 min reticulation and 24 h of culture, by apoptotic/necrotic/healthy cell detection kit based on SI Fig. 1. Results are means of two independent experiments. * Significant difference with "cells" condition ($p < 0.05$). (For interpretation of the references to colour in this figure legend, the reader is referred to the Web version of this article.)

structure in the culture medium (data not shown). It was therefore chosen to test 3 and 5 min in reticulation times. For DPSCs cultured 24 h in bioink without microscaffolds, survival rate reach 83.3% for 3 min of reticulation (Figs. 3 and SI Fig. 2) that decreased to 57.9% for 5 min of reticulation (SI Fig. 3). Inversely, DPSCs cultured 24 h in bioink with PLL-coated microscaffold or with microscaffold without coating, their survival rate remained lower than DPSCS cultured 24 h in bioink without microscaffold (cell alone in bioink^{hd}, Table 1) showing

respectively 60 and 70.7% of survival (Figs. 3B) and 75.5% in bioink with PLL-coated microscaffold for 5 min of reticulation (SI Fig. 3). DPSCs cultured 24 h in bioink with collagen-coated microscaffold reached 80 and 90% of viability respectively for 3 (Fig. 3B) and for 5 min reticulation (SI Fig. 3).

For HCS-2/8 cells cultured 24 h in bioink without microscaffolds, 72.2% of cells survived after 3 min of reticulation. We observe that for HCS-2/8 cell survival significant increased in bioink with PLL and collagen-coated microscaffolds for 3 of cross-linking compared to survival in bioink without microscaffolds (respectively 93.8, 81.8 and 72.2% Fig. 3B). As for HCS-2/8 cells, survival of NIH 3T3 cells cultured in bioink was significantly higher in the presence of microscaffolds (70.7% without coating, 73.7% for PLL-coating and 83.3% for collagen-coating compared to 58.2% for cells alone). Of note, after 5 min cross-link, the survival rate in bioink with microscaffolds are similar to cells alone in bioink (67.8% for cells alone, 74.1% for PLL coated microscaffold and 73.9% for collagen coated microscaffolds, SI Fig. 3) except for cells with microscaffold without coating for which the survival rate decreased to 49.5% (SI Fig. 3).

In summary the data showed that for HCS-2/8 cells, NIH 3T3 cells and DPSCs, the use of collagen coated microscaffolds in bioink with 3 min reticulation improve cell viability. These results suggest that microscaffolds mechanically protect the cells during hand deposition, increasing cell viability 24 h after this process. Therefore, the condition "collagen coated microscaffolds" is retained for the rest of this work.

3.4. Collagen coated cell-laden microscaffolds incorporated in bioink enhance cell viability after bioprinting

Bioink^{hd} hand deposition was a necessary step to select best culture condition to be used with the extrusion bio-printer. We next evaluated cell viability using the bioprinter with the bioink^{bb} containing collagen coated cell-laden microscaffolds. In order to evaluate the best condition in the viability of cells in the bioink^{bb}, 2 min of cross-linking was also compared to 3 min. For HCS-2/8 cells, we added the condition microscaffolds coated with PLL since it was the condition with the highest survival rate in our preliminary experiments by hand deposition.

The 3D printed structure was a single cylindrical shape strain with a diameter of 800 μm and a length of 10 mm (Fig. 4A) or a cylinder of 3 layers wrapped around itself to form an organoid (Fig. 4B). Our data shows that HSC-2/8 cells in bioink printed with collagen coated microscaffold allowed the best survival rate (Fig. 4C and 91.3% survival) in comparison with all the other conditions (Fig. 4C). We found the highest survival rate for DPSCs cells in bioink printed with collagen coated microscaffolds (89.7% and 85.4%, respectively, Fig. 4C for 3 min and SI Fig. 4 for 2 min duration cross-linking). Of note, survival rate was always lower for cells printed in bioink without microscaffold compared to conditions with micro-scaffold (for 2 min, 77.4 and 81.7% respectively SI Fig. 4, for 3 min, 85.9 and 89.7% respectively, Fig. 4C).

NIH 3T3 cells show similar viability to DPSCs. NIH 3T3 cell survival printed in bioink increases in presence of collagen coated microscaffold after 2 or 3 min cross-linking compared to cells cultured without microscaffold (with microscaffolds 85.5% for 2 or 3 min cross-linking

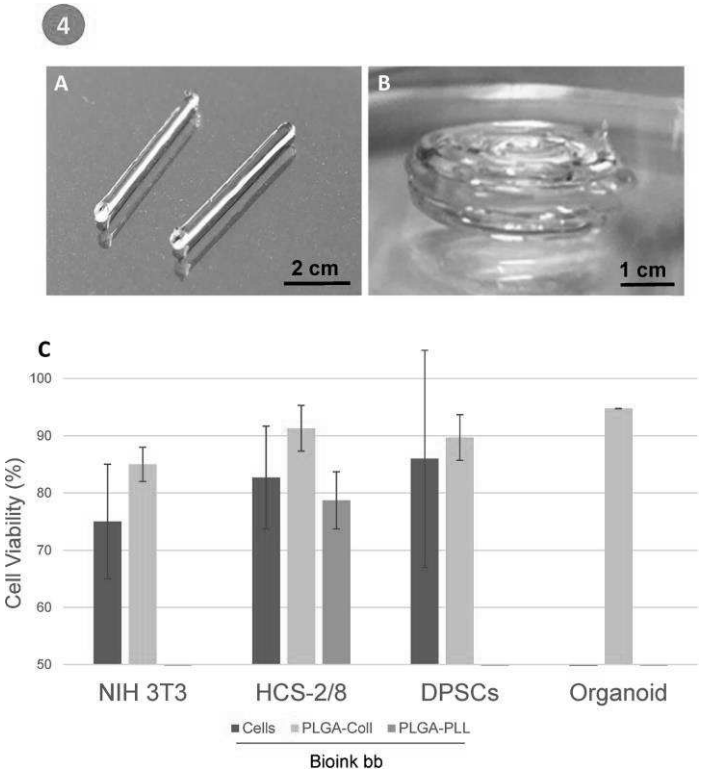

Fig. 4. Cell-laden micro-scaffolds incorporated in bioink enhance cell viability after BioBot extrusion A) Printed structure for survival analyses of NIH 3T3, HCS-2/8 and DPSCs, B) Printed structure of an organoid for survival analyses of HCS-2/8 + DPSCs co-culture. C) Survival percentage of NIH 3T3, HCS-2/8, DPSCs and HCS-2/8 + DPSCs co-culture in an organoid. Bioink extruded by BioBot technology using 3 min reticulation and after 24 h of culture, analyzed with the apoptotic/necrotic/healthy cell detection kit (PromoKine). Results are means of two independent experiments.

and without particles 69.5 and 80.1% for 2 and 3 min, respectively, Figs. 4C and SI Fig. 4 for 2 min).

In conclusion, as with hand deposition, the presence of collagen-coated microscaffolds in the printed bioink has a tendency to increase the viability of NIH 3T3 cells, HCS-2/8 cells and DPSCs as compared to the printed bioink without microscaffolds.

3.5. Cell-laden microscaffolds incorporated in bioink enhance DPSCs migration towards HCS-2/8 cells after bioprinting

The development of complex cellular models by 3D bioprinting could be relevant to better mimic *in vivo* environments and study inter-cellular responses. After demonstrating that pre-cellularized micro-scaffold increased cell viability, we choose to study their ability to create viable 3D multicellular environments by bioprinting. The main advantage of printing a co-culture of pre-cellularized microscaffolds was to precisely choose their 3D localization while protecting their viability and proliferation abilities.

As an example we selected a co-culture to study interactions between DPSCs cells and HSC-2/8 cells. DPSCs are multipotent mesenchymal progenitors (MSC) from dental pulp, a biologically relevant cellular model for tissue engineering applications [34]. They can differentiate into odontoblast and maintain pulp homeostasis by formation of new dentin protecting underlying pulp. They have also a great differentiation capacity into adipogenic, neurogenic and chondrogenic cells. Chondrosarcomas HCS 2/8 cells are aggressive malignant tumorous cells and tumorigenicity depends on their localization in the bone into central, peripheral and juxtacortical [35]. A very characteristic phenomenon is that MSCs exhibited preferential recruitment into regions of tumor growth [36]. Cancerous cells can recruit MSCs to release inflammatory mediators into the tumor microenvironment [37]. Our aim was to determine whether DPSCs and HCS-2/8 cells could interact in a 3D printed co-culture and to mimic a physiologic process. A 2D control experiment was developed to determine whether DPSCs and HSC-2/8 interact using culture-insert (Ibidi system). HCS 2/8 were seeded inside the inserts while DPSCs outside, both at 4×10^4 cells/mL. By optical microscopy, we showed that at 1 day after removing the insert, the insert footprint was cell free between areas colonized by HCS-2/8 cells (SI Fig. 5 A, red dotted line delimiting HCS-2/8 cells). At 7 days after removing the insert, in the same area, DPSCs fully colonized insert footprints, creating physical contact with the HCS-2/8 cells (SI Fig. 5 B, red dotted line delimiting HCS 2/8 cells). DPSCs coming from outside footprints, proliferated and filled the areas that were initially cell-free (insert footprints) between the HCS-2/8 that no longer had space

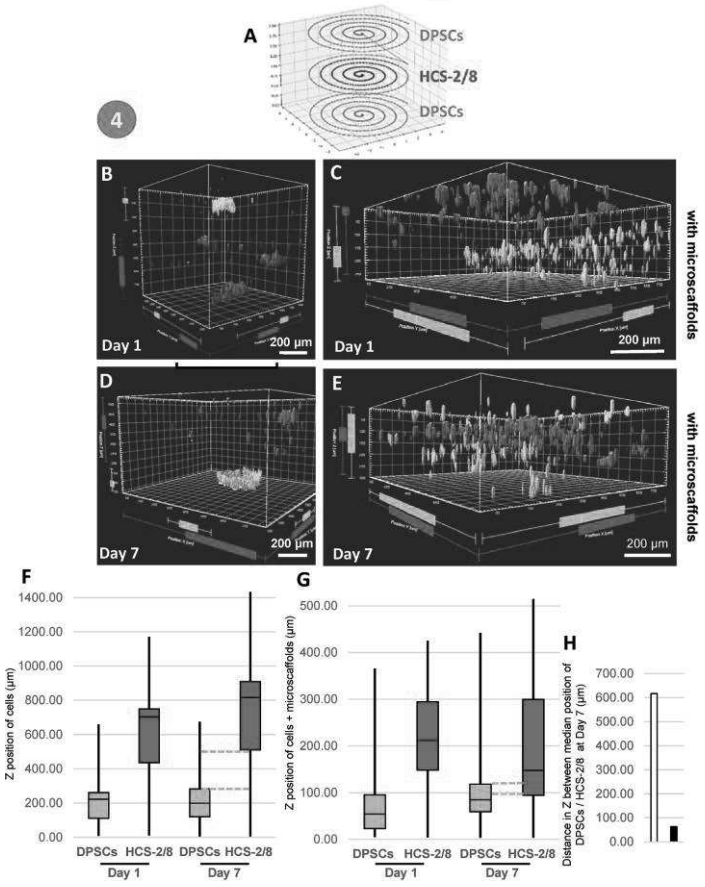

Fig. 5. Cell-laden PLGA microscaffolds incorporated in bioink enhance DPSCs migration within HCS-2/8 cells after bioprinting extrusion. A) Experimental design of an organoid composed of DPSCs (in green) and HCS 2/8 cells (in red). This printed structure is shaped like a spiral. B) Representative vertical section images of organoid by confocal microscopy B) and D) without PLGA microscaffolds, C and E) with collagen coated PLGA microscaffolds, B and C) 1 day after printing, D and E) 7 days after printing. F) boxplots of the Z position of cells without microscaffolds from B and D. G) boxplots of the Z position of cells with microscaffolds from C and E. H) Distance in Z between median position of DPSCs/HCS 2/8 at day 7 from E. (For interpretation of the references to colour in this figure legend, the reader is referred to the Web version of this article.)

available to proliferate. This result showed that the DPSCs prevented the extension of the HSC 2/8 cells in a 2D environment.

We then determined the interaction of these two cell models in a 3D environment. The use of the 3D bioprinter allowed us to create a 3D architecture with precise insertion of DPSC and HCS-2/8 cells into defined areas. We designed a model composed by a core of cancerous cells surrounded by stem cells. These printed structures measured approximately 7 mm × 7 mm x 3 mm (see experimental design, Fig. 5A). By confocal microscopy and Imaris 3D image reconstruction, we showed that at 1 day after bioprinting of pre-cellularized microscaffolds with HSC-2/8 cells (in red) and microscaffolds with DPSCs (in green) achieve two distinctly separated red and green cell areas (Fig. 5B). 7 days after bioprinting, we showed by confocal microscopy that DPSCs (in green) were colocalized with HCS-2/8 (cells in red). DPSCs surrounded the HSC-2/8 region above and below and some infiltrated the cancer cells suggesting that the migration direction is from DPSC to HCS-2/8. At this timepoint separation ceased to exist (Fig. 5D). The evaluation of DPSCs and HCS-2/8 z positions, based on Imaris 3D image reconstruction (Fig. 5C and E), showed that at day 1 the two cell models were 157.4 µm separated (median to median) while at day 7 they overlaped (Fig. 5G and H). We tested a control condition with HCS-2/8 and DPSCs without microscaffold printed as described above. At 1 day after bioprinting, we observed two distinctly cell areas separated from 480 µm materialized in red by HSC-2/8 cells and in green by DPSCs cells (Fig. 5C and F). 7 days after bioprinting, we showed that the red region (HCS-2/8 cells) remained 616.5 µm separated from the green region (DPSCs cells) (Fig. 5D, F and 5H). This data suggests that aggregated cells printed without microscaffolds were not able to migrate inside the organoid. Indeed, migration of DPSCs to HSC-2/8 cells was observed only when the cells were pre-cultured in the presence of microscaffolds preventing their aggregation.

4. Discussion

Cell proliferation. The amount of cells required for bioprinting is huge. Indeed, billions of cells are needed in bioprinting for the smallest of constructs. To print larger and complex architectures, it is necessary to produce a quantity of cells even more substantial. This is often problematic, as it is time consuming and very expensive. Therefore, inserting micro-scaffold into the bioink offers a larger surface area for cell adhesion and proliferation, increasing the number of cells available for bioprinting.

For DPSCs cells, the highest proliferation comes from cells cultured with microscaffolds coated with collagen. They can grow faster and reach a higher concentration thanks to the micro-scaffold which provides a larger surface area available for cell proliferation. In addition, the collagen coating increases the adherence of cells to the microscaffolds, rendering the scaffolds more attractive to the cells. Cells can bind to collagen via the adhesion molecule integrin α2β1 which recognizes a specific sequence, glycine-phenylalanine-proline-glycine-glutamic acid-arginine, located in the α2-1 domain of collagen [38]. Our results are in agreement with previous work showing that PLGA microparticle offers adherent platform for cells to proliferate in suspension [39] or in bioink and constructs hand deposited [17].

The presence of microscaffolds renders the environment more attractive to the cells, as evidenced by the increase in cell proliferation. This increase is higher when PLL is used as a coating.

As for HCS 2/8 cells, NIH 3T3 cells alone do not proliferate as fast in bioreactors as in culture flasks (decrease in the Alamar Blue signal from T0h to T72h). Again, this is compensated by the addition of microscaffolds and particularly by the presence of coated microscaffolds (48 h of culture, the proliferation rate for coated collagen microscaffolds is 3.2 times higher than for cells alone). This can be explained by the presence of microscaffolds for cell proliferation, giving them a needed 3D space and moreover the presence of coating has improved their attractiveness and adhesion.

Cell survival during bioink hand deposition. The results showed that collagen coated microscaffolds are the best candidate to preserves HCS-2/8 cells, NIH 3T3 cells and DPSCs survival within bioink after hand deposition compared to the conditions without micro-scaffold. The 3D structure probably protects the cells from the mechanical shear stresses induced during the hand deposition process. The uniform localization of the DPSCs at the periphery of the microscaffolds after hand deposition suggests that they are able to proliferate and to migrate on their surface and around (microscaffolds free areas), contrary to DPSCs without microscaffolds organized in aggregates.

Extrusion BioBot bio-printer. The bioprinters allows precise control of the pressure applied to the printing nozzle, the printing speed, the amount of bioink and the design of the printed architecture. Thanks to these precise controls, the survival rate of the cells is improved for all the conditions tested compared to those with hand deposition process. We also determined whether the duration of UV cross-linking of the bioink could be harmful for cell viability. Although the UV duration was reduced to 2 min, the cell viability decreases. This is probably due to a lower mechanical stability of the bioink, even in the presence of microscaffolds, limiting cell adhesion and proliferation. As for hand deposition, the condition with 3 min of cross-linking" in the presence of this collagen-coated microscaffolds allowed the best cell viability. We can note that the viability of NIH 3T3 cells did not change as a function of cross-linking time, when printed with collagen-coated microscaffolds, contrary to other cell types. The presence of a solid material provided by the microscaffolds is the determining factor to increase their survival during their bioprinting. In the absence of these microscaffolds, NIH 3T3 forms isolated aggregates.

In conclusion, our results show that when using collagen-coated microscaffolds, before printing and after printing, cell proliferation and cell viability are higher, compared with cells alone.

Co-culture assisted printing. Thanks to extrusion bioprinting using microscaffolds, we focused on the patterning of two co-cultured cell models. Therefore, mechanisms of chondrogenesis were determined by bioprinting of chondrocytes and bone-marrow-derived mesenchymal cell-laden bioinks [40]. In an *in vivo* model, Nakamizo et al. showed that marrow-derived mesenchymal stem cells injected into the carotid artery of mice tumor models migrate within brain tumors that they bear [36]. In the present work, we bioprinted a structure containing in its center HCS-2/8 cells-laden bioinks surrounded at the top and bottom with DPSCs-laden bioinks. 1 day after printing, the two cell types were physically separated whereas 7 days after, DPCSs were colocalized within HCS-2/8 cells. Concerning a possible gravity that attracts the microscaffolds down, anyway after crosslinking by UV, the loss modulus of the ink amounts to 148 Pa (SI Table 1) at a frequency of 10 Hz this corresponds to a dynamic viscosity of about 1500 Pa. In such a medium, an overestimation of the sedimentation rate of the PLGA particles (specific density of 1250 kg m^{-3}) can be given and it amounts to 9.1 × 10^{-4} µm s^{-1} and hence to 78 µm.day^{-1}. This value is however largely overestimated due to the porosity of the PLGA particles which hence have a much lower apparent density and sediment slowlier accordingly. In addition, the real cell loaden ink in crowded in particles and in cells and much more viscous than the ink by itself again inducing a reduction in the sedimentation rate. Hence, we believe that most of the added PLGA particles will not have time to sediment to the bottom of the ink during our biological evaluation lasting over 7 days. Our results found by extrusion printing are in accordance with those of Nakamizo et al. [36]. Of note, DPSCs were able to migrate to HSC-2/8 only when these two cell types were associated to microscaffolds in the laden bioinks. Recently, Heilshorn and co-workers showed that endothelial cell migration was promoted into 3D printed structures depending upon void fractions that they contain [41]. In our model, the microscaffolds within the bioink do not structure void fraction favorable to cell migration. However, we can hypothesize that specific growth factors [42] from HSC-2/8 cells mediating the tropism of DPSCs are more effective when DPSCs are uniformly localized on the microscaffolds rather than

organized in aggregates without microscaffolds. Recent works determined how the distribution of the cells within bioprinted architecture regulates its mechanical properties, structural feature and ultimately the biological functionality of the construct [43–45]. For example, hydrogels containing clustered cells have a significantly different modulus than those with random cell distribution [46]. Our 3D bioprinting approach showing that DPSCs have a tropism for chondrosarcomas HCS 2/8 cells offers interesting perspectives. Stem cells could be used as a 3D *in vitro* bioprinting model of delivery vehicles for sarcoma therapy [47].

5. Conclusion

In this work, we developed a bioink, based on methacrylated collagen and hyaluronic acid, in combination with porous poly(D,L-lactic-co-glycolic acid) solid microscaffolds to protect cells against mechanical stress during extrusion printing. We found that porosities of the microscaffolds allowed human chondosarcoma cells to colonize the structure. Moreover, proliferation of chondrosarcoma cells, fibroblast cells, and dental pulp stem cells (DPSCs) incorporated within bioink (before printing) increased 4-fold in presence of a polylysine- or collagen-coated microscaffolds compared with those cultured without microscaffolds. Their survival increased by 10% either by hand deposition or by bioprinting extrusion compared to cells in bioink without microscaffolds. In addition to the mechanoshield properties provided by microscaffolds, they allow the migration of DPSCs stem cells towards HCS-2/8 cancer cells after 7 days of co-culture in an organoid created by bioprinting extrusion while without microscaffolds the cells aggregated and remained static.

CRediT authorship contribution statement

Adrien Rousselle: designed the studies, performed the experiments, Formal analysis, Writing – original draft. **Arielle Ferrandon:** performed the experiments. **Eric Mathieu:** performed the experiments. **Julien Godet:** Formal analysis, Writing – original draft. **Vincent Ball:** performed the experiments, Formal analysis, Writing – original draft. **Leo Comperat:** performed the experiments. **Hugo Oliveira:** Formal analysis, Writing – original draft. **Philippe Lavalle:** Writing – original draft. **Dominique Vautier:** designed the studies, performed the experiments, Formal analysis, Writing – original draft. **Youri Arntz:** designed the studies, Formal analysis, Writing – original draft, and all authors edited the final submission.

Declaration of competing interest

The authors declare that they have no known competing financial interests or personal relationships that could have appeared to influence the work reported in this paper.

Data availability

Data will be made available on request.

Acknowledgements

Financial support was received from Region Grand-Est MIPPI4D (Programmable Informed Material 4D Printing).

Appendix A. Supplementary data

Supplementary data to this article can be found online at https://doi.org/10.1016/j.bprint.2022.e00247.

References

[1] A.S. Moghaddam, H.A. Khonakdar, M. Arjmand, S.H. Jafari, Z. Bagher, Z. S. Moghaddam, M. Chimerad, M.M. Sisakht, S. Shojaei, Review of bioprinting in regenerative medicine: naturally derived bioinks and stem cells, ACS Appl. Bio Mater. 4 (2021) 4049–4070, https://doi.org/10.1021/acsabm.1c00219.
[2] S.V. Murphy, A. Atala, 3D bioprinting of tissues and organs, Nat. Biotechnol. 32 (2014) 773–785, https://doi.org/10.1038/nbt.2958.
[3] W. Peng, P. Datta, B. Ayan, V. Ozbotat, D. Sosnoski, I.T. Ozbolat, 3 D bioprinting for drug discovery and development in pharmaceutics, Acta Biomater. 57 (2017) 26–46, https://doi.org/10.1016/j.actbio.2017.05.025.
[4] J. Hagenbuchner, D. Nothdurfter, M.J. Ausserlechner, 3D bioprinting: novel approaches for engineering complex human tissue equivalents and drug testing, Essays Biochem. 65 (2021) 417–427, https://doi.org/10.1042/EBC20200153.
[5] R. Augustine, S.N. Kalva, R. Ahmad, A.A. Zahid, S. Hasan, A. Nayeem, L. McClements, A. Hasan, 3D bioprinted cancer models: revolutionizing personalized cancer therapy, Transl. Oncol. 14 (2021), 101015, https://doi.org/10.1016/j.tranon.2021.101015.
[6] K. Hölzl, S. Lin, L. Tytgat, S. Van Vlierberghe, L. Gu, A. Ovsianikov, Bioink properties before, during and after 3D bioprinting, Biofabrication 8 (2016), 032002, https://doi.org/10.1088/1758-5090/8/3/032002.
[7] S.M. Hull, L.G. Brunel, S.C. Heilshorn, 3D bioprinting of cell-laden hydrogel for improved biological functionality, Adv. Mater 34 (2022), e2103691, https://doi.org/10.1002/adma.202103691.
[8] K. Zhou, Y. Sun, J. Yang, H. Mao, Z. Gu, Hydrogels for 3D embedded bioprinting: a focused review on bioink and support baths, J. Mater. Chem. B. 10 (2022) 1897–1907, https://doi.org/10.1039/d1tb02554f.
[9] S.V. Murphy, A. Atala, 3D bioprinting of tissues and organs, Nat. Biotechnol. 32 (2014) 773–785, https://doi.org/10.1038/nbt.2958.
[10] Y. Zhao, Y. Li, S. Mao, W. Sun, R. Yao, The influence of printing parameter on cell survival rate and printability in microextrusion-based 3D printing technology, Biofabrication 7 (2015), 045002, https://doi.org/10.1088/1758-5090/7/4/045002.
[11] L. Ning, B. Yang, F. Mohabatpour, N. Betancourt, M.D. Sarker, P. Papagerakis, X. Chen, Process-induced cell damage: pneumatic versus screw-driven bioprinting, Biofabrication 12 (2020), 025011, https://doi.org/10.1088/1758-5090/ab5f53.
[12] L. Ning, N. Betancourt, D.J. Schreyer, X. Chen, Characterization of cell damage and proliferative ability during and after bioprinting, ACS Biomater. Sci. Eng. 4 (2018) 3906–3918, https://doi.org/10.1021/acsbiomaterials.8b00714.
[13] H. Oliveira, C. Médina, M.L. Stachowicz, B. Paiva dos Santos, L. Chagot, N. Dusserre, J.C. Fricain, Extracellular matrix (ECM)-derived bioinks designed to foster vasculogenesis and neurite outgrowth: characterization and bioprinting, Bioprinting 22 (2021), e00134, https://doi.org/10.1016/j.bprint.2021.e00134.
[14] W.Y. Wang, A.T. Pearson, M.L. Kutys, C.K. Choi, M.A. Wozniak, B.M. Baker, C. S. Chen, Extracellular matrix alignment dictates the organization of focal adhesions and directs uniaxial cell migration, APL Bioeng 2 (2018), 046107, https://doi.org/10.1063/1.5052239.
[15] E.D.F. Ker, A.S. Nain, L.E. Weiss, J. Wang, J. Suhan, C.H. Amon, P.G. Campbell, Bioprinting of growth factors onto aligned sub-micron fibrous scaffolds for simultaneous control of cell differentiation and alignment, Biomaterials 32 (2011) 8097–8107, https://doi.org/10.1016/j.biomaterials.2011.07.025.
[16] L. Riley, L. Schirmer, T. Segura, Granular hydrogels: emergent properties of jammed hydrogel microparticles and their applications in tissue repair and regeneration, Curr. Opin. Biotechnol. 60 (2019) 1–8, https://doi.org/10.1016/j.copbio.2018.11.001.
[17] Y.J. Tan, X. Tan, W.Y. Yeong, S.B. Tor, Hybrid microscaffold-based 3D bioprinting of multi-cellular constructs with high compressive strength: a new biofabrication strategy, Sci. Rep. 6 (2016), 39140, https://doi.org/10.1038/srep39140.
[18] I. Donderwinkel, J.C.M. van Hestb, N.R. Cameron, Bio-inks for 3D bioprinting: recent advances and future prospects, Polym. Chem. 8 (2017) 4451, https://doi.org/10.1039/c7py00826k.
[19] A. Wenz, K. Borchers, G.E.M. Tovar, P.J. Kluger, Bone matrix production in hydroxyapatite-modified hydrogels suitable for bone bioprinting, Biofabrication 9 (2017), 044103, https://doi.org/10.1088/1758-5090/aa91ec.
[20] X. Cui, J. Li, Y. Hartanto, M. Durham, J. Tang, H. Zhang, G. Hooper, K. Lim, T. Woodfield, Advances in extrusion 3D bioprinting: a focus on multicomponent hydrogel based bioinks, Adv. Healthc. Mater. 9 (2020), e1901648, https://doi.org/10.1002/adhm.201901648.
[21] A. Mazzocchi, M. Devarasetty, R. Huntwork, S. Soker, A. Skardal, Optimization of collagen type I-hyaluronan hybrid bioink for 3D bioprinted liver microenvironments, Biofabrication 11 (2018), 015003, https://doi.org/10.1088/1758-5090.
[22] A.E. Kuriakose, W. Hu, K.T. Nguyen, J.U. Menon, Scaffold-based lung tumor culture on porous PLGA microparticle substrates, PLoS One 15 (2019), e0217640, https://doi.org/10.1371/journal.pone.0217640.
[23] O. Qutachi, J.R. Vetsch, D. Gill, H. Cox, D.J. Scurr, S. Hofmann, R. Müller, R. A. Quirk, K.M. Shekesheff, C.V. Rahman, Injectable and porous PLGA microspheres that form highly porous scaffolds at body temperature, Acta Biomater. 10 (2014) 5090–5098, https://doi.org/10.1016/J.ACTBIO.2014.08.015.
[24] D. Dhamecha, D. Le, R. Movsas, A. Gonsalves, J.U. Menon, Porous polymeric microspheres with controllable pore diameters for tissue engineered lung tumor Model development, Front. Bioeng. Biotechnol. 8 (2020) 799, https://doi.org/10.3389/fbioe.2020.00799.
[25] C. Ehlinger, E. Mathieu, M. Rabineau, V. Ball, P. Lavalle, D. Vautier, L. Kocgozlu, Insensitivity of dental pulp stem cells migration to substrate stiffness, Biomaterials 275 (2021), 120969, https://doi.org/10.1016/j.biomaterials.2021.120969.

[26] M. Takigawa, K. Tajima, H.O. Pan, M. Enomoto, A. Kinoshita, F. Suzuki, Y. Takano, Y. Mori, Establishment of a clonal human chondrosarcoma cell line with cartilage phenotype, Cancer Res. 49 (1989) 3996–4002.
[27] D. Smith, C. Herman, S. Razdan, M.R. Abedin, W. Van Stoecker, S. Barua, Microparticles for suspension culture of mammalian cells, ACS Appl. Bio Mater. 2 (2019) 2791–2801, https://doi.org/10.1021/acsabm.9b00215.
[28] B. D.v Fairbanks, M.P. Schwaetz, C.N. Bowman, K.S. Anseth, Photoinitiated polymerization of PEG-diacrylate with lithium phenyl-2,4,6-trimethylbenzoylphosphinate: polymerization rate and cytocompatibility, Biomaterials 30 (2009) 6702–6707, https://doi.org/10.1016/j.biomaterials.2009.08.055.
[29] L. Ouyang, J.P.K. Armstrong, Y. Lin, J.P. Wojciechowski, C. Lee-Reeves, D. Hachim, K. Zhou, J.A. Burdick, M.M. Stevens, Expanding and optimizing 3D bioprinting capabilities using complementary network bioinks, Sci. Adv. 6 (2020) 5529–5547, https://doi.org/10.1126/sciadv.abc5529.
[30] J. O'Brien, I. Wilson, T. Orton, F. Pognan, Investigation of the Alamar Blue (resazurin) fluorescent dye for the assessment of mammalian cell cytotoxicity, Eur. J. Biochem. 267 (2000) 5421–5426, https://doi.org/10.1046/j.1432-1327.2000.01606.x.
[31] R. Suntornnond, E. Yong Sheng Tan, J. An, C. Kai Chua, A mathematical model on the resolution of extrusion bioprinting for the development of new bioinks, Materials 9 (2006) 756, 103390/ma9090756.
[32] E. Gioffredia, M. Boffitoa, S. Calzonea, S.M. Giannitellib, A. Rainerb, M. Trombettab, P. Mozeticb, V. Chiono, Pluronic F127 hydrogel characterization and biofabrication in cellularized constructs for tissue engineering applications, Procedia CIRP 49 (2016) 125–132, https://doi.org/10.1016/j.2015.11.001.
[33] S. Knowlton, B. Yenilmez, S. Anand, S. Tasoglu, Photocrosslinking-based bioprinting: examining crosslinking schemes, 5, Bioprinting 10 (2017) 8.
[34] M. Marrelli, B. Codispoti, R.M. Shelton, B.A. Scheven, P.R. Cooper, M. Tatullo, F. Paduano, Dental pulp stem cell mechanoresponsiveness : effects of mechanical stimuli on dental pulp stem cell behavior, Front. Physiol. 9 (2018) 1685, https://doi.org/10.3389/fphys.2018.01685.
[35] H. Gelderblom, P.C.W. Hogendoorn, S.D. Dijkstra, C.S. van Rijswijk, A.D. Krol, A. H.M. Taminiau, J.V.M.G. Bovée, The clinical approach towards chondrosarcoma, Oncol. 13 (2008) 320–329, https://doi.org/10.1634/theoncologist.2007-0237.
[36] A. Nakamizo, F. Marini, T. Amano, A. Khan, M. Studeny, J. Gumin, J. Chen, S. Hentschel, G. Vecil, J. Dembinski, M. Andreeff, F.F. Lang, Human bone marrow-derived mesenchymal stem cells in the treatment of gliomas, Cancer Res. 65 (2005) 3307–3318, https://doi.org/10.1158/0008-5472.CAN-04-1874.
[37] E. Spaeth, A. Klopp, J. Dembinski, M. Andreeff, F. Marini, Inflammatin and tumor microenvironments: defining the migratory itinerary of mesenchymal stem cells, Gene Ther. 15 (2008) 730–738, https://doi.org/10.1038/gt.2008.39. Epub 2008 Apr 10.
[38] R.O. Hynes, Integrins: bidirectional, allosteric signaling machines, Cell 110 (2002) 673–687, https://doi.org/10.1016/s0092-8674(02)00971-6.
[39] D. Smith, C. Herman, S. Razdan, M. Raisul Abedin, W. Van Stoecker, S. Barua, Microparticles for suspension culture of mammalian cells, ACS Appl. Bio Mater. 2 (2019) 2791–2801, https://doi.org/10.1021/acsabm.9boo215.
[40] J.H. Möller, M. Amoroso, D. Hägg, C. Brantsing, N. Rotter, P. Apelgren, A. Lindahl, L. Kölby, P. Gatenholm, Plast. Reconstr. Surg. Glob. Open. 5 (2017) e1227, https://doi.org/10.1097/GOX.0000000000001227.
[41] A.J. Seymour, S. Shin, S.C. Heilshorn, 3D printing of microgel scaffolds with tunable void fraction to promote cell infiltration, Adv. Healthcare Mater. 10 (2021), e2100644, https://doi.org/10.1002/adhm.202100644.
[42] F. Giner, J.A. López-Guerrero, I. Machado, Z. García-Casado, A. Fernández-Serre, A. Peydró-Olaya, A. Llombart-Bosch, Expression profiles of angiogenesis in two high grade chondrosarcomas: a xenotransplant experience in nude mice, Histol. Histopathol. 32 (2017) 1281–1291, https://doi.org/10.14670/HH-11-880.
[43] M.A. Skylar-Scott, S.G.M. Uzel, L.L. Nam, J.H. Ahrens, R.L. Truby, S. Damaraju, J. A. Lewis, Biomanufacturing of organ-specific tissues with high cellular density and embedded vascular channels, Sci. Adv. 5 (2019), eaaw2459, https://doi.org/10.1126/sciadv.aaw2459.
[44] V. Mironov, R.P. Visconti, V. Kasyanov, G. Forgacs, C.J. Drake, R.R. Markwald, Organ printing : tissue spheroids as building blocks, Biomaterials 30 (2009) 2164–2174, https://doi.org/10.1016/j.biomaterials.2008.12.084.
[45] A.M. Blakely, K.L. Manning, A. Tripathi, J.R. Morgan, Bio-Pick, place, and perfuse : a new instrument for three-dimensional tissue engineering, Tissue Eng. C Methods 21 (2015) 737–746, https://doi.org/10.1089/ten.TEC.2014.0439.
[46] K. Hölzl, S. Lin, L. Tytgat, S. Van Vlierberghe, L. Gu, A. Ovsianikov, Bioink properties before, during and after 3D bioprinting, Biofabrication 8 (2016), 032002, https://doi.org/10.1088/1758-5090/8/3/032002.
[47] M. Studeny, F.C. Marini, R.E. Champlin, C. Zompetta, I.J. Fidler, M. Andreeff, Bone marrow-derived mesenchymal stem cells as vehicles for interferon-β delivery into tumors, Cancer Res. 62 (2002) 3603–3608.

SI Table 1

	Storage modulus (Pa)	Loss modulus (Pa)
CollHAMA	85±15	43±15
CollHAMAGel	354±60	144±50
CollHAMAGel + UV irradiation	1310±200	148±40

SI Figure 1

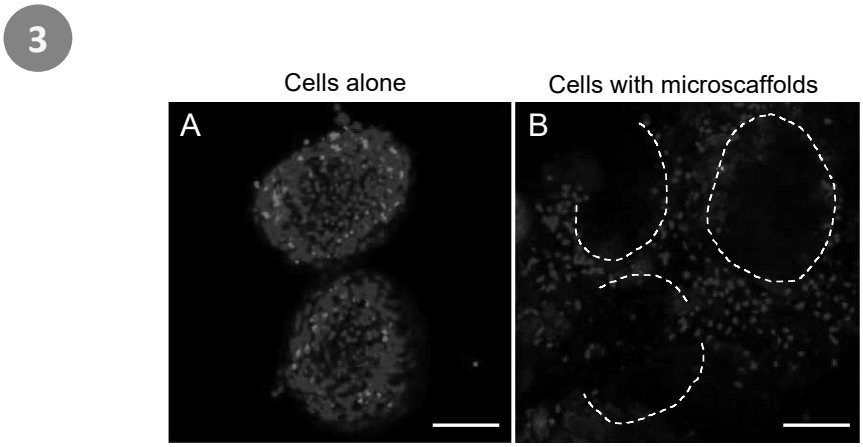

Representative confocal microscopy images of DPSCs cells within bioink hand deposited A) Without PLGA micro-scaffold, B) With PLGA micro-scaffold (collagen coated) using the apoptotic/necrotic/healthy cells kit. Cell superpositions with Hoechst 33342 (blue: nucleus), EthD-III (red: necrotic cells), Annexin V-FITC (green: apoptotics cells). White dotted lines delimiting the micro-scaffolds. Scale bar: 60 µm.

SI Figure 2

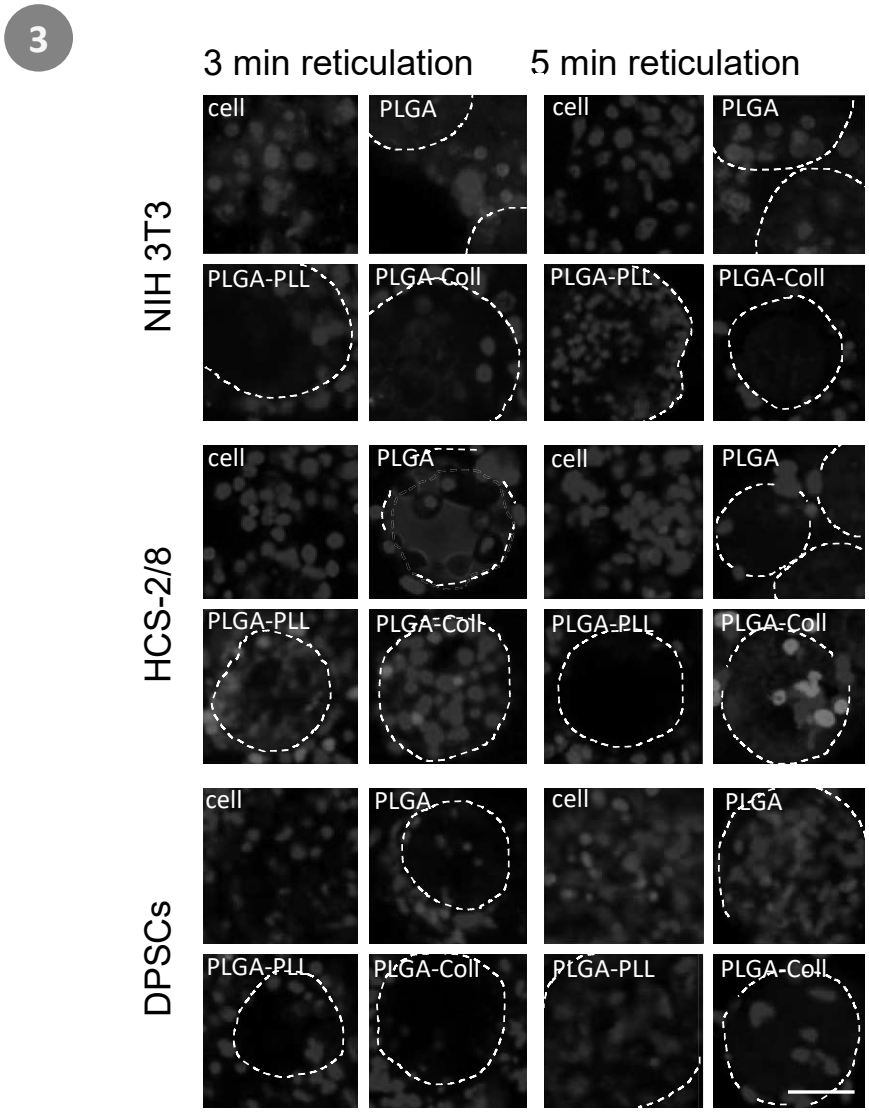

Representative confocal microscopy images of NIH 3T3, HCS-2/8 and DPSCs hand deposited with or without PLGA micro-scaffolds (PLL or Collagen coated) 3 min or 5 min reticulation and after 24 of culture using the apoptotic/necrotic/healthy cells kit. Cell superpositions with Hoechst 33342 (blue: nucleus), EthD-III (red: necrotic cells). White dotted lines delimiting the micro-scaffolds. Scale bar: 50 µm.

SI Figure 2

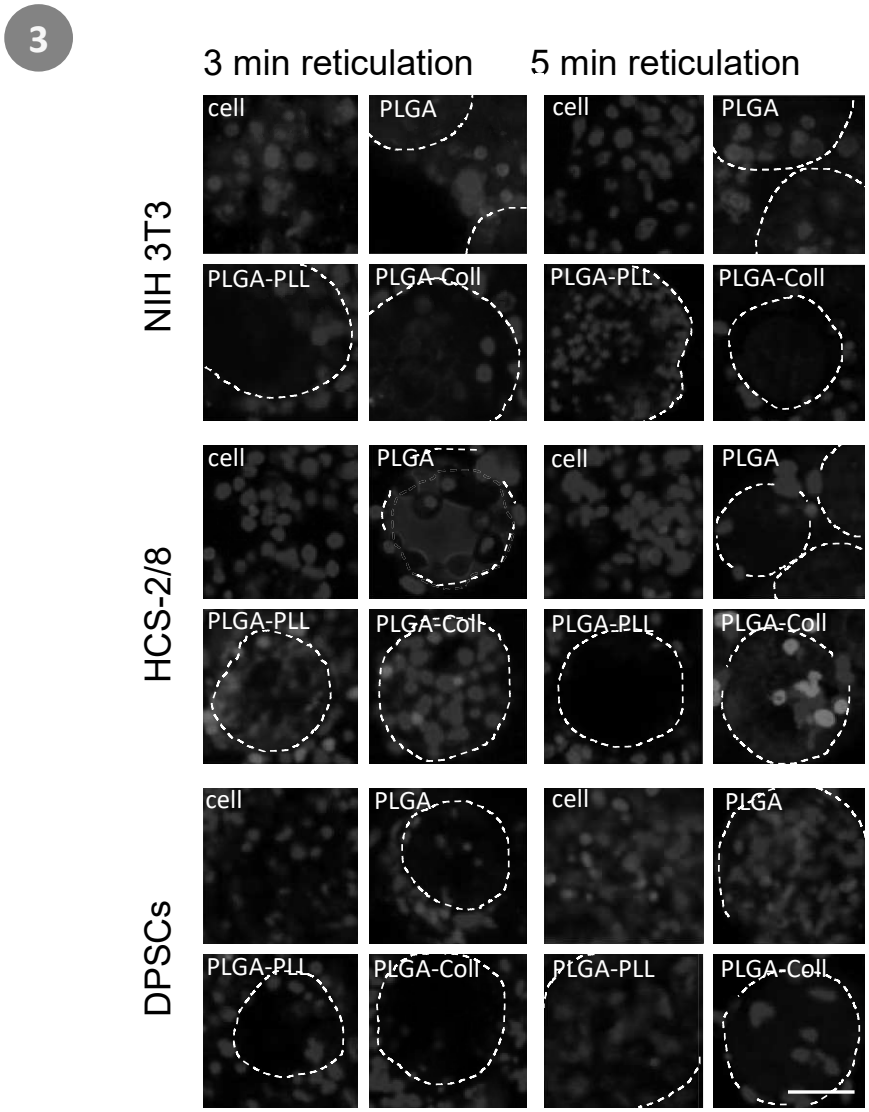

Representative confocal microscopy images of NIH 3T3, HCS-2/8 and DPSCs hand deposited with or without PLGA micro-scaffolds (PLL or Collagen coated) 3 min or 5 min reticulation and after 24 of culture using the apoptotic/necrotic/healthy cells kit. Cell superpositions with Hoechst 33342 (blue: nucleus), EthD-III (red: necrotic cells). White dotted lines delimiting the micro-scaffolds. Scale bar: 50 µm.

SI Figure 3

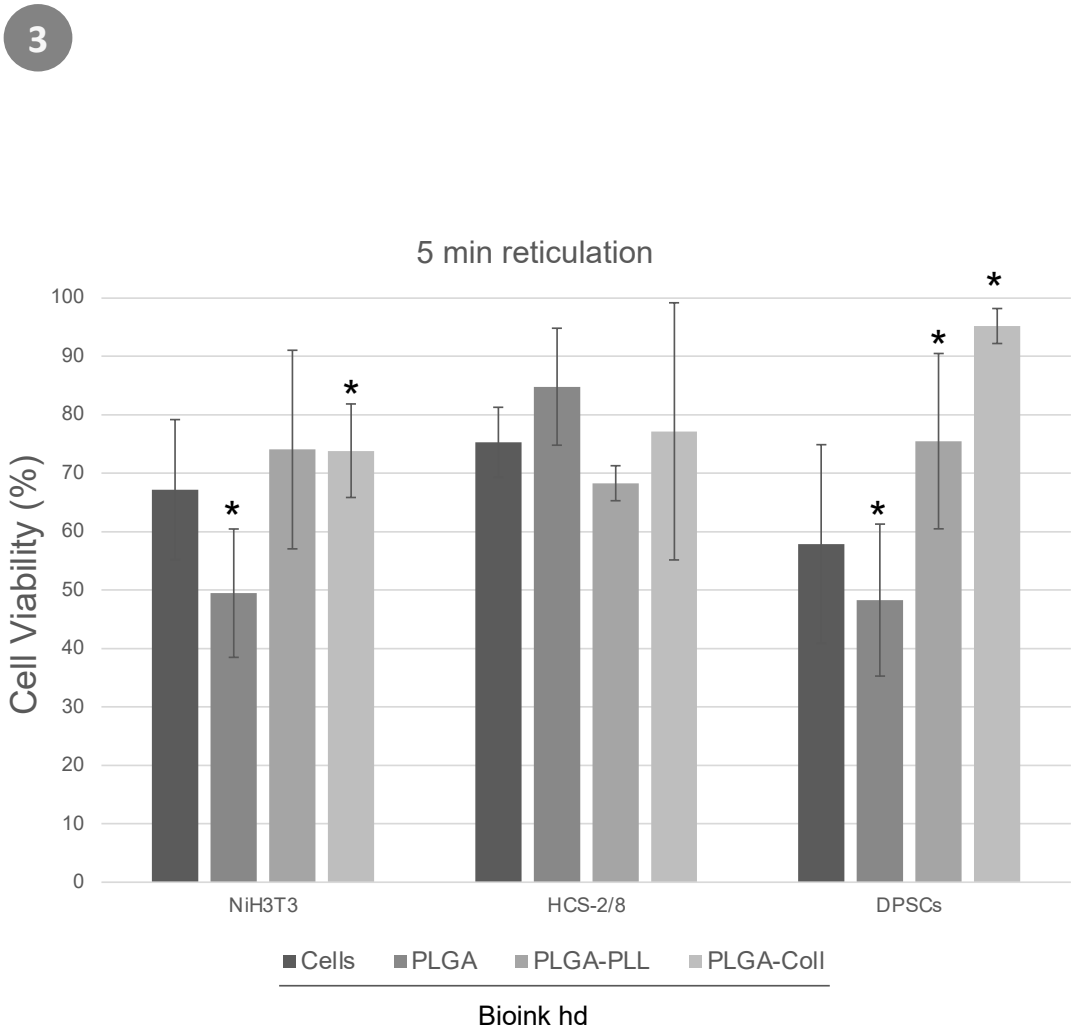

NIH 3T3, HCS-2/8 and DPSCs cells viability in bioink hand deposited with 5 min reticulation and after 24h of culture, analyzed with the apoptotic/necrotic/healthy cell detection kit (PromoKine) based on SI Fig. 1 . Results are means of three independent experiments. ***** Significant difference with “cells” condition ($p<0.05$).

SI Figure 4

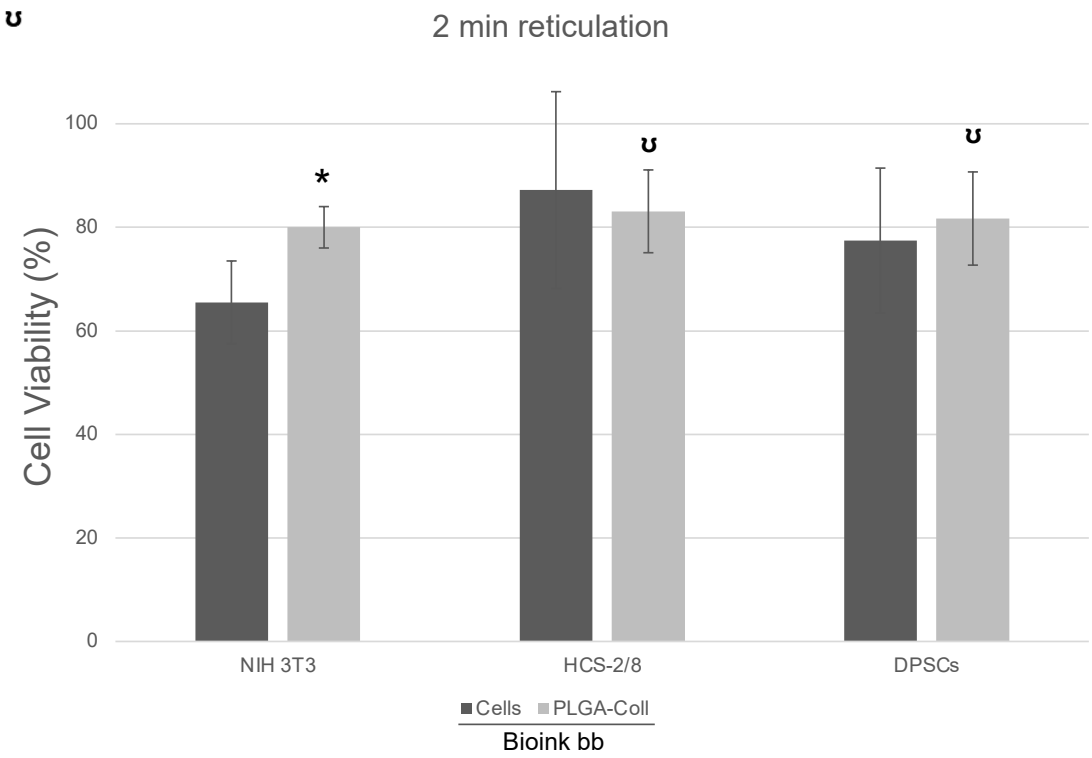

Cell-laden micro-scaffolds incorporated in bioink enhance cell viability after bio-bot extrusion A) Percentage of surviving NIH3T3, HCS-2/8, DPSCs (HCS-2/8 and with bio-bot extrusion using 2 min reticulation and after 24h of culture, analyzed with the apoptotic/necrotic/healthy cell detection kit (PromoKine). Results are means of two independent experiments. ***** Significant difference with "cells" condition ($p<0.05$), **ʊ** Significant difference with "cells" condition ($p<0.06$).

SI Figure 5

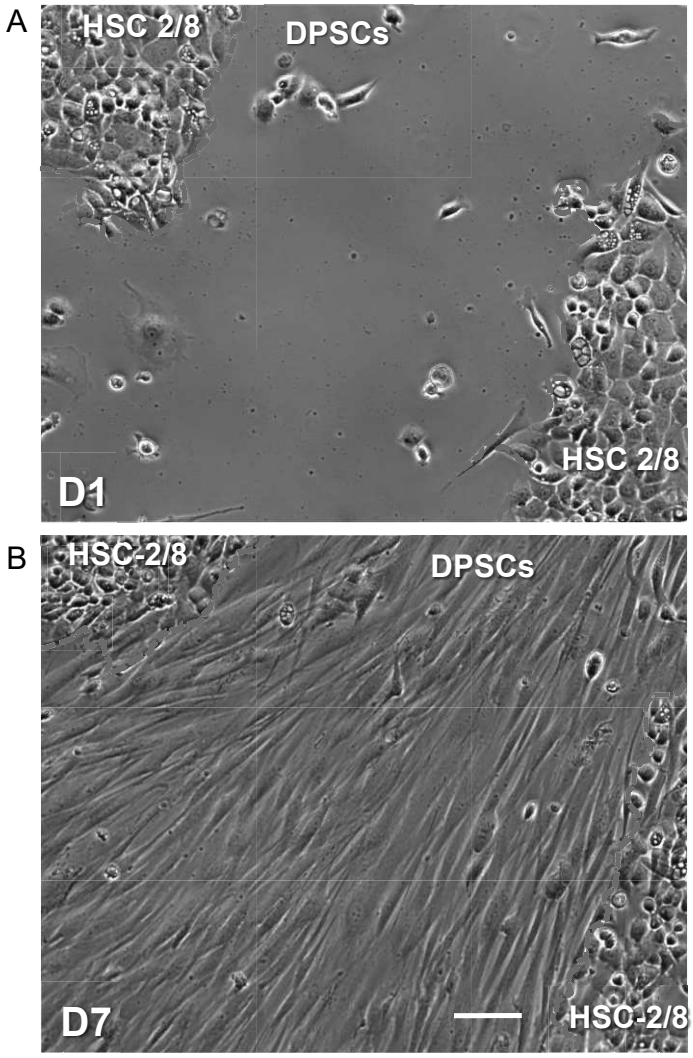

DPSCs prevented the extension of the HSC 2/8 cells in a 2D environment. Representative images acquired by phase contract microscopy. HCS 2/8 cells were seeded inside inserts while DPSCs outside both 4 x 10^4 cell . mL^{-1}. A) 1 day after removing the insert, B) 7 days after removing the insert. Red dotted line delimiting HCS-2/8 cells from DPSCs. Scale bar : 100µm.

3. Supplementary data

Further work on this article has been conducted, some of which are being optimized and constitute prospects for the continuation of this work. We expose here additional information concerning the process of diameter and pore size optimization of the PLGA microscaffolds and the bioprinting of PDLSc cells.

3.1 Diameter and pore size optimization of the PLGA microscaffolds

To develop our microscaffolds, we chose to work with PLGA, a biocompatible polymer. We produced particles using PLGA 50/50 and PLGA 75/25 and tested the different variations of PVA concentration, emulsion 1 and 2 speed of agitation, temperature, PLGA concentration, porogen concentration and nature.

We found that the PVA concentration have an effect on particle size. Indeed, the particles will be smaller with an increase in PVA concentration. The PLGA concentration will have an effect on the particle size and density, higher the concentration, bigger the particle but only up to a point where the particles will not have a more important diameter but will be denser and less porous. In addition, the PLGA concentration effect can be regulated with other parameters. Indeed, we adapted protocols using 2% of PLGA instead of using 20% of PLGA and obtained the same results. The agitation time and speed in both emulsions is primordial for the size and porosity of the particles. For the first agitation, the concentration and nature of the porgen is also of capital importance and will greatly influence the porosity of the formed particles. The speed and temperature of the second emulsion will impact the size of the particles and indirectly the size and amount of porosity. Indeed, in our case, the porogen mainly used gelatin which is temperature sensitive. By cooling our second emulsion at 0°C, we assured the maintaining of the microparticles of gelatin formed during the first emulsion, which form the porosities of the bigger PLGA particles.

Furthermore, other parameters have a crucial importance, such as the cell culture parameters. Indeed, the cell culture and culture agitation time have a primordial role on the cell adhesion. To do so we first coated our microscaffolds with PLL and collagen coating. We then tested different cell agitation speeds and times and cell culture without agitation times. To compare the different conditions, we used alamar blue

assays and confocal imaging to evaluate the cell adhesion. For cells study in our work, we determined that an agitation speed of 50 rpm during 3 hours followed by a cell culture of 48 hours without agitation was the best condition, with the maximum adhesion for cells with microscaffolds. Of note, for other type of cells, new agitation speed and time would need to be investigated.

3.2 Peridontal ligaments cells (PDLSc)

Another cell type of stem cells was analyzed in this work: the PDLSc cells. We chose to work on models for periodontal regeneration. These cells showed a proliferation rate before printing very interesting, with an increase up to 400% with microscaffolds coated with PLL compared to cells alone (Figure 19). The cell viability when bioprinted was also increased by 10% when printing with microscaffolds coated with collagen compared to cells printed alone (Figure 20).

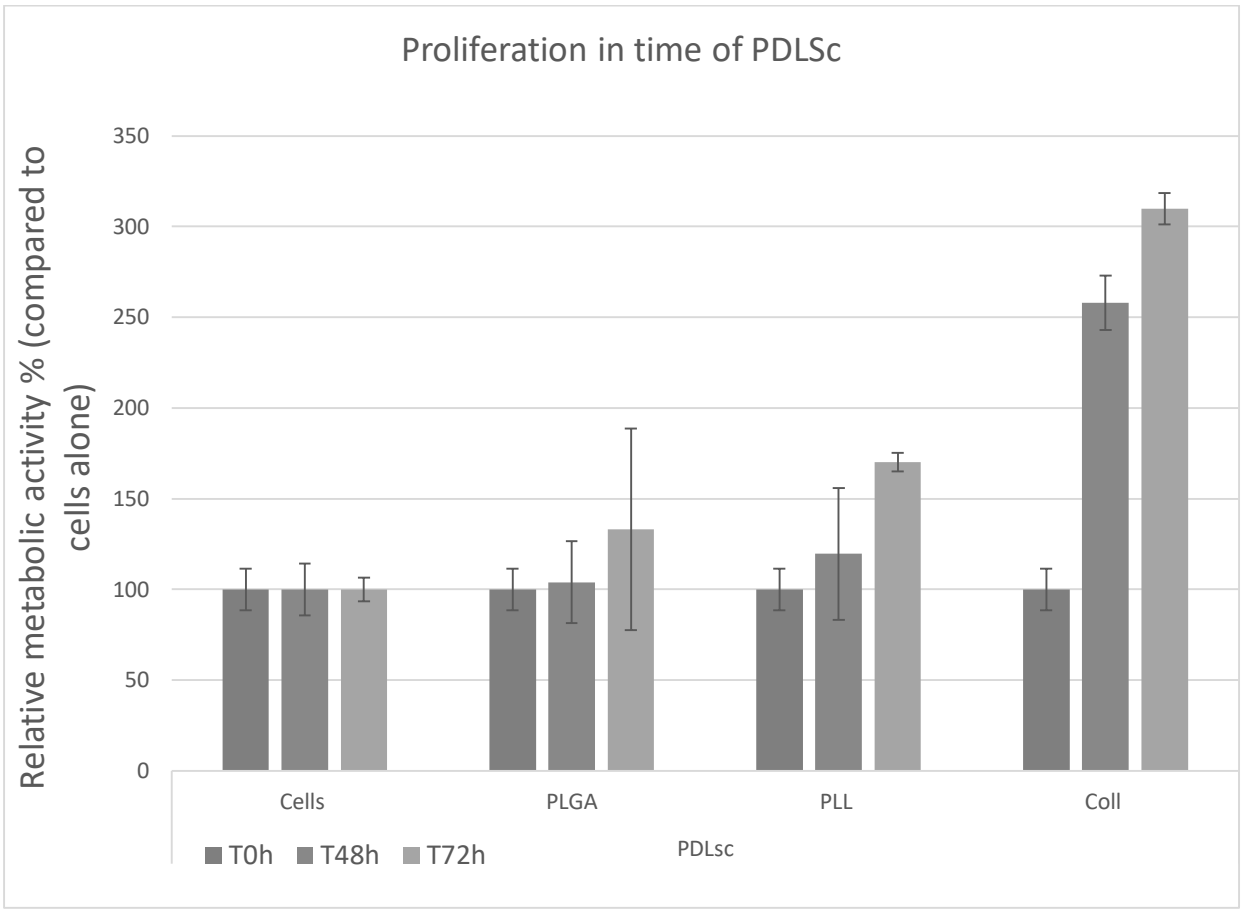

Figure 19 Metabolic activity of PDLSc cells before printing

PDLSc cell proliferation **on the microscaffolds coated with Collagen and PLL.** Proliferation was monitored after 48h and 72h of culture by resazurin measurements using alamar blue assay. 100% corresponds to the proliferation of cells alone for each time. Results are means of three independent experiments.

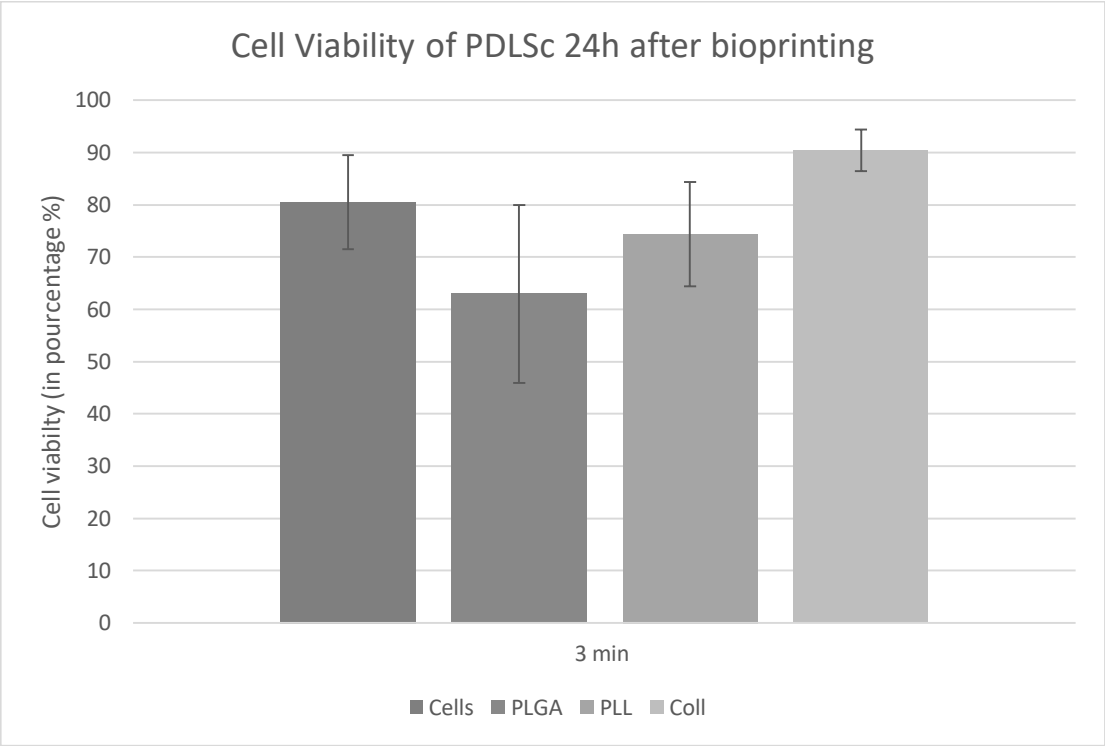

Figure 20 PDLSc cells viability 24h after bioprinting

PDLSc cell viability **on the microscaffolds coated with Collagen and PLL after 3 minutes of reticulation.** 100% corresponds to all the cells alive. Results are means of three independent experiments.

4. Conclusion

In this chapter, we have developed porous biodegradable porous PLGA microscaffolds and have demonstrated their benefic action for extrusion bioprinting. Indeed, the presence of the microscaffolds increased up to 4-fold the proliferation of chondrosarcoma cells, fibroblast cells, and dental pulp stem cells (DPSCs) before being incorporated within bioink (i.e. before printing) compared with those cultured without microscaffolds. The cell survival rate increased by 10% when bioprinting with coated microscaffolds compared to cells in bioink without microscaffolds. In addition, the microscaffolds allowed the migration of DPSCs stem cells towards HCS-2/8 cancer cells after 7 days of co-culture in a cellular construct created by bioprinting extrusion while without microscaffolds the cells aggregated and remained static meaning the production of a cellular model closer to the *in vivo* model when bioprinting with the microscaffolds.

These results could be enhanced by adapting the microscaffolds to the bioprinted cells, by adapting the cell culture conditions and coating. Indeed, it is possible to use generic microscaffolds with an average size adapted to most cells, an interesting coating of collagen which will increase the adhesion and have very interesting results as shown in this article. But each cell type, application, is different and to obtain optimal results, such as optimal cell adhesion, proliferation and thus viability, the size and coating of the microscaffolds should be investigated.

In the next chapter a direct application of our microscaffolds, was investigated for a medical application. Indeed, in the chapter 4, we investigated the use of our microscaffolds, and adapted them, to produce a new type of diaphragmatic patch with membranes of bovine serum albumin (BSA) and muscular cells.

Chapitre 4: Bioprinting muscular cells onto BSA membranes for diaphragm regeneration

1. Introduction

Following our first study and after having demonstrated the interest of the porous microscaffolds in bioprinting, we studied a direct application of this technology with the pediatrician Dr. Isabelle Talon. Indeed, bioprinting can be used to print patches and tissues to help heal damaged tissue. In this context, we collaborated with Dr. Isabelle Talon to study a new model of diaphragmatic patches by bioprinting muscular cells on BSA membranes to help heal Congenital diaphragmatic hernia (CDH). CDH is a malformation of the diaphragm where a hole is formed in the diaphragm during the development of the tissue. To help heal this malformation patches are implanted on the diseased area. Unfortunately, the patches used today are not ideal and in some cases new surgeries are necessary to implant new patches and remove the prior ones. For this reason, a new generation of diagrammatic patches is needed. In a previous work, Dr. Talon *et al* have worked on the functionalization of polytetrafluoroethylene (e-PTFE) membranes (Talon *et al.*, 2019). However, these membranes are non-biodegradable. To remedy this, in this study we choose to work with bovine serum albumin (BSA) membranes produced by *Albupad*, which are biodegradable and cytocompatible membranes. By combining these novel membranes with extrusion bioprinting, we were able to print muscular cells into precise structures to reproduce the configuration of the diaphragm. To increase the cellular density and cellular viability before and after bioprinting, two major limitations of this technology, we used porous PLGA microscaffolds. Indeed, in our previous work, we demonstrated the enhancement of cell proliferation before and printing and the increase in cell viability by protecting them during the extrusion process.

In this work, we found that during cell culture under agitation, the cell proliferation of the muscular cells was increased two fold with coated microscaffolds before printing. When printing muscular cells in well plates, the addition of the coated microscaffolds increased the viability by 29%. Finally, we found that 7 days after bioprinting the presence of the microscaffolds in combination with one type of BSA membrane increased the cellular proliferation inside the bioprinted construct by 655%.

These results are presented in the form of a draft article.

2. Paper draft

Bioprinting muscle patches for the treatment of Congenital diaphragmatic hernia on BSA membranes.

1. Introduction

Congenital diaphragmatic hernia (CDH) is a naturally occurring malformation, where a hole appears in the diaphragm during the development of the fetus. The diaphragm is a thin layer of muscle and tendon separating the chest cavity and abdominal cavity and is the principal muscle in the respiratory system in humans. With the contraction of the diaphragm a depression is created in the lungs leading to the inspiration of air. The expulsion of air is done with the relaxation of the diaphragm. When a hole occurs in this organ, during the fetus development, organs such as the bowls, lever or stomach can crowd the chest cavity. The presence of additional organ in the chest cavity can lead to respiratory complications and death. CDH occurs in 1 in 2 500 births without having determined causes (The Congenital Diaphragmatic Hernia Study Group, 2007).

In the case of mild CDH, few complications and negative effects on the development of lungs occur and the treatment can be delayed after the birth to surgically close the hole in the diaphragm. To close the defect, surgically implanted biomaterials are used such as membranes of polytetrafluoroethylene (e-PTFE), a synthetic non-degradable biomaterial. This membrane, which has been functionalized (Talon *et al.*, 2019), helps news cells colonize the newly formed tissue. But these biomaterials are not biodegradable are often supplementary surgeries are needed to replace the membranes with the growth of the patient. Furthermore, cell adhesion and colonization are not optimal, thus, new biomaterials and inoculation methods are needed.

Therefore, in this work, we implemented the use of membranes of bovine serum albumin (BSA, from Albupad) to produce new patches for diaphragm defaults combined with the emerging technology of extrusion bioprinting with PLGA microscaffolds (Rousselle *et al.*, 2022) to enhance proliferation, viability and cell colonization before and after printing.

Indeed, bioprinting has been used in tissue engineering (Murphy and Atala, 2014) as it has the ability to create complex 3D structures with an organization and functionality similar to native tissues. This is due in part to the precise placement of bioprinted cell and the precise control of the cellular environment. Extrusion bioprinting is the most used technology today but has limitations such as the cell concentration needed to reproduce tissues and organs and the low viability rate due to shear stress. In our previous work, we demonstrated that porous PLGA microscaffolds enhanced the cell proliferation cell viability.

In this work we adapted PLGA microscaffolds to bioprinting muscular cells. We first determined the most adapted microscaffold coating and 3D cell agitation to enhance the cell proliferation before bioprinting. We tested different coatings, the first one of collagen and the second one of Pol-Lysine (PLL) and determined the best condition to achieve the highest proliferation rate of our muscular cells. Following this, we bioprinted the muscular cells on two different BSA membranes. The first membrane is produced by mixing $CaCl_2$ with BSA and the second by mixing NaBr with BSA. To bioprint our cells we worked with a bioink created and characterized in the work of Oliveira *et al* (Oliveira *et al.*, 2021). We then determined wheter the microscaffolds and membranes affected cell viability at 24 hours and 7 days after printing. Indeed, the shear stress would affect the viability of the cells during the first 24 hours after printing, whereas the membranes would have an effect on the viability later in time after the bioprinting. We also determined the effect of the microscaffolds and the membranes on the proliferation of the bioprinted muscular cells 7 days after bioprinting.

Finally, the differentiation of the muscular cells into mature myotubes was induced. The adhesion and colonization of the muscular cells on the BSA membranes was also determined.

2. Materials and methods

a. PLGA microscaffolds synthesis

Poly (D,L-lactide-co-glycolide) PLGA (lactide-glycolide ratio of 50-50, ref P2191), Mowiol®, PVA (Polyvinyl alcohol, ref 81383), DCM (Dichloromethane, ref 270997)

Bovine skin gelatin (ref G9391) were purchased from Sigma Aldrich. The porous PLGA microscaffolds were prepared following a double emulsion technique using gelatin as porogen. The process is described in our previous study.

The characterization of the microscaffolds is detailed in the same study. In addition, before each experiment with the microscaffolds, their size and porosity are determined by optical imaging with the **Keyance VHX digital microscope**.

b. Surface Treatment and coating

Different coatings were tested to increase the cell adhesion on the microscaffolds (data not shown) and the condition selected is a coating of PLL.

To obtain this PLL coating, the PLGA microscaffolds were filtered using a 140 µm nylon mesh (Sigma) and immersed in a 0.25 M NaOH solution at room temperature for 30 minutes under agitation. PLGA microscaffolds were then washed three times with DW and immersed for 24 hours in a 1 mg/mL PLL, in Tris NaCl 0.25M, solution at 4°C overnight. After etching and/or coating, the microscaffolds were washed with DW and lyophilized for further uses and stocked at 4°C.

c. Albupad membrane production and characterization

The fabrication protocol and characterization are described in the work of *Aloui et al.* Briefly, NaBr and $CaCl_2$ salts are mixed with bovine serum albumin (BSA) and evaporated into specific molds.

d. Cell preparation and culture

C2C12 Murrin myoblast cell line is a subclone (produced by H. Blau, et al) of the mouse myoblast cell line established by D. Yaffe and O. Saxel purchased from ATCC (CRL-1772). The cells were cultured in DMEM high glucose and supplemented with 20% and 100 units/mL of penicillin, 100 mg/mL streptomycin in an incubator at 37°C and 5% CO_2. Cells are cultured and before reaching 70% confluence, they were removed with

trypsine (Dutscher, L0615-500) and used for experimentation. Cells were used from passages 8 to 25.

C2C12 grow as undifferentiated myoblasts when cultured in this cell medium. When replacing the cell medium with a medium enriched with 2% horse serum, the C2C12 differentiate into mature myotubes.

e. Cell expansion with PLGA-PLL coated microscaffolds

Before printing, bioreactors are used to culture the cells in bioreactors with and without microscaffolds to increase the number of cells available for the bioprinting process. The microscaffolds of PLGA-PLL were used at a concentration of 10mg of microscaffolds for 1 mL of cell medium and with 5 x 10^5cells/mL. The cell culture was done in sterile 50 mL bioreactor tubes (Tubespin® Bioreaktor 50). Cell culture by 3D agitation with microscaffolds and bioreactors was adapted from a study of (Smith *et al.*, 2019). To increase the adhesion of cells on the microscaffolds in the bioreactors. We proceeded as follows: The microscaffolds were put in the bioreactors at a concentration of 10mg/mL and sterilized with the UV lamp BioGlow® with an intensity of 6W and a wavelength of 365nm and used at 3cm of the particles. The cells were detached from their cell culture flask with a mild trypsin solution. The trypsin treatment was stopped with the suspensions of the cells in fresh cell medium with serum and counted with a Neubauer chamber. The cells were then seeded into the bioreactors with and without microscaffolds at a concentration of 5 x 10^5cells/mL. The bioreactors were then agitated at 50rpm in an incubator, at 37°C and with 5% CO_2, during 3 hours. After the agitation, the bioreactors were left in the incubators for 72 hours before extracting the cells and microscaffolds for bioprinting.

f. Bio-ink preparation and characterization

The hydrogel used to produce the bioink was composed of CollMa collagen methacrylate 0.2% (w/v), HAMA hyaluronic acid methacrylate 2% (w/v) and gelatin 5% (w/v). The preparation of the hydrogel is detailed in our previous study (Rousselle

et al., 2022) and is adapted from the study of Oliveira *et al* (Oliveira *et al.*, 2021). Briefly the hydrogel is prepared by mixing a gelatin solution with HAMA and a neutralized CollMa solution with the photoinitiator LAP (final 0.1% (w/v)). Gelatin was included in the formulation as a hydrogel support, as it increases the mechanical strength of the bioink during printing. This bioink is doubly reticulated, a first reticulation of the gelatin with the temperature of the printing platform (10°C), to improve the structural integrity. Secondly, a UV reticulation in induced with a UV lamps. After the second reticulation, the gelatin was removed with successive baths of heated PBS or cell medium at 37°C, leaching the gelatin without losing cells or structural integrity, as previously shown by the team of L. Ouyang et al (Ouyang *et al.*, 2020). The hydrogel without cells are designated as biomaterial inks, and the ones including live cells are designated as bioinks. The cells were added to the biomaterial ink by removing the cell medium from the bioreactors with a centrifugation and gently adding the ink. The newly formed bioink was homogenized and printed right after.

g. Cell metabolic activity evaluation

The metabolic activity or cell proliferation of the cells before and after printing was evaluated with and without the microscaffolds. This metabolic activity was evaluated using the Alamar Blue™ assay (O'Brien *et al.*, 2000). Alamar Blue™ is a non-fluorescent compound which is reduced into a fluorescent product. The reduction is done by living cells (Gloeckner, Jonuleit and Lemke, 2001). Contrary to other viability or proliferation assays, Alamar blue™ is non-toxic and environment friendly, thus allowing to keep the same samples for all the time of the experiment. In this work, we establish a correlation between cellular activity measured by Alamar blue™ and cell proliferation as was done in the works of Gloeckner et al; 2001. Indeed, the rate of dye reduction is directly proportional to the number of viable cells present (O'Brien *et al.*, 2000), thus as a direct measure of the metabolic competence of cell cultures (Magnani and Bettini, 2000) resazurin reduction can give a cell proliferation index (Vega-Avila and Pugsley, 2011).

Before printing 5 x 10^5 cells by mL were seeded in bioreactors with and without microscaffolds with the appropriate culture medium. For the micro-scaffold condition, the concentration was 10 mg / mL of microscaffolds. The metabolic evaluation was done at T0, T24 hours, T72 hours and T168 hours. 6 mL of cell medium with resazurin

(10% (v/v)) was added to each well and the bioreactors were incubated at 37 °C for 2 h. Subsequently, 300µL of supernatant was transferred to dark 96 wells and the fluorescence was measured (excitation 640 nm, emission 690 nm, SAFAS, Xenius XC, Safas Monaco). Such measurements were done at T0h, T48h, and T72h. The metabolic activity was calculated with the difference between the measurement and a blank composed of cell medium with 10% resazurin.

h. Statistical experiments

The results and data are shown for two independent experiments. All data are shown as means ± standard deviations. All statistical analyses were performed using the SigmaPlot v. 14.0 software and the analysis were done with the test (ANOVA) by an appropriate pairwise comparison or comparison versus control group procedure ($P < 0.05$ considered significant).

i. Cell viability

Cell viability percentage, after printing, was determined using the PromoKine Apoptotic / Necrotic / Healthy Cells Detection Kit. Briefly, cells were stained with Annexin V-FITC (green for apoptotic cells), Hoechst 33342 (blue for viable cells) and EthD-III (red for dead cells) for 15 minutes, according to the kit's protocol. Stained cells were then analyzed using a Zeiss LSM 510 confocal microscope equipped with a x20/0.40na objective. Five random images by sample were taken. Using the software ImageJ 1.53c (http://rsb.info.nih.gov/ij/), the images were analyzed to determine the percentage of viable cells compared to apoptotic or necrotic cells. To do so, the total number of blue cells (live) per image were counted, compared to green and red cells (apoptotic and necrotic cells). 100% represents that all cells are alive in the experiment.

j. Extrusion Bioprinting

The 3D printer used for this study was a pneumatic extrusion based 3D bioprinter BioX (CellInk). The bioinks were loaded into 3cc syringe (CellInk), and 18G (0.8 mm diameter) conical tips (FTM Technologies, Nanterre, France) were used during the printing process. The geometry and the printing path was created using FreeCAD or Scl3er softwares. The slicing of the constructs was done either with the software Scl3er or the built in slicer of the BioX. For the printing, the parameters used were set within a range of 15 to 20 Kpa, with a displacement speed of 10 mm/s. The syringes were heated at 30°C and the printing bed was set at 10°C. Immediately after printing, the printed structures were cross-linked using 365 nm UV light, for a duration of 3 minutes. After UV reticulation, the constructs were washed 3 times with cell medium or sterile PBS at 37°C to remove all the gelatin from the construct.

To print on the BSA membranes, the calibration was done manually and adjusted to account for the height of each membrane. All printed constructs were identical for each experiment and consisted of a block 10 by 10 mm with a height of 0.8mm and used the same STL and slicing parameters.

Six different conditions of bioprinting were tested, the first was the printing of cells without microscaffolds on the surface of a 12 well plate. The second was a printing of cells with microscaffolds on the surface of a 12 well plate. The third condition was the printing of cells without microscaffolds on the surface of a NaBr BSA membrane. The fourth condition was a printing of cells with microscaffolds on the surface of a NaBr BSA membrane. The fifth condition was the printing of cells without microscaffolds on the surface of a $CaCl_2$ BSA membrane. The sixth and last condition was a printing of cells with microscaffolds on the surface of a $CaCl_2$ BSA membrane. Table 2.1 summarized all bioprinting conditions with and without microscaffolds, as well as the surface on which bioprinting were performed.

TABLE 3.1 ALL BIOPRNTING CONDITIONS

/	With microscaffolds	On Well plate surface	On NaBr BSA	On $CaCl_2$ BSA
Condition 1	-	+	-	-
Condition 2	+	+	-	-
Condition 3	-	-	+	-
Condition 4	+	-	+	-
Condition 5	-	-	-	+
Condition 6	+	-	-	+

All extrusion bioprinting conditions for each experiment were done at the same time, in the same printing conditions, with a printing speed of 10 mm/s, a pressure of 15-20 Kpa and a temperature of nozzle of 30°C.

3. Results

a. PLGA microscaffolds of ideal size and porosity and two relevant coating

As showed in our previous work (Rousselle *et al.*, 2022), the produced microscaffolds have an average size of 102.8 µm ± 15.8 µm and 91.12% of the pores on the microscaffolds have a size superior to 8 µm. The microscaffolds are filtered through 140 µm meshes membranes. These results show that the size and porosities are of sufficient dimension to allow cells adhere and penetrate the microscaffolds. Indeed, microcarriers usually have a size between 60-400µm (Ayyildiz-Tamis, Avcı and Deliloglu-Gurhan, 2014; Levato *et al.*, 2014) and the 140 µm filtration prevents the printing nozzle from clogging with the microscaffolds.

Collagen and PLL coatings have been demonstrated to increase cell adhesion on PLGA surfaces (Zheng *et al.*, 2019; Dhamecha *et al.*, 2020). These coatings were performed as described in Rousselle et al (Rousselle *et al.*, 2022).

b. Collagen and PLL coated microscaffolds enhance C2C12 cell proliferation before printing

The cell activity of C2C12 cells was evaluated and increased 2.1 times at 72h when cultured with PLL coated microscaffolds compared to cells without microscaffolds. At 48h, the cell activity of PLL-coated microscaffodls was 1.4 fold higher than that of cells alone at T0. For collagen coated microscaffolds, we first observe a decrease in cell proliferation, with a decrease of 37.5% compared to cells alone at T0. At 72 hours of culture, cells cultured with collagen coated microscaffolds have the same cell activity as cells alone at T0. For microscaffolds without coating, there is a decrease of 10.5% of the cell proliferation at 48 hours of culture compared to cells alone at T0. Finally, there is no difference in cell activity between cells culture alone and cells cultured with uncoated PLGA microscaffolds at 72 hours of culture (Figure 21).

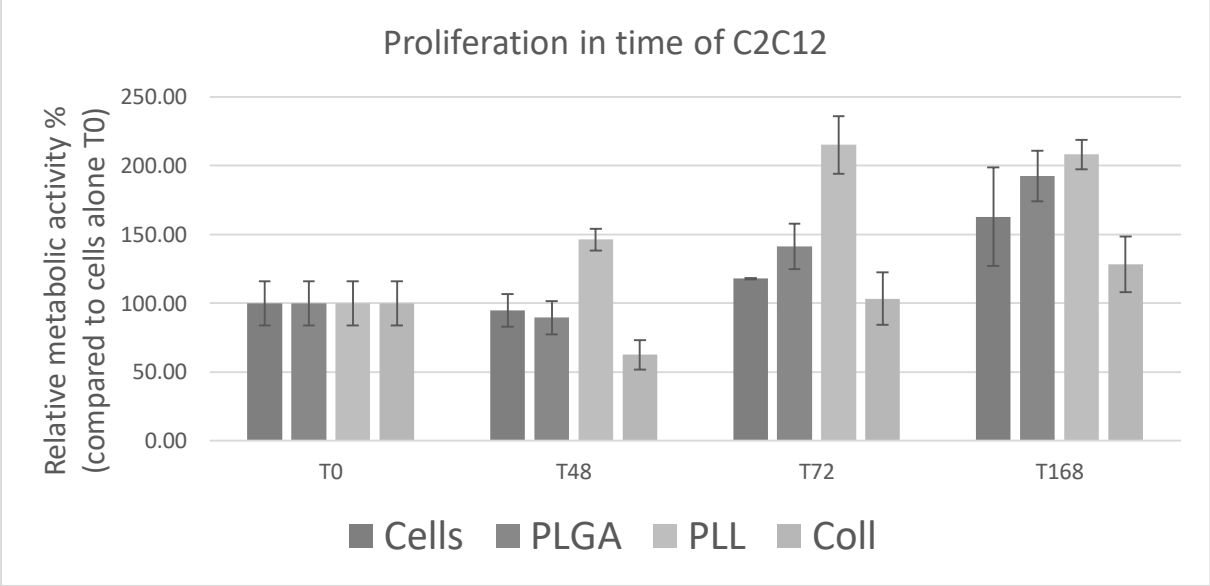

Figure 21 Relative metabolic activity of C2C12 cells before printing

C2C12 **cell proliferation on the microscaffolds coated with PLL, Collagen and without coating.** Proliferation was monitored after 48h, 72h and 168h of culture by resazurin measurements using alamar blue assay. 100% corresponds to the proliferation of cells alone for each time. Results are means of three independent experiments.

TABLE 4.1 SUMMARY RELATIVE METABOLIC ACTIVITY OF C2C12 CELLS BEFORE BIOPRINTING

Time/Condition	Cells	PLGA	PLL	Collagen
48 hours	94.7 %	89.5 %	146.2 %	62.5 %
72hours	117.9 %	141.2 %	**215.1 %**	103.3 %
168 hours	162.9 %	192.5 %	208.0 %	128.3 %

In summary, there is an increase in cell proliferation for the C2C12 cells when they are cultured in the presence of PLL coated microscaffolds compared to those cultured without microscaffolds. Cell proliferation is highest when cultured for 72 hours with PLL-coated microscaffolds.

c. *Cell proliferation is increased with PLL coated microscaffolds and NaBr membranes after bioprinting*

Having found the most adapted cell culture conditions and coatings for C2C12 cells, we bioprinted our precellurized PLL coated microscaffolds and cells alone on our BSA membranes. We printed the six conditions described in *Fig 1.* The cell activity of our cells inside the bioink products was measured.

We demonstrated that as before printing, without the BSA membranes, the adding of the PLL coated microscaffolds the cell activity was increased by 2.0, 7 days after printing.

There is no difference when printing on $CaCl_2$ BSA membranes when printing with or without microscaffolds. The cell activity is even decreased by 40% compared to cells alone bioprinted on well plates.

When printing on NaBr BSA membranes without microscaffolds, we also have a 40% decrease in cell activity compared to cells alone bioprinted on well plates. But when bioprinting on NaBr BSA membranes with PLL-coated microscaffolds, there is a 500% increase in cell activity compared to cells alone bioprinted on a well plate. The cell activity of bioprinted constructs is also increased by 2.5 compared to cells printed with PLL coated microscaffolds in well plates (Figure 22 and Table 4.2).

We also inoculated, without bioprinting, NaBr BSA and $CaCl_2$ membranes with C2C12 cells and compared, after one week, the metabolic activity of the cells with that of C2C12 cells in a well-plate (Figure 23 and Table 4.3).

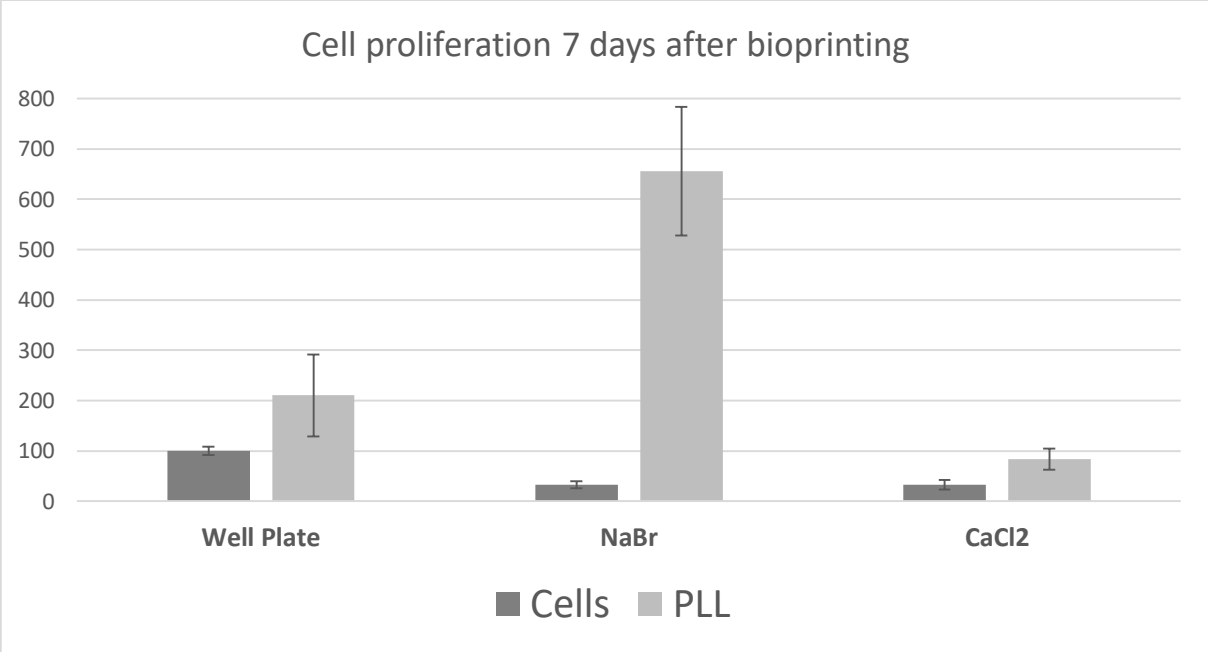

Figure 22 Survival rate of C2C12 cells one week after bioprinting

C2C12 cell proliferation on the microscaffolds coated with PLL, on well-plate, NaBr BSA and $CaCl_2$ BSA membranes. Proliferation was monitored after one week after bioprinting by resazurin measurements using alamar blue assay. 100% corresponds to the proliferation of cells alone. Results are means of three independent experiments.

TABLE 5.3 SUMMARY RELATIVE METABOLIC ACTIVITY OF C2C12 ONE WEEK AFTER BIOPRINTING

	Well Plate	NaBr	$CaCl_2$
Cells Alone	100 %	32.7 %	32.4 %
PLL	210.4 %	**655.5 %**	83.5 %

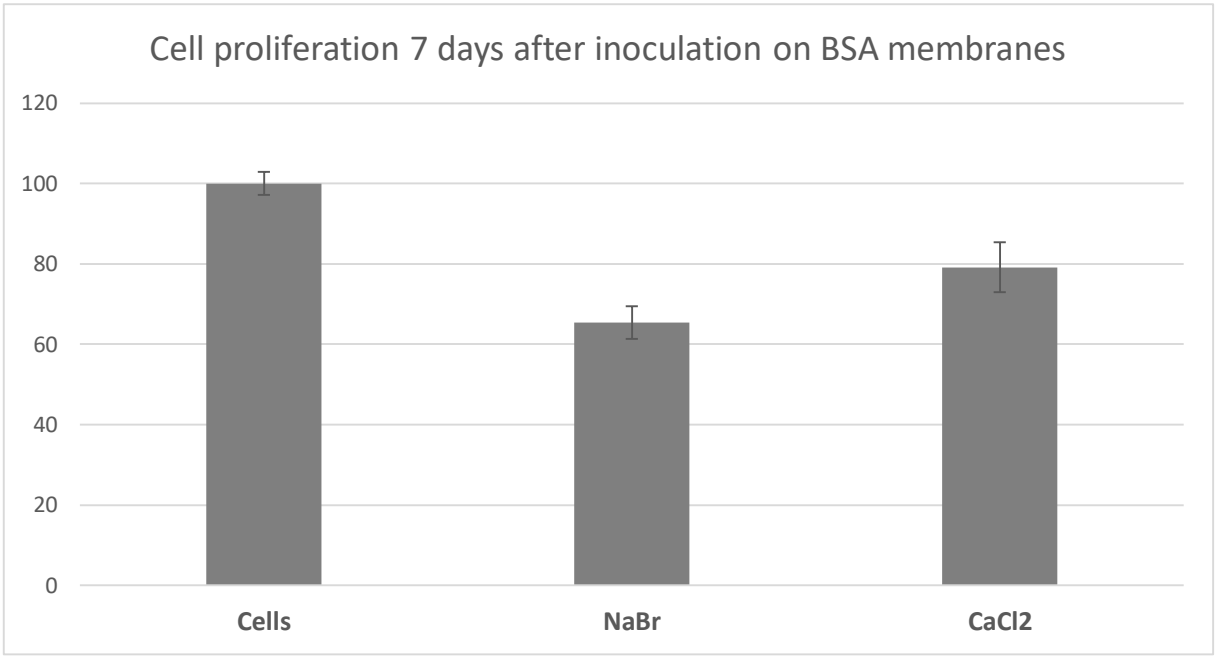

Figure 23 Relative metabolic activity of C2C12 cells one week after inoculation

C2C12 cell proliferation **on well-plate, NaBr BSA and $CaCl_2$ BSA membranes.** Proliferation was monitored after one week after inoculation by resazurin measurements using alamar blue assay. 100% corresponds to the proliferation of cells alone. Results are means of three independent experiments.

TABLE 6.4 SUMMARY RELATIVE METABOLIC ACTIVITY OF C2C12 ONE WEEK AFTER INOCULATION

	Well Plate	NaBr	$CaCl_2$
Cells Alone	100 %	65.4 %	79.1 %

To summarize, we can demonstrate the same increase in cell activity when printing cells with PLL-coated microscaffolds compared to cells printed without microscaffolds as before printing. When bioprinting on $CaCl_2$ BSA membranes with and without microscaffolds and when printing on NaBr BSA membranes without microscaffolds, we can observe a decrease in cell activity compared to products bioprinted with cells alone on well plates. But when bioprinting on NaBr BSA membranes with PLL coated microscaffolds, we can observe a significant increase of the cell activity.

d. Bioprinting with PLL coated microscaffolds on BSA membranes enhances C2C12 cell viability after bioprinting

24 hours and 7 days after bioprinting for our 6 conditions, we determined the cell viability of the C2C12 cells. Our data show that 24 hours after bioprinting C2C12 cells on well plates with and without microscaffolds, the survival rate in inferior to 65%. When printing on the BSA membranes (NaBr or $CaCl_2$) without microscaffolds, the survival rate is between 85-90%. We found the highest survival rate when bioprinting the C2C12 cells with PLL coated microscaffolds on the BSA membranes (NaBr and $CaCl_2$) with survival rates superior to 95% and no significant difference between NaBr and $CaCl_2$ membranes.

After 7 days the viability rate of all conditions is above 95% with no significative difference between the 6 conditions.

In conclusion, we can observe that bioprinting with BSA membranes improves cell viability at 24 hours and that bioprinting with PLL-coated microscaffolds on BSA

membranes yields the best cellular viability. After 7 days there are no more differences between the 6 conditions for the survival rate of C2C12 cells (Figure 24).

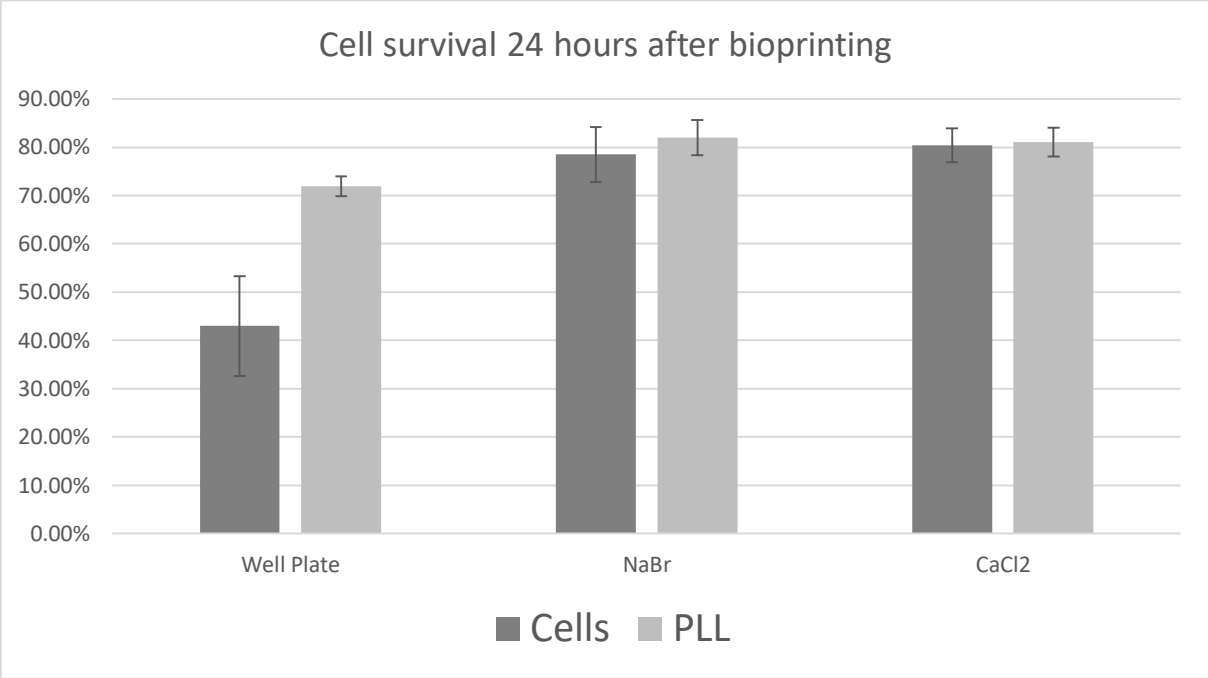

Figure 24 Survival rate of C2C12 cells one week after bioprinting

C2C12 cell viability on the microscaffolds coated with PLL on well-plate, NaBr BSA and $CaCl_2$ BSA membranes. 100% corresponds to all the cells alive. Results are means of three independent experiments.

TABLE 7.5 SUMMARY SURVIVAL CELL RATE 24H AFTER BIOPRINTING

	Well Plate	**NaBr**	**$CaCl_2$**
Cells Alone	43.0 %	78.5 %	80.4 %
PLL	71.9 %	82.0 %	81.1 %

e. Colonization of BSA membranes after bioprinting

C2C12 muscular cells can be differentiated into mature myotubes to form the precursors to muscle tissue. When adding horse serum to the cell culture medium C2C12 cells are differentiated into mature myotubes. Futhermore, we could observe mature myotubes not only in the bioprinted constructs but also on NaBr BSA

membranes, outside the bioink. The cells were able to migrate from the bioink onto the NaBr BSA membrane and colonize it (Figure 25). This wasn't observed on $CaCl_2$ BSA membranes but could be due to the difficulties of observing the surface of the $CaCl_2$ BSA membranes.

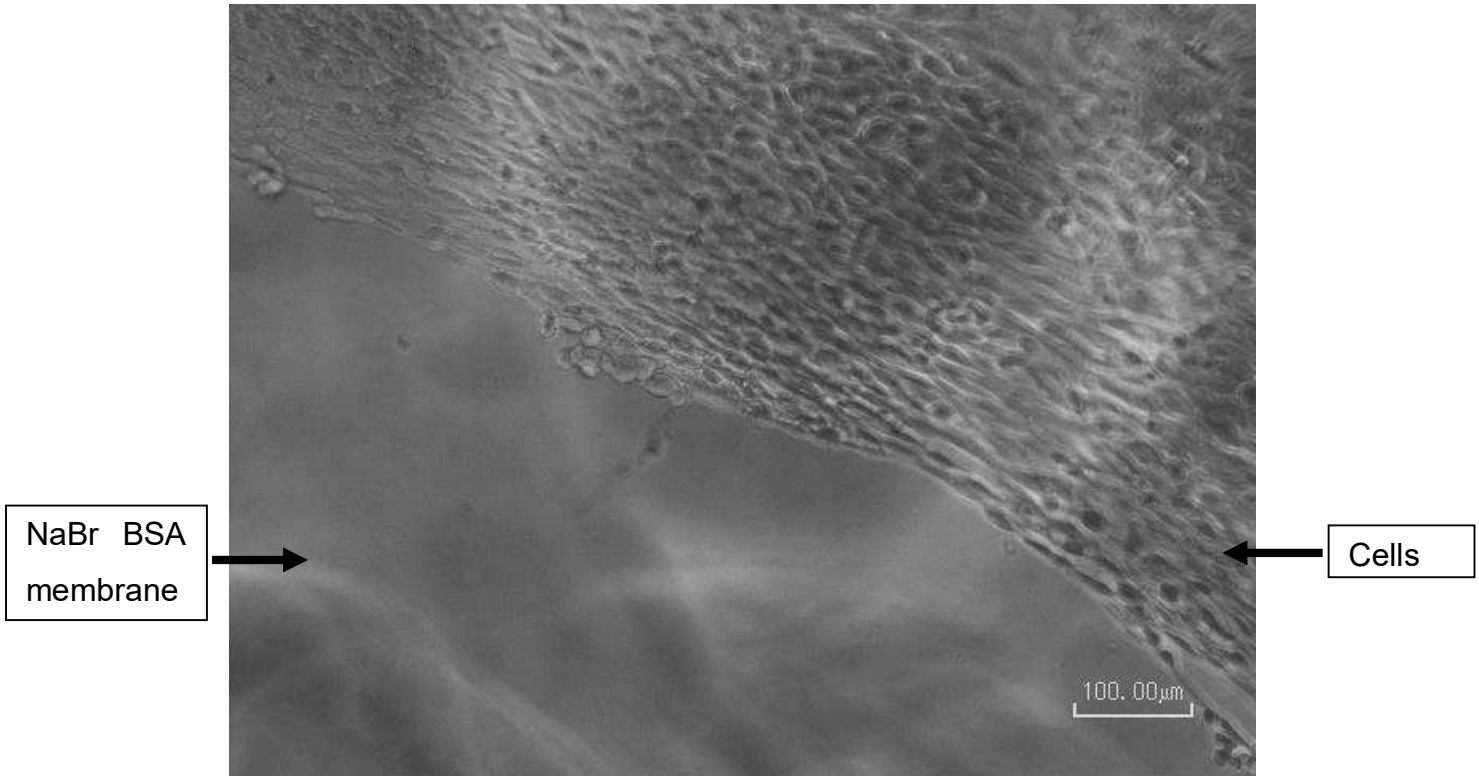

Figure 25 C2C12 adhesion on NAbR BSA membranes one month after bioprinting

C2C12 cell adhesion on NaBr BSA membranes one month after bioprinting. Adhesion was observed by optical imaging and confocal imaging.

4. Discussion

Cell proliferation before printing. When bioprinting any tissue or cell construct, the number of cells needed is considerable. Indeed, according to McClelland *et al* (McClelland *et al.*, 2012), there are between 10^9 and 10^{11}cells by mL in any human tissue or organ. Such numbers are needed for the biofabrication of tissues or constructs mimicking human tissue. The production of this quantity of cells is often complicated and would necessitate important resources in cell medium and time. Thus, the use of our PLL coated PLGA microscaffolds for the cell culture of the C2C12 cells before bioprinting allows us to have more cells, faster and at lower cost. Indeed, the microscaffolds increase the surface area where cells can proliferate and the PLL coating increase the cell adhesion to the surface of our microscaffolds. This two fold increase in proliferation with our PLL coated microscaffolds could be further increased with the use of spinner flask, instead of individual bioreactors, with large volumes and more agitation cycles.

Cell proliferation 7 days after printing. As for the results of cell proliferation before bioprinting, the cells with microscaffolds have an increase in cell activity compared to cells alone. The microscaffolds provide an additional surface on which cells can proliferate. Regarding bioprinted cells on BSA membrane, the cells can proliferate on coated microscaffolds, in the bioink but also on BSA membranes. Since the NaBr BSA surface is attractive to C2C12 cells, the proliferation rate of the cells is increased compared to cells printed with microscaffolds on well plates. This is not the case with the $CaCl_2$ BSA membrane, which does not increase the metabolic activity of the cells. It appears that the NaBr BSA membrane is attractive to the cells and allow cell adhesion and proliferation after printing, thus increasing cellular activity with the microscaffolds. Indeed, when inoculating the membranes without bioprinting and without microscaffolds, there is a decrease of the cellular activity after 7 days compared to a culture in a well-plate.

Cell survival at 24 hours after bioprinting. During the extrusion bioprinting process, cells are exposed to shear stress which can damage, kill or incapacitate the cells (Zhao *et al.*, 2015; Ning, 2020). This will have an effect on the cell viability and will be visible 24 hours after the extrusion process which for extrusion bioprinting can range from 40-

86% (Murphy and Atala, 2014). In extrusion bioprinting of C2C12 cells without microscaffolds, the survival rate is very low, bellow 43%. With microscaffolds, it is increased to 72%. But when printing on BSA membranes, with and without microscaffolds, the survival rate is increased to 80%. This can be explained by the fact that the surface of the well plates is stiffer than the BSA membranes, which increases the shear stress applied to the cells when printing in well plates. When printing on the BSA membranes the shear stress is reduced but not completely harmless for the cell. We can deduce this from the increase in cell viability when printing on BSA membranes with PLL coated microscaffolds. Indeed, the microscaffolds can further protect the cells from the shear stress during the extrusion process, increasing the viability rate. We can observe this when comparing the survival rate of cell printed alone in well plates to cells printing with microscaffolds in well plates which have a higher survival rate.

The best condition, where the shear stress is the most reduced for the cells, is obtained when printing with PLL-coated microscaffolds and on the softer surface of BSA membranes.

Cell survival at 7 days after bioprinting. 7 days after printing shear stress will have no effect on the survival rate but the bioink will. In this case, we used the bioink used in our previous work, adapted from the work of Oliveria et al (Oliveira *et al.*, 2021). This bioink was created and tunned to be environment friendly for cells, having very good cell viability rates. Thus, explaining the very high cellular viability of the C2C12 cells in all 6 conditions 7 days after printing.

C2C12 cell colonization on NaBr BSA membranes Indeed, for NaBr BSA membranes, a layer of myotubes was able to colonize the surface of the membranes in the same space as the bioprinted products even after removing the construct. This could demonstrate that the bioprinted construct could be progressively replaced by muscular tissue. Muscle tissue could take the space of the bioprinted product after differentiation of the C2C12 cells.

Conclusion

Our results show a two-fold increase in proliferation before and after bioprinting with the aid of our adapted microscaffolds for C2C12 cells. These microscaffolds aid in the

cell survival against the shear stress induced by the extrusion process, which is enhanced by the bioprinting on BSA membranes. These BSA membranes have also been shown to allow the differentiation of the muscular cells into mature myotubes.

In this study, NaBr BSA membranes paired with PLL-coated microscaffolds showed the most promise, with the highest cellular activity before printing and 7 days after printing. This condition demonstrated the highest survival rate. Finally, NaBr BSA membranes enabled the colonization of cells on their surface with mature myotubes, the first step in the production of mature tissue able to replace or patch defects in the diaphragm.

In future studies, human myoblasts cells could be used to adapt with adapted microscaffolds and bioprinted into constructs with the same morphology and architecture than the diaphragm. The cellular activity, viability and maturation of the cells on the BSA membranes could be studied to work with the best conditions. This work could be the first step into the production of a new type of patches to help treat Congenital diaphragmatic hernia with cells extracted from the patient to recreate a functional diaphragm.

3. Perspective and conclusion

This study shows that bioprinting of muscular cells on biocompatible membranes BSA combined with coated microscaffolds improves cell proliferation and viability. Indeed, by adapting porous PLGA microscaffolds for C2C12 cells, the cellular proliferation increased by 100% before and after printing. When bioprinting with the coated microscaffolds in well plates, the cellular viability at 24h was increased by almost 30%. When bioprinting on the BSA membranes the cellular viability was above 80%. After 7 days, the cell viability for all conditions was higher than 95%. Finally, we were able to observe the colonization of the BSA-NaBr membranes with muscular cells directly on the membrane.

In future studies, we will print anatomically relevant structures (Figure 26 similar to the configuration of the diaphragm) with human myoblastsand tendon cells, to create viable patches to heal diseased diaphragms. Indeed, we are working with human myoblast cells by adapting our microscaffolds to these cells. This is the first step towards bioprinting patches with human muscular and tendon cells.

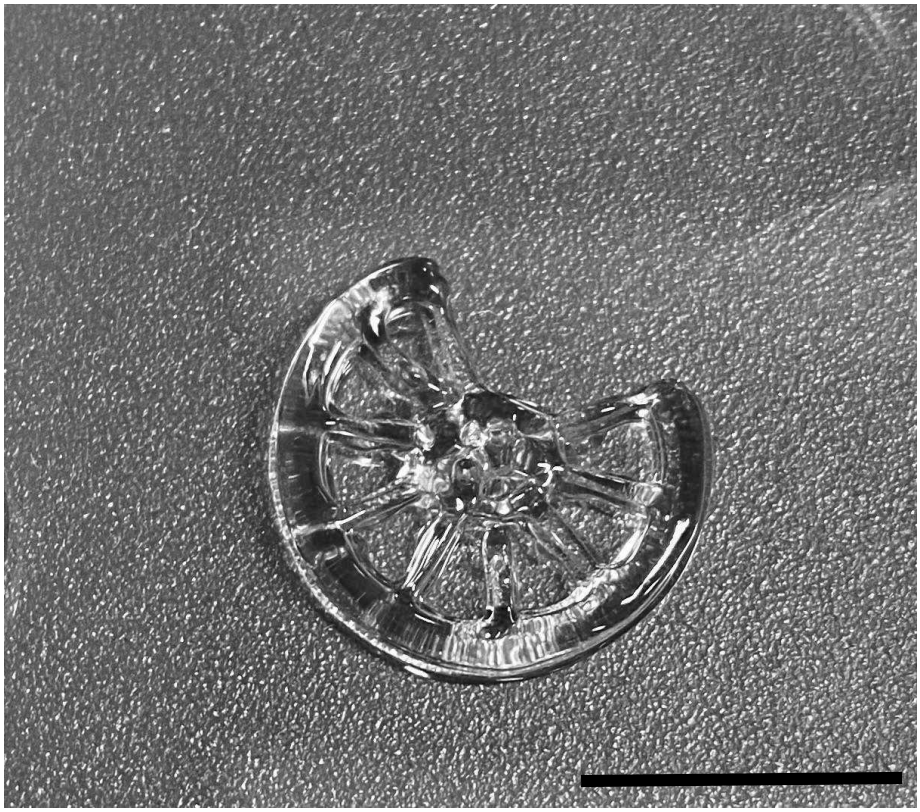

*Figure **26** Bioprinted diaphragm model*

Bioprinted diaphragm model, printed with BioX and ink cellink start using a 0.405mm nozzle. The axis represents muscular cells, to induce the direction of maturation of myoblastic cells into a desired direction. The center represents the tendon center. Scale bar 0.75 cm.

Furthermore, these patches could be made to completely replace diseased or absent diaphragms with patient-derived cells.

Conclusion and future work

Bioprinting is a powerful and versatile technology which can be used in numerous domains, from tissue engineering to drug discovery. In this work we have presented the different technologies of bioprinting. We have demonstrated the need for a solution for two significant limitations of extrusion bioprinting, the most frequent bioprinting technology. Indeed, the cell density and cell viability are lacking after and before bioprinting. The solution we have implemented is the production, adaptation and use of porous PLGA microscaffolds to act as proliferation surfaces for the cells before bioprinting, increasing the proliferation rates up to 450%. During the extrusion process the microscaffolds protect the cells and increase the cell viability 24 hours after printing. After printing, the use of microscaffolds increased stem cell migration towards cancer cells in an organoid cell construct, rendering the 3D model with microscaffolds more similar to the *in vivo* model and increasing cell proliferation up to 500%.

After producing and demonstrating these novel microscaffolds, we bioprinted new diaphragm patches on BSA membranes as a first model to treat congenital diaphragmatic hernia with the help of these microscaffolds. Indeed, we bioprinted myoblast cells in specific spatial configuration on the biocompatible membranes with our porous microscaffolds. The microscaffolds increased the cell proliferation before printing by 100%, increasing the amont of cells available before printing. By bioprinting with our microscaffolds, we were able to obtain a cell viability after 24 hours above 80% and a cell viability above 95% one week after printing. The use of the microscaffolds increased the cell proliferation by 500% one week after printing, demonstrating the benefic effect of the microscaffolds for the development of the muscular patch on BSA membranes. Finally, the cells printed with the microscaffolds, on the BSA membranes were able to differentiate into mature myotubes 4 weeks after printing. This study demonstrates the benefices in using the microscaffolds for tissue engineering, in proliferation rate before printing, cell viability during the printing process and tissue maturation in time.

These new PLGA microscaffolds are a new solution to render extrusion bioprinting more accible and reduce its two major limitations. The microscaffolds can be adapted to most cells and extrusion based applications.

Bioprinting is a revolutionary technology that could overcome organs shortages and find new drugs to treat the most serious diseases. But bioprinting is still in its infancy and new methods are needed. Thancks to these microscaffolds it is my conviction that bioprinting is a step closer to becoming a mature tissue engineering technology.

- Future work

This work is still in progress and a pre-maturation project is planned with the Satt Conectus and could lead to industrial applications.

We are also working to produce organoids to reproduce diseased organs with adapted PLGA microscaffolds. Indeed, as discussed before, scaffolds can be adapted and used to help produce organoids (Kaur *et al.*, 2021). These scaffolds help control the spatial positioning of the cells and limit the necrosis in the center of the cell aggregate. As was done by Dye *et al* (Dye *et al.*, 2020), we want to use the morphology of the scaffolds to promote cell maturation and control the organoid's size. To do so, we produced PLGA microscaffolds with an average size of 180µm with an important porosity. Indeed, we intend to use these scaffolds to create a porous 3D environment for the cell adhesion, proliferation and development of an organoid while diminishing the necrotic center of an organoid.

References

Ahmed, E.M. (2015) 'Hydrogel: Preparation, characterization, and applications: A review', *Journal of Advanced Research*, 6(2), pp. 105–121. Available at: https://doi.org/10.1016/j.jare.2013.07.006.

Arcaute, K., Mann, B.K. and Wicker, R.B. (2006) 'Stereolithography of Three-Dimensional Bioactive Poly(Ethylene Glycol) Constructs with Encapsulated Cells', *Annals of Biomedical Engineering*, 34(9), pp. 1429–1441. Available at: https://doi.org/10.1007/s10439-006-9156-y.

Augustine, R. *et al.* (2021) '3D Bioprinted cancer models: Revolutionizing personalized cancer therapy', *Translational Oncology*, 14(4), p. 101015. Available at: https://doi.org/10.1016/j.tranon.2021.101015.

Aydin, L., Kucuk, S. and Kenar, H. (2020) 'A universal self-eroding sacrificial bioink that enables bioprinting at room temperature', *Polymers for Advanced Technologies*, 31(7), pp. 1634–1647. Available at: https://doi.org/10.1002/pat.4892.

Ayyildiz-Tamis, D., Avcı, K. and Deliloglu-Gurhan, S.I. (2014) 'Comparative investigation of the use of various commercial microcarriers as a substrate for culturing mammalian cells', *In Vitro Cellular & Developmental Biology - Animal*, 50(3), pp. 221–231. Available at: https://doi.org/10.1007/s11626-013-9717-y.

Bae, S.E. *et al.* (2009) 'Fabrication of covered porous PLGA microspheres using hydrogen peroxide for controlled drug delivery and regenerative medicine', *Journal of Controlled Release*, 133(1), pp. 37–43. Available at: https://doi.org/10.1016/j.jconrel.2008.09.006.

Baier, C. *et al.* (2007) 'Hyaluronan is organized into fiber-like structures along migratory pathways in the developing mouse cerebellum', *Matrix Biology*, 26(5), pp. 348–358. Available at: https://doi.org/10.1016/j.matbio.2007.02.002.

Baier Leach, J. *et al.* (2003) 'Photocrosslinked hyaluronic acid hydrogels: Natural, biodegradable tissue engineering scaffolds', *Biotechnology and Bioengineering*, 82(5), pp. 578–589. Available at: https://doi.org/10.1002/bit.10605.

Bartfeld, S. and Clevers, H. (2015) 'Organoids as Model for Infectious Diseases: Culture of Human and Murine Stomach Organoids and Microinjection of Helicobacter Pylori', *Journal of Visualized Experiments*, (105), p. 53359. Available at: https://doi.org/10.3791/53359.

Bertassoni, L.E. *et al.* (2014) 'Direct-write bioprinting of cell-laden methacrylated gelatin hydrogels', *Biofabrication*, 6(2), p. 024105. Available at: https://doi.org/10.1088/1758-5082/6/2/024105.

Bhattacharjee, T. *et al.* (2015) 'Writing in the granular gel medium', *Science Advances*, 1(8), p. e1500655. Available at: https://doi.org/10.1126/sciadv.1500655.

Bible, E. *et al.* (2009) 'The support of neural stem cells transplanted into stroke-induced brain cavities by PLGA particles', *Biomaterials*, 30(16), pp. 2985–2994. Available at: https://doi.org/10.1016/j.biomaterials.2009.02.012.

Bishop, E.S. *et al.* (2017) '3-D bioprinting technologies in tissue engineering and regenerative medicine: Current and future trends', *Genes & Diseases*, 4(4), pp. 185–195. Available at: https://doi.org/10.1016/j.gendis.2017.10.002.

Blaeser, A. *et al.* (2016) 'Controlling Shear Stress in 3D Bioprinting is a Key Factor to Balance Printing Resolution and Stem Cell Integrity', *Advanced Healthcare Materials*, 5(3), pp. 326–333. Available at: https://doi.org/10.1002/adhm.201500677.

Boularaoui, S. (2020) 'An overview of extrusion-based bioprinting with a focus on induced shear stress and its effect on cell viability', p. 17.

Brassard, J.A. *et al.* (2021) 'Recapitulating macro-scale tissue self-organization through organoid bioprinting', *Nature Materials*, 20(1), pp. 22–29. Available at: https://doi.org/10.1038/s41563-020-00803-5.

Breathwaite, E. *et al.* (2020) '3D Bioprinted Osteogenic Tissue Models for In Vitro Drug Screening', *Molecules*, 25(15), p. 3442. Available at: https://doi.org/10.3390/molecules25153442.

Cao, X. *et al.* (2019) 'A Tumor-on-a-Chip System with Bioprinted Blood and Lymphatic Vessel Pair', *Advanced Functional Materials*, 29(31), p. 1807173. Available at: https://doi.org/10.1002/adfm.201807173.

Carmeliet, P. and Jain, R.K. (2000) 'Angiogenesis in cancer and other diseases', 407, p. 9.

Catros, S. *et al.* (2011) 'Effect of laser energy, substrate film thickness and bioink viscosity on viability of endothelial cells printed by Laser-Assisted Bioprinting', *Applied Surface Science*, 257(12), pp. 5142–5147. Available at: https://doi.org/10.1016/j.apsusc.2010.11.049.

Celikkin, N. *et al.* (2018) 'Gelatin methacrylate scaffold for bone tissue engineering: The influence of polymer concentration: GELATIN METHACRYLATE SCAFFOLD FOR BONE TISSUE ENGINEERING', *Journal of Biomedical Materials Research Part A*, 106(1), pp. 201–209. Available at: https://doi.org/10.1002/jbm.a.36226.

Chen, E.P. *et al.* (2021) '3D Bioprinting of Vascularized Tissues for in vitro and in vivo Applications', *Frontiers in Bioengineering and Biotechnology*, 9, p. 664188. Available at: https://doi.org/10.3389/fbioe.2021.664188.

Chen, Y.-C. *et al.* (2012) 'Functional Human Vascular Network Generated in Photocrosslinkable Gelatin Methacrylate Hydrogels', *Advanced Functional Materials*, 22(10), pp. 2027–2039. Available at: https://doi.org/10.1002/adfm.201101662.

Chew, D. *et al.* (2020) 'The Changing Face of in vitro Culture Models for Thyroid Cancer Research: A Systematic Literature Review', *Frontiers in Surgery*, 7, p. 43. Available at: https://doi.org/10.3389/fsurg.2020.00043.

Chimene, D., Kaunas, R. and Gaharwar, A.K. (2020) 'Hydrogel Bioink Reinforcement for Additive Manufacturing: A Focused Review of Emerging Strategies', *Advanced Materials*, 32(1), p. 1902026. Available at: https://doi.org/10.1002/adma.201902026.

'Chimene et al. - 2020 - Hydrogel Bioink Reinforcement for Additive Manufac.pdf' (no date).

Choi, S.-W. *et al.* (2010) 'Uniform Beads with Controllable Pore Sizes for Biomedical Applications', *Small*, 6(14), pp. 1492–1498. Available at: https://doi.org/10.1002/smll.201000544.

Christensen, K. *et al.* (2015) 'Freeform inkjet printing of cellular structures with bifurcations: Approach Freeform Fabrication of Bifurcated Cellular Structures by Using a Liquid Support-Based Inkjet Printing Approach', *Biotechnology and Bioengineering*, 112(5), pp. 1047–1055. Available at: https://doi.org/10.1002/bit.25501.

Chun, K.W. *et al.* (2004) 'Biodegradable PLGA Microcarriers for Injectable Delivery of Chondrocytes: Effect of Surface Modification on Cell Attachment and Function', *Biotechnology Progress*, 20(6), pp. 1797–1801. Available at: https://doi.org/10.1021/bp0496981.

Chung, H.J. *et al.* (2008) 'Highly Open Porous Biodegradable Microcarriers: *In Vitro* Cultivation of Chondrocytes for Injectable Delivery', *Tissue Engineering Part A*, 14(5), pp. 607–615. Available at: https://doi.org/10.1089/tea.2007.0263.

Clark (1939) 'Microscopic observations on the growth of blood capillaries in the living mammal', p. 51.

Correia Carreira, S., Begum, R. and Perriman, A.W. (2020) '3D Bioprinting: The Emergence of Programmable Biodesign', *Advanced Healthcare Materials*, 9(15), p. 1900554. Available at: https://doi.org/10.1002/adhm.201900554.

Costa, E.C. *et al.* (2018) 'Spheroids Formation on Non-Adhesive Surfaces by Liquid Overlay Technique: Considerations and Practical Approaches', *Biotechnology Journal*, 13(1), p. 1700417. Available at: https://doi.org/10.1002/biot.201700417.

Daly, A.C. *et al.* (2021) 'Bioprinting for the Biologist', *Cell*, 184(1), pp. 18–32. Available at: https://doi.org/10.1016/j.cell.2020.12.002.

Danhier, F. *et al.* (2012) 'PLGA-based nanoparticles: An overview of biomedical applications', *Journal of Controlled Release*, 161(2), pp. 505–522. Available at: https://doi.org/10.1016/j.jconrel.2012.01.043.

Datta, P. (2017) 'Bioprinting for Vascular and Vascularized Tissue Biofabrication', p. 59.

De Moor, L. *et al.* (2018) 'High-throughput fabrication of vascularized spheroids for bioprinting', *Biofabrication*, 10(3), p. 035009. Available at: https://doi.org/10.1088/1758-5090/aac7e6.

Decker, C. (2002) 'Kinetic Study and New Applications of UV Radiation Curing', *Macromolecular Rapid Communications*, 23(18), pp. 1067–1093. Available at: https://doi.org/10.1002/marc.200290014.

DeForest, C.A. and Anseth, K.S. (2012) 'Advances in Bioactive Hydrogels to Probe and Direct Cell Fate', *Annual Review of Chemical and Biomolecular Engineering*, 3(1), pp. 421–444. Available at: https://doi.org/10.1146/annurev-chembioeng-062011-080945.

Derakhshanfar, S. *et al.* (2018) '3D bioprinting for biomedical devices and tissue engineering: A review of recent trends and advances', *Bioactive Materials*, 3(2), pp. 144–156. Available at: https://doi.org/10.1016/j.bioactmat.2017.11.008.

Dhamecha, D. *et al.* (2020) 'Porous Polymeric Microspheres With Controllable Pore Diameters for Tissue Engineered Lung Tumor Model Development', *Frontiers in Bioengineering and Biotechnology*, 8. Available at: https://doi.org/10.3389/fbioe.2020.00799.

Dou, C. *et al.* (2021) 'A State-of-the-Art Review of Laser-Assisted Bioprinting and its Future Research Trends', *ChemBioEng Reviews*, 8(5), pp. 517–534. Available at: https://doi.org/10.1002/cben.202000037.

Dunne, M., Corrigan, O.I. and Ramtoola, Z. (2000) 'In#uence of particle size and dissolution conditions on the degradation properties of polylactide-co-glycolide particles', p. 10.

Dutta, D., Heo, I. and Clevers, H. (2017) 'Disease Modeling in Stem Cell-Derived 3D Organoid Systems', *Trends in Molecular Medicine*, 23(5), pp. 393–410. Available at: https://doi.org/10.1016/j.molmed.2017.02.007.

Dye, B.R. *et al.* (2020) 'Human lung organoids develop into adult airway-like structures directed by physico-chemical biomaterial properties', *Biomaterials*, 234, p. 119757. Available at: https://doi.org/10.1016/j.biomaterials.2020.119757.

Ehlinger, C. *et al.* (2021) 'Insensitivity of dental pulp stem cells migration to substrate stiffness', *Biomaterials*, 275, p. 120969. Available at: https://doi.org/10.1016/j.biomaterials.2021.120969.

Ehsan, S.M. *et al.* (2014) 'A three-dimensional in vitro model of tumor cell intravasation', *Integrative Biology*, 6(6), p. 603. Available at: https://doi.org/10.1039/c3ib40170g.

Elmowafy, E.M., Tiboni, M. and Soliman, M.E. (2019) 'Biocompatibility, biodegradation and biomedical applications of poly(lactic acid)/poly(lactic-co-glycolic acid) micro and nanoparticles', *Journal of Pharmaceutical Investigation*, 49(4), pp. 347–380. Available at: https://doi.org/10.1007/s40005-019-00439-x.

Essentials of 3D Biofabrication and Translation (2015). Elsevier. Available at: https://doi.org/10.1016/C2013-0-18665-5.

Fairbanks, B.D. *et al.* (2009) 'Photoinitiated polymerization of PEG-diacrylate with lithium phenyl-2,4,6-trimethylbenzoylphosphinate: polymerization rate and cytocompatibility', *Biomaterials*, 30(35), pp. 6702–6707. Available at: https://doi.org/10.1016/j.biomaterials.2009.08.055.

Fedorovich, N.E. *et al.* (2009) 'The effect of photopolymerization on stem cells embedded in hydrogels', *Biomaterials*, 30(3), pp. 344–353. Available at: https://doi.org/10.1016/j.biomaterials.2008.09.037.

Fennema, E. *et al.* (2013) 'Spheroid culture as a tool for creating 3D complex tissues', *Trends in Biotechnology*, 31(2), pp. 108–115. Available at: https://doi.org/10.1016/j.tibtech.2012.12.003.

Ferreira, A.M. *et al.* (2012) 'Collagen for bone tissue regeneration', *Acta Biomaterialia*, 8(9), pp. 3191–3200. Available at: https://doi.org/10.1016/j.actbio.2012.06.014.

Ford Versypt, A.N., Pack, D.W. and Braatz, R.D. (2013) 'Mathematical modeling of drug delivery from autocatalytically degradable PLGA microspheres — A review', *Journal of Controlled Release*, 165(1), pp. 29–37. Available at: https://doi.org/10.1016/j.jconrel.2012.10.015.

Forget, A. *et al.* (2017) 'Mechanically Tunable Bioink for 3D Bioprinting of Human Cells', p. 7.

Fu, K. *et al.* (2000) 'Visual Evidence of Acidic Environment Within Degrading Poly(lactic-co-glycolic acid) (PLGA) Microspheres', p. 7.

Gao, Q. *et al.* (2015) 'Coaxial nozzle-assisted 3D bioprinting with built-in microchannels for nutrients delivery', *Biomaterials*, 61, pp. 203–215. Available at: https://doi.org/10.1016/j.biomaterials.2015.05.031.

Garcez, P.P. *et al.* (2016) 'Zika virus impairs growth in human neurospheres and brain organoids', *Science*, 352(6287), pp. 816–818. Available at: https://doi.org/10.1126/science.aaf6116.

Gaspar, V.M. *et al.* (2019) 'Advanced Bottom-Up Engineering of Living Architectures', *Adv. Mater.*, p. 41.

Gasperini, L., Mano, J.F. and Reis, R.L. (2014) 'Natural polymers for the microencapsulation of cells', *Journal of The Royal Society Interface*, 11(100), p. 20140817. Available at: https://doi.org/10.1098/rsif.2014.0817.

Gauvin, R. *et al.* (2012) 'Microfabrication of complex porous tissue engineering scaffolds using 3D projection stereolithography', *Biomaterials*, 33(15), pp. 3824–3834. Available at: https://doi.org/10.1016/j.biomaterials.2012.01.048.

Gjorevski, N. *et al.* (2022) 'Tissue geometry drives deterministic organoid patterning', *Science*, 375(6576), p. eaaw9021. Available at: https://doi.org/10.1126/science.aaw9021.

Gloeckner, H., Jonuleit, T. and Lemke, H.-D. (2001) 'Monitoring of cell viability and cell growth in a hollow-fiber bioreactor by use of the dye Alamar Bluee', p. 8.

Gribova, V. *et al.* (2013) 'Effect of RGD functionalization and stiffness modulation of polyelectrolyte multilayer films on muscle cell differentiation', *Acta Biomaterialia*, 9(5), pp. 6468–6480. Available at: https://doi.org/10.1016/j.actbio.2012.12.015.

Gu, Q. *et al.* (2016) 'Functional 3D Neural Mini-Tissues from Printed Gel-Based Bioink and Human Neural Stem Cells', *Advanced Healthcare Materials*, 5(12), pp. 1429–1438. Available at: https://doi.org/10.1002/adhm.201600095.

Guarecuco, R. *et al.* (2018) 'Immunogenicity of pulsatile-release PLGA microspheres for single-injection vaccination', *Vaccine*, 36(22), pp. 3161–3168. Available at: https://doi.org/10.1016/j.vaccine.2017.05.094.

Gudapati, H., Dey, M. and Ozbolat, I. (2016) 'A comprehensive review on droplet-based bioprinting: Past, present and future', *Biomaterials*, 102, pp. 20–42. Available at: https://doi.org/10.1016/j.biomaterials.2016.06.012.

Guillotin, B. *et al.* (2010) 'Laser assisted bioprinting of engineered tissue with high cell density and microscale organization', *Biomaterials*, 31(28), pp. 7250–7256. Available at: https://doi.org/10.1016/j.biomaterials.2010.05.055.

Gullberg, D.E. and Lundgren-Åkerlund, E. (2002) 'Collagen-binding I domain integrins — what do they do?', *Progress in Histochemistry and Cytochemistry*, 37(1), pp. 3–54. Available at: https://doi.org/10.1016/S0079-6336(02)80008-0.

Gunti, S. *et al.* (2021) 'Organoid and Spheroid Tumor Models: Techniques and Applications', *Cancers*, 13(4), p. 874. Available at: https://doi.org/10.3390/cancers13040874.

Hagenbuchner, J., Nothdurfter, D. and Ausserlechner, M.J. (2021) '3D bioprinting: novel approaches for engineering complex human tissue equivalents and drug testing', *Essays in Biochemistry*. Edited by J. Jang, 65(3), pp. 417–427. Available at: https://doi.org/10.1042/EBC20200153.

Han, S. *et al.* (2020) '3D Bioprinted Vascularized Tumour for Drug Testing', *International Journal of Molecular Sciences*, 21(8), p. 2993. Available at: https://doi.org/10.3390/ijms21082993.

Harrison, R.G. (1906) 'Observations on the living developing nerve fiber', *Experimental Biology and Medicine*, 4(1), pp. 140–143. Available at: https://doi.org/10.3181/00379727-4-98.

Hayden, P.J. and Harbell, J.W. (2021) 'Special review series on 3D organotypic culture models: Introduction and historical perspective', *In Vitro Cellular & Developmental Biology - Animal*, 57(2), pp. 95–103. Available at: https://doi.org/10.1007/s11626-020-00500-2.

Hazur, J. *et al.* (2020) 'Improving alginate printability for biofabrication: establishment of a universal and homogeneous pre-crosslinking technique', *Biofabrication*, 12(4), p. 045004. Available at: https://doi.org/10.1088/1758-5090/ab98e5.

He, Y. *et al.* (2016) 'Research on the printability of hydrogels in 3D bioprinting', *Scientific Reports*, 6(1). Available at: https://doi.org/10.1038/srep29977.

Heinrich, M.A. *et al.* (2019) '3D Bioprinting: from Benches to Translational Applications', *Small*, p. 1805510. Available at: https://doi.org/10.1002/smll.201805510.

Helary, C. *et al.* (2010) 'Concentrated collagen hydrogels as dermal substitutes', *Biomaterials*, 31(3), pp. 481–490. Available at: https://doi.org/10.1016/j.biomaterials.2009.09.073.

Hennink, W.E. and van Nostrum, C.F. (2012) 'Novel crosslinking methods to design hydrogels', *Advanced Drug Delivery Reviews*, 64, pp. 223–236. Available at: https://doi.org/10.1016/j.addr.2012.09.009.

Heredia-Guerrero, J.A. *et al.* (2018) 'Antimicrobial, antioxidant, and waterproof RTV silicone-ethyl cellulose composites containing clove essential oil', *Carbohydrate Polymers*, 192, pp. 150–158. Available at: https://doi.org/10.1016/j.carbpol.2018.03.050.

Highley, C.B., Rodell, C.B. and Burdick, J.A. (2015) 'Direct 3D Printing of Shear-Thinning Hydrogels into Self-Healing Hydrogels', *Advanced Materials*, 27(34), pp. 5075–5079. Available at: https://doi.org/10.1002/adma.201501234.

Hofer, M. and Lutolf, M.P. (2021) 'Engineering organoids', *Nature Reviews Materials*, 6(5), pp. 402–420. Available at: https://doi.org/10.1038/s41578-021-00279-y.

Hölzl, K. *et al.* (2016) 'Bioink properties before, during and after 3D bioprinting', *Biofabrication*, 8(3), p. 032002. Available at: https://doi.org/10.1088/1758-5090/8/3/032002.

Hopp, B. (2012) 'Femtosecond laser printing of living cells using absorbing film-assisted laser-induced forward transfer', *Optical Engineering*, 51(1), p. 014302. Available at: https://doi.org/10.1117/1.OE.51.1.014302.

Hospodiuk, M. *et al.* (2017) 'The bioink: A comprehensive review on bioprintable materials', *Biotechnology Advances*, 35(2), pp. 217–239. Available at: https://doi.org/10.1016/j.biotechadv.2016.12.006.

J M Yuhas (1977) 'A simplified method for production and growth of multicellular tumor spheroids'.

Jeong, S.Y. *et al.* (2020) 'Fabrication of Dentin-Pulp-Like Organoids Using Dental-Pulp Stem Cells', *Cells*, 9(3), p. 642. Available at: https://doi.org/10.3390/cells9030642.

Jiang, Y. *et al.* (2005) 'A Multiscale Model for Avascular Tumor Growth', *Biophysical Journal*, 89(6), pp. 3884–3894. Available at: https://doi.org/10.1529/biophysj.105.060640.

Jung, R. *et al.* (2009) 'Antimicrobial Properties of Hydrated Cellulose Membranes With Silver Nanoparticles', *Journal of Biomaterials Science, Polymer Edition*, 20(3), pp. 311–324. Available at: https://doi.org/10.1163/156856209X412182.

Jungst, T. *et al.* (2016) 'Strategies and Molecular Design Criteria for 3D Printable Hydrogels', *Chemical Reviews*, 116(3), pp. 1496–1539. Available at: https://doi.org/10.1021/acs.chemrev.5b00303.

Junk, S. and Kuen, C. (2016) 'Review of Open Source and Freeware CAD Systems for Use with 3D-Printing', *Procedia CIRP*, 50, pp. 430–435. Available at: https://doi.org/10.1016/j.procir.2016.04.174.

Karakaidos, P. *et al.* (2022) 'Laser Bioprinting of Cells Using UV and Visible Wavelengths: A Comparative DNA Damage Study', *Bioengineering*, 9(8), p. 378. Available at: https://doi.org/10.3390/bioengineering9080378.

Kaur, S. *et al.* (2021) 'Non-matrigel scaffolds for organoid cultures', *Cancer Letters*, 504, pp. 58–66. Available at: https://doi.org/10.1016/j.canlet.2021.01.025.

Khoeini, R. *et al.* (2021) 'Natural and Synthetic Bioinks for 3D Bioprinting', *Advanced NanoBiomed Research*, 1(8), p. 2000097. Available at: https://doi.org/10.1002/anbr.202000097.

Klebe, R. (1988) 'Cytoscribing: A method for micropositioning cells and the construction of two- and three-dimensional synthetic tissues', *Experimental Cell Research*, 179(2), pp. 362–373. Available at: https://doi.org/10.1016/0014-4827(88)90275-3.

Kozlowski, M.T., Crook, C.J. and Ku, H.T. (2021) 'Towards organoid culture without Matrigel', *Communications Biology*, 4(1), p. 1387. Available at: https://doi.org/10.1038/s42003-021-02910-8.

Kumar, P., Ebbens, S. and Zhao, X. (2021) 'Inkjet printing of mammalian cells – Theory and applications', *Bioprinting*, 23, p. e00157. Available at: https://doi.org/10.1016/j.bprint.2021.e00157.

Kumari, A., Yadav, S.K. and Yadav, S.C. (2010) 'Biodegradable polymeric nanoparticles based drug delivery systems', *Colloids and Surfaces B: Biointerfaces*, 75(1), pp. 1–18. Available at: https://doi.org/10.1016/j.colsurfb.2009.09.001.

Kunz-Schughart, L.A. *et al.* (2001) 'A Heterologous 3-D Coculture Model of Breast Tumor Cells and Fibroblasts to Study Tumor-Associated Fibroblast Differentiation', *Experimental Cell Research*, 266(1), pp. 74–86. Available at: https://doi.org/10.1006/excr.2001.5210.

Kuriakose, A.E. *et al.* (2019) 'Scaffold-based lung tumor culture on porous PLGA microparticle substrates', *PLOS ONE*. Edited by N. Cordes, 14(5), p. e0217640. Available at: https://doi.org/10.1371/journal.pone.0217640.

Landers, R. *et al.* (2002) 'Rapid prototyping of scaffolds derived from thermoreversible hydrogels and tailored for applications in tissue engineering', *Biomaterials*, 23(23), pp. 4437–4447. Available at: https://doi.org/10.1016/S0142-9612(02)00139-4.

Langer, E.M. *et al.* (2019) 'Modeling Tumor Phenotypes In Vitro with Three-Dimensional Bioprinting', *Cell Reports*, 26(3), pp. 608-623.e6. Available at: https://doi.org/10.1016/j.celrep.2018.12.090.

Lee, A. *et al.* (2019) '3D bioprinting of collagen to rebuild components of the human heart', *Science*, 365(6452), pp. 482–487. Available at: https://doi.org/10.1126/science.aav9051.

Lee, K.Y. and Mooney, D.J. (2012) 'Alginate: Properties and biomedical applications', *Progress in Polymer Science*, 37(1), pp. 106–126. Available at: https://doi.org/10.1016/j.progpolymsci.2011.06.003.

Lee, Y.-B. *et al.* (2010) 'Bio-printing of collagen and VEGF-releasing fibrin gel scaffolds for neural stem cell culture', *Experimental Neurology*, 223(2), pp. 645–652. Available at: https://doi.org/10.1016/j.expneurol.2010.02.014.

Leucht, A. (2020) 'Advanced gelatin-based vascularization bioinks for extrusion-based bioprinting of vascularized bone equivalents', p. 15.

Levato, R. *et al.* (2014) 'Biofabrication of tissue constructs by 3D bioprinting of cell-laden microcarriers', *Biofabrication*, 6(3), p. 035020. Available at: https://doi.org/10.1088/1758-5082/6/3/035020.

Li, M. *et al.* (2011) 'Effect of needle geometry on flow rate and cell damage in the dispensing-based biofabrication process', *Biotechnology Progress*, 27(6), pp. 1777–1784. Available at: https://doi.org/10.1002/btpr.679.

Li, X. *et al.* (2020) 'Inkjet Bioprinting of Biomaterials', *Chemical Reviews*, 120(19), pp. 10793–10833. Available at: https://doi.org/10.1021/acs.chemrev.0c00008.

Lin, H. *et al.* (2017) 'Projection Stereolithographic Fabrication of BMP-2 Gene-activated Matrix for Bone Tissue Engineering', *Scientific Reports*, 7(1), p. 11327. Available at: https://doi.org/10.1038/s41598-017-11051-0.

Liu, W. *et al.* (2017) 'Extrusion Bioprinting of Shear-Thinning Gelatin Methacryloyl Bioinks', *Advanced Healthcare Materials*, 6(12), p. 1601451. Available at: https://doi.org/10.1002/adhm.201601451.

Lo, B. and Parham, L. (2009) 'Ethical Issues in Stem Cell Research', *Endocrine Reviews*, 30(3), pp. 204–213. Available at: https://doi.org/10.1210/er.2008-0031.

Loh, Q.L. and Choong, C. (2013) 'Three-Dimensional Scaffolds for Tissue Engineering Applications: Role of Porosity and Pore Size', *Tissue Engineering Part B: Reviews*, 19(6), pp. 485–502. Available at: https://doi.org/10.1089/ten.teb.2012.0437.

Ma, Z. *et al.* (2022) '3D bioprinting of proangiogenic constructs with induced immunomodulatory microenvironments through a dual cross-linking procedure using laponite incorporated bioink', *Composites Part B: Engineering*, 229, p. 109399. Available at: https://doi.org/10.1016/j.compositesb.2021.109399.

Magnani, E. and Bettini, E. (2000) 'Resazurin detection of energy metabolism changes in serum-starved PC12 cells and of neuroprotective agent effect', *Brain Research Protocols*, 5(3), pp. 266–272. Available at: https://doi.org/10.1016/S1385-299X(00)00022-2.

Makadia, H.K. and Siegel, S.J. (2011) 'Poly Lactic-co-Glycolic Acid (PLGA) as Biodegradable Controlled Drug Delivery Carrier', *Polymers*, 3(3), pp. 1377–1397. Available at: https://doi.org/10.3390/polym3031377.

Malda, J. *et al.* (2013) '25th Anniversary Article: Engineering Hydrogels for Biofabrication', *Advanced Materials*, 25(36), pp. 5011–5028. Available at: https://doi.org/10.1002/adma.201302042.

Malekpour, A. and Chen, X. (2022) 'Printability and Cell Viability in Extrusion-Based Bioprinting from Experimental, Computational, and Machine Learning Views', *Journal of Functional Biomaterials*, 13(2), p. 40. Available at: https://doi.org/10.3390/jfb13020040.

Mandrycky, C. *et al.* (2016) '3D bioprinting for engineering complex tissues', *Biotechnology Advances*, 34(4), pp. 422–434. Available at: https://doi.org/10.1016/j.biotechadv.2015.12.011.

Marga, F. *et al.* (2012) 'Toward engineering functional organ modules by additive manufacturing', *Biofabrication*, 4(2), p. 022001. Available at: https://doi.org/10.1088/1758-5082/4/2/022001.

Martin, G.D., Hoath, S.D. and Hutchings, I.M. (2008) 'Inkjet printing - the physics of manipulating liquid jets and drops', *Journal of Physics: Conference Series*, 105, p. 012001. Available at: https://doi.org/10.1088/1742-6596/105/1/012001.

McClelland, R.E. *et al.* (2012) 'Tissue Engineering', in *Introduction to Biomedical Engineering*. Elsevier, pp. 273–357. Available at: https://doi.org/10.1016/B978-0-12-374979-6.00006-X.

McCormack, A. *et al.* (2020) '3D Printing in Suspension Baths: Keeping the Promises of Bioprinting Afloat', *Trends in Biotechnology*, 38(6), pp. 584–593. Available at: https://doi.org/10.1016/j.tibtech.2019.12.020.

Meléndez, P.A. *et al.* (2008) 'Thermal Inkjet Application in the Preparation of Oral Dosage Forms: Dispensing of Prednisolone Solutions and Polymorphic Characterization by Solid-State Spectroscopic Techniques', *Journal of Pharmaceutical Sciences*, 97(7), pp. 2619–2636. Available at: https://doi.org/10.1002/jps.21189.

Miri, A.K. *et al.* (2019) 'Multiscale bioprinting of vascularized models', *Biomaterials*, 198, pp. 204–216. Available at: https://doi.org/10.1016/j.biomaterials.2018.08.006.

Moghaddam, A.S. *et al.* (2021) 'Review of Bioprinting in Regenerative Medicine: Naturally Derived Bioinks and Stem Cells', *ACS Applied Bio Materials*, 4(5), pp. 4049–4070. Available at: https://doi.org/10.1021/acsabm.1c00219.

Moldovan, N.I., Hibino, N. and Nakayama, K. (2017) 'Principles of the *Kenzan* Method for Robotic Cell Spheroid-Based Three-Dimensional Bioprinting <sup/>', *Tissue Engineering Part B: Reviews*, 23(3), pp. 237–244. Available at: https://doi.org/10.1089/ten.teb.2016.0322.

Mouser, V.H.M. *et al.* (2016) 'Yield stress determines bioprintability of hydrogels based on gelatin-methacryloyl and gellan gum for cartilage bioprinting', *Biofabrication*, 8(3), p. 035003. Available at: https://doi.org/10.1088/1758-5090/8/3/035003.

Muller, C. *et al.* (2020) 'Polyarginine Decorated Polydopamine Nanoparticles With Antimicrobial Properties for Functionalization of Hydrogels', *Frontiers in Bioengineering and Biotechnology*, 8, p. 982. Available at: https://doi.org/10.3389/fbioe.2020.00982.

Murphy, S.V. and Atala, A. (2014) '3D bioprinting of tissues and organs', *Nature Biotechnology*, 32(8), pp. 773–785. Available at: https://doi.org/10.1038/nbt.2958.

Muthukrishnan, L. (2021) 'Imminent antimicrobial bioink deploying cellulose, alginate, EPS and synthetic polymers for 3D bioprinting of tissue constructs', *Carbohydrate Polymers*, 260, p. 117774. Available at: https://doi.org/10.1016/j.carbpol.2021.117774.

Naseri, E. *et al.* (2020) 'Low-temperature solvent-based 3D printing of PLGA: a parametric printability study', *Drug Development and Industrial Pharmacy*, 46(2), pp. 173–178. Available at: https://doi.org/10.1080/03639045.2019.1711389.

Ning, L. (2020) 'Process-induced cell damage: pneumatic versus screw-driven bioprinting', p. 16.

Novosel, E.C. (2011) 'Vascularization is the key challenge in tissue engineering', *Advanced Drug Delivery Reviews*, p. 12.

O'Brien, J. *et al.* (2000) 'Investigation of the Alamar Blue (resazurin) fluorescent dye for the assessment of mammalian cell cytotoxicity: Resazurin as a cytotoxicity assay', *European Journal of Biochemistry*, 267(17), pp. 5421–5426. Available at: https://doi.org/10.1046/j.1432-1327.2000.01606.x.

O'Connell, C.D. *et al.* (2019) 'Evaluation of sterilisation methods for bio-ink components: gelatin, gelatin methacryloyl, hyaluronic acid and hyaluronic acid methacryloyl', *Biofabrication*, 11(3), p. 035003. Available at: https://doi.org/10.1088/1758-5090/ab0b7c.

O'Connell, C.D. *et al.* (2020) 'Free-form co-axial bioprinting of a gelatin methacryloyl bio-ink by direct in situ photo-crosslinking during extrusion', *Bioprinting*, 19, p. e00087. Available at: https://doi.org/10.1016/j.bprint.2020.e00087.

Oliveira, H. *et al.* (2021) 'Extracellular matrix (ECM)-derived bioinks designed to foster vasculogenesis and neurite outgrowth: Characterization and bioprinting', *Bioprinting*, 22, p. e00134. Available at: https://doi.org/10.1016/j.bprint.2021.e00134.

Oryan, A. *et al.* (2018) 'Chemical crosslinking of biopolymeric scaffolds: Current knowledge and future directions of crosslinked engineered bone scaffolds', *International Journal of Biological Macromolecules*, 107, pp. 678–688. Available at: https://doi.org/10.1016/j.ijbiomac.2017.08.184.

Ouyang, L. *et al.* (2015) 'Three-dimensional bioprinting of embryonic stem cells directs highly uniform embryoid body formation', *Biofabrication*, 7(4), p. 044101. Available at: https://doi.org/10.1088/1758-5090/7/4/044101.

Ouyang, L. *et al.* (2020) 'Expanding and optimizing 3D bioprinting capabilities using complementary network bioinks', *Science Advances*, 6(38), p. eabc5529. Available at: https://doi.org/10.1126/sciadv.abc5529.

Ozbolat, I.T. (2017) 'Extrusion-Based Bioprinting * *With minor contributions by Monika Hospodiuk, The Pennsylvania State University.', in *3D Bioprinting*. Elsevier, pp. 93–124. Available at: https://doi.org/10.1016/B978-0-12-803010-3.00004-4.

Ozbolat, I.T. and Hospodiuk, M. (2016) 'Current advances and future perspectives in extrusion-based bioprinting', *Biomaterials*, 76, pp. 321–343. Available at: https://doi.org/10.1016/j.biomaterials.2015.10.076.

Özçelik, H. *et al.* (2015) 'Harnessing the Multifunctionality in Nature: A Bioactive Agent Release System with Self-Antimicrobial and Immunomodulatory Properties', *Advanced Healthcare Materials*, 4(13), pp. 2026–2036. Available at: https://doi.org/10.1002/adhm.201500546.

Pati, F. *et al.* (2015) 'Extrusion Bioprinting', in *Essentials of 3D Biofabrication and Translation*. Elsevier, pp. 123–152. Available at: https://doi.org/10.1016/B978-0-12-800972-7.00007-4.

Patuzzo, S. *et al.* (2017) '3D Bioprinting Technology: Scientific Aspects and Ethical Issues', *Science and Engineering Ethics* [Preprint]. Available at: https://doi.org/10.1007/s11948-017-9918-y.

Peng, W. *et al.* (2017) '3D bioprinting for drug discovery and development in pharmaceutics', *Acta Biomaterialia*, 57, pp. 26–46. Available at: https://doi.org/10.1016/j.actbio.2017.05.025.

Pourchet, L.J. *et al.* (2017) 'Human Skin 3D Bioprinting Using Scaffold-Free Approach', *Advanced Healthcare Materials*, 6(4), p. 1601101. Available at: https://doi.org/10.1002/adhm.201601101.

Pugliese, L. *et al.* (2018) 'The clinical use of 3D printing in surgery', *Updates in Surgery*, 70(3), pp. 381–388. Available at: https://doi.org/10.1007/s13304-018-0586-5.

Qutachi, O. *et al.* (2014) 'Injectable and porous PLGA microspheres that form highly porous scaffolds at body temperature', *Acta Biomaterialia*, 10(12), pp. 5090–5098. Available at: https://doi.org/10.1016/j.actbio.2014.08.015.

Qutachi, O. *et al.* (2018) 'Improved delivery of PLGA microparticles and microparticle-cell scaffolds in clinical needle gauges using modified viscosity formulations', *International Journal of Pharmaceutics*, 546(1–2), pp. 272–278. Available at: https://doi.org/10.1016/j.ijpharm.2018.05.025.

Raghavan, S. *et al.* (2017) 'Personalized Medicine–Based Approach to Model Patterns of Chemoresistance and Tumor Recurrence Using Ovarian Cancer Stem Cell Spheroids', *Clinical Cancer Research*, 23(22), pp. 6934–6945. Available at: https://doi.org/10.1158/1078-0432.CCR-17-0133.

Reid, J.A. *et al.* (2019) 'A 3D bioprinter platform for mechanistic analysis of tumoroids and chimeric mammary organoids', *Scientific Reports*, 9(1), p. 7466. Available at: https://doi.org/10.1038/s41598-019-43922-z.

Ren, Y. *et al.* (2021) 'Developments and Opportunities for 3D Bioprinted Organoids', *International Journal of Bioprinting*, 7(3), p. 364. Available at: https://doi.org/10.18063/ijb.v7i3.364.

Rivron, N.C. *et al.* (2009) 'Tissue assembly and organization: Developmental mechanisms in microfabricated tissues', *Biomaterials*, 30(28), pp. 4851–4858. Available at: https://doi.org/10.1016/j.biomaterials.2009.06.037.

Rousselle, A. *et al.* (2022) 'Enhancing cell survival in 3D printing of organoids using innovative bioinks loaded with pre-cellularized porous microscaffolds', *Bioprinting*, p. e00247. Available at: https://doi.org/10.1016/j.bprint.2022.e00247.

Rouwkema, J., Rivron, N.C. and van Blitterswijk, C.A. (2008) 'Vascularization in tissue engineering', p. 8.

Rowley, J.A., Madlambayan, G. and Mooney, D.J. (1999) 'Alginate hydrogels as synthetic extracellular matrix materials', *Biomaterials*, 20(1), pp. 45–53. Available at: https://doi.org/10.1016/S0142-9612(98)00107-0.

Rutz, A.L., Lewis, P.L. and Shah, R.N. (2017) 'Toward next-generation bioinks: Tuning material properties pre- and post-printing to optimize cell viability', *MRS Bulletin*, 42(08), pp. 563–570. Available at: https://doi.org/10.1557/mrs.2017.162.

Santi, M. *et al.* (2020) 'Production of 3D Tumor Models of Head and Neck Squamous Cell Carcinomas for Nanotheranostics Assessment', *ACS Biomaterials Science & Engineering*, 6(9), pp. 4862–4869. Available at: https://doi.org/10.1021/acsbiomaterials.0c00617.

Santoni, S. (2022) '3D bioprinting: current status and trends—a guide to the literature and industrial practice', p. 29.

Saunders, R.E. and Derby, B. (2014) 'Inkjet printing biomaterials for tissue engineering: bioprinting', *International Materials Reviews*, 59(8), pp. 430–448. Available at: https://doi.org/10.1179/1743280414Y.0000000040.

Shamma, R.N. *et al.* (2022) 'Triblock Copolymer Bioinks in Hydrogel Three-Dimensional Printing for Regenerative Medicine: A Focus on Pluronic F127', *Tissue Engineering Part B: Reviews*, 28(2), pp. 451–463. Available at: https://doi.org/10.1089/ten.teb.2021.0026.

Shpichka, A. *et al.* (2020) 'Fibrin-based Bioinks: New Tricks from an Old Dog', *International Journal of Bioprinting*, 6(3). Available at: https://doi.org/10.18063/ijb.v6i3.269.

Sigaux, N. *et al.* (2019) '3D Bioprinting:principles, fantasies and prospects', *Journal of Stomatology, Oral and Maxillofacial Surgery*, 120(2), pp. 128–132. Available at: https://doi.org/10.1016/j.jormas.2018.12.014.

Smith, C.M. *et al.* (2004) 'Three-Dimensional BioAssembly Tool for Generating Viable Tissue-Engineered Constructs', p. 11.

Smith, D. *et al.* (2019) 'Microparticles for Suspension Culture of Mammalian Cells', *ACS Applied Bio Materials*, 2(7), pp. 2791–2801. Available at: https://doi.org/10.1021/acsabm.9b00215.

Sorkio, A. *et al.* (2018) 'Human stem cell based corneal tissue mimicking structures using laser-assisted 3D bioprinting and functional bioinks', *Biomaterials*, 171, pp. 57–71. Available at: https://doi.org/10.1016/j.biomaterials.2018.04.034.

Suo, H. *et al.* (2021) 'Low-temperature 3D printing of collagen and chitosan composite for tissue engineering', *Materials Science and Engineering: C*, 123, p. 111963. Available at: https://doi.org/10.1016/j.msec.2021.111963.

Sutherland, R.M. (1971) 'Growth of Multicell Spheroids in Tissue Culture as a Model of Nodular Carcinomas2', *JNCI: Journal of the National Cancer Institute* [Preprint]. Available at: https://doi.org/10.1093/jnci/46.1.113.

Takigawa, M. *et al.* (1989) 'Establishment of a Clonal Human Chondrosarcoma Cell Line with Cartilage Phenotypes', *American Association for Cancer Research*, p. 8.

Talon, I. *et al.* (2019) 'Polydopamine Functionalization: A Smart and Efficient Way to Improve Host Responses to e-PTFE Implants', *Frontiers in Chemistry*, 7, p. 482. Available at: https://doi.org/10.3389/fchem.2019.00482.

Tan, H. *et al.* (2009) 'RGD modified PLGA/gelatin microspheres as microcarriers for chondrocyte delivery', *Journal of Biomedical Materials Research Part B: Applied Biomaterials*, 91B(1), pp. 228–238. Available at: https://doi.org/10.1002/jbm.b.31394.

Tan, Y.J. *et al.* (2016) 'Hybrid microscaffold-based 3D bioprinting of multi-cellular constructs with high compressive strength: A new biofabrication strategy', *Scientific Reports*, 6(1), p. 39140. Available at: https://doi.org/10.1038/srep39140.

Tarassoli, S.P. *et al.* (2021) 'Candidate Bioinks for Extrusion 3D Bioprinting—A Systematic Review of the Literature', *Frontiers in Bioengineering and Biotechnology*, 9, p. 616753. Available at: https://doi.org/10.3389/fbioe.2021.616753.

Tenover, F.C. and McGowan, J.E. (1996) 'Reasons for the Emergence of Antibiotic Resistance', *The American Journal of the Medical Sciences*, 311(1), pp. 9–16. Available at: https://doi.org/10.1016/S0002-9629(15)41625-8.

The Congenital Diaphragmatic Hernia Study Group (2007) 'Defect Size Determines Survival in Infants With Congenital Diaphragmatic Hernia', *Pediatrics*, 120(3), pp. e651–e657. Available at: https://doi.org/10.1542/peds.2006-3040.

Thomas, B.H. *et al.* (2009) 'Hydrophilic–hydrophobic hydrogels for cartilage replacement', *Journal of the Mechanical Behavior of Biomedical Materials*, 2(6), pp. 588–595. Available at: https://doi.org/10.1016/j.jmbbm.2008.08.001.

Tibbitt, M.W. and Anseth, K.S. (2009) 'Hydrogels as extracellular matrix mimics for 3D cell culture', *Biotechnology and Bioengineering*, 103(4), pp. 655–663. Available at: https://doi.org/10.1002/bit.22361.

Timmins, N.E. and Nielsen, L.K. (2007) 'Generation of Multicellular Tumor Spheroids by the Hanging-Drop Method', in H. Hauser and M. Fussenegger (eds) *Tissue Engineering*. Totowa, NJ: Humana Press (Methods in Molecular Medicine™), pp. 141–151. Available at: https://doi.org/10.1007/978-1-59745-443-8_8.

Tirella, A. *et al.* (2011) 'Substrate stiffness influences high resolution printing of living cells with an ink-jet system', *Journal of Bioscience and Bioengineering*, 112(1), pp. 79–85. Available at: https://doi.org/10.1016/j.jbiosc.2011.03.019.

Tomás-Bort, E. *et al.* (2020) '3D approaches to model the tumor microenvironment of pancreatic cancer', *Theranostics*, 10(11), pp. 5074–5089. Available at: https://doi.org/10.7150/thno.42441.

Van Norman, G.A. (2016) 'Drugs, Devices, and the FDA: Part 1', *JACC: Basic to Translational Science*, 1(3), pp. 170–179. Available at: https://doi.org/10.1016/j.jacbts.2016.03.002.

Vanaei, S. *et al.* (2021) 'An Overview on Materials and Techniques in 3D Bioprinting Toward Biomedical Application', *Engineered Regeneration*, 2, pp. 1–18. Available at: https://doi.org/10.1016/j.engreg.2020.12.001.

Vega-Avila, E. and Pugsley, M.K. (2011) 'An overview of colorimetric assay methods used to assess survival or proliferation of mammalian cells', *Proceedings of the Western Pharmacology Society*, 54, pp. 10–14.

Ventura, R.D. (2021) 'An Overview of Laser-assisted Bioprinting (LAB) in Tissue Engineering Applications', *Medical Lasers*, 10(2), pp. 76–81. Available at: https://doi.org/10.25289/ML.2021.10.2.76.

Vijayavenkataraman, S., Lu, W.F. and Fuh, J.Y.H. (2016) '3D bioprinting – An Ethical, Legal and Social Aspects (ELSA) framework', *Bioprinting*, 1–2, pp. 11–21. Available at: https://doi.org/10.1016/j.bprint.2016.08.001.

Vinci, M. *et al.* (2012) 'Advances in establishment and analysis of three-dimensional tumor spheroid-based functional assays for target validation and drug evaluation', *BMC Biology*, 10(1), p. 29. Available at: https://doi.org/10.1186/1741-7007-10-29.

Wallace, D. (2003) 'Collagen gel systems for sustained delivery and tissue engineering', *Advanced Drug Delivery Reviews*, 55(12), pp. 1631–1649. Available at: https://doi.org/10.1016/j.addr.2003.08.004.

Wang, L. *et al.* (2021) 'Epsilon-poly-L-lysine: Recent Advances in Biomanufacturing and Applications', *Frontiers in Bioengineering and Biotechnology*, 9, p. 748976. Available at: https://doi.org/10.3389/fbioe.2021.748976.

Wang, X. *et al.* (2017) 'Gelatin-Based Hydrogels for Organ 3D Bioprinting', *Polymers*, 9(12), p. 401. Available at: https://doi.org/10.3390/polym9090401.

Wang, X. *et al.* (2018) 'Tumor-like lung cancer model based on 3D bioprinting', *3 Biotech*, 8(12), p. 501. Available at: https://doi.org/10.1007/s13205-018-1519-1.

Wang, Z. *et al.* (2015) 'A simple and high-resolution stereolithography-based 3D bioprinting system using visible light crosslinkable bioinks', *Biofabrication*, 7(4), p. 045009. Available at: https://doi.org/10.1088/1758-5090/7/4/045009.

Wang, Z. *et al.* (2018) 'Visible Light Photoinitiation of Cell-Adhesive Gelatin Methacryloyl Hydrogels for Stereolithography 3D Bioprinting', *ACS Applied Materials & Interfaces*, 10(32), pp. 26859–26869. Available at: https://doi.org/10.1021/acsami.8b06607.

Waran, V. *et al.* (2014) 'Utility of multimaterial 3D printers in creating models with pathological entities to enhance the training experience of neurosurgeons: Technical note', *Journal of Neurosurgery*, 120(2), pp. 489–492. Available at: https://doi.org/10.3171/2013.11.JNS131066.

Wells, M.F. *et al.* (2016) 'Genetic Ablation of AXL Does Not Protect Human Neural Progenitor Cells and Cerebral Organoids from Zika Virus Infection', *Cell Stem Cell*, 19(6), pp. 703–708. Available at: https://doi.org/10.1016/j.stem.2016.11.011.

Wilson, W.C. and Boland, T. (2003) 'Cell and organ printing 1: Protein and cell printers', *The Anatomical Record*, 272A(2), pp. 491–496. Available at: https://doi.org/10.1002/ar.a.10057.

Wouters, O.J., McKee, M. and Luyten, J. (2020) 'Research and Development Costs of New Drugs—Reply', *JAMA*, 324(5), p. 518. Available at: https://doi.org/10.1001/jama.2020.8651.

Wu, Z. *et al.* (2016) 'Bioprinting three-dimensional cell-laden tissue constructs with controllable degradation', *Scientific Reports*, 6(1). Available at: https://doi.org/10.1038/srep24474.

Xu, H. *et al.* (2018) 'Organoid technology and applications in cancer research', *Journal of Hematology & Oncology*, 11(1), p. 116. Available at: https://doi.org/10.1186/s13045-018-0662-9.

Xu, Y. *et al.* (2017) 'Polymer degradation and drug delivery in PLGA-based drug-polymer applications: A review of experiments and theories: REVIEW ON BIODEGRADATION AND

DRUG DELIVERY FROM PLGA POLYMERS', *Journal of Biomedical Materials Research Part B: Applied Biomaterials*, 105(6), pp. 1692–1716. Available at: https://doi.org/10.1002/jbm.b.33648.

Yan, Y. *et al.* (2022) 'Preparation and In Vitro Characterization of Gelatin Methacrylate for Corneal Tissue Engineering', *Tissue Engineering and Regenerative Medicine*, 19(1), pp. 59–72. Available at: https://doi.org/10.1007/s13770-021-00393-6.

Yang, H.-W. *et al.* (2017) 'Ebola Vaccination Using a DNA Vaccine Coated on PLGA-PLL/γPGA Nanoparticles Administered Using a Microneedle Patch', *Advanced Healthcare Materials*, 6(1), p. 1600750. Available at: https://doi.org/10.1002/adhm.201600750.

Yi, H.-G. *et al.* (2019) 'A bioprinted human-glioblastoma-on-a-chip for the identification of patient-specific responses to chemoradiotherapy', *Nature Biomedical Engineering*, 3(7), pp. 509–519. Available at: https://doi.org/10.1038/s41551-019-0363-x.

Yoo, J.-W., Doshi, N. and Mitragotri, S. (2010) 'Endocytosis and Intracellular Distribution of PLGA Particles in Endothelial Cells: Effect of Particle Geometry: Endocytosis and Intracellular Distribution of PLGA Particles in Endothelial Cells …', *Macromolecular Rapid Communications*, 31(2), pp. 142–148. Available at: https://doi.org/10.1002/marc.200900592.

Yoon, J.J. and Park, T.G. (2001) 'Degradation behaviors of biodegradable macroporous scaffolds prepared by gas foaming of effervescent salts', *Journal of Biomedical Materials Research*, 55(3), pp. 401–408. Available at: https://doi.org/10.1002/1097-4636(20010605)55:3<401::AID-JBM1029>3.0.CO;2-H.

Yue, J. *et al.* (2015) '3D-Printable Antimicrobial Composite Resins', *Advanced Functional Materials*, 25(43), pp. 6756–6767. Available at: https://doi.org/10.1002/adfm.201502384.

Zhao, Y. *et al.* (2015) 'The influence of printing parameters on cell survival rate and printability in microextrusion-based 3D cell printing technology', *Biofabrication*, 7(4), p. 045002. Available at: https://doi.org/10.1088/1758-5090/7/4/045002.

Zheng, S. *et al.* (2019) 'Poly- L -lysine-coated PLGA/poly(amino acid)-modified hydroxyapatite porous scaffolds as efficient tissue engineering scaffolds for cell adhesion, proliferation, and differentiation', *New Journal of Chemistry*, 43(25), pp. 9989–10002. Available at: https://doi.org/10.1039/C9NJ01675A.

Zhong, S.P. *et al.* (1994) 'Biodegradation of hyaluronic acid derivatives by hyaluronidase', *Biomaterials*, 15(5), pp. 359–365. Available at: https://doi.org/10.1016/0142-9612(94)90248-8.

Zhu, J. and Marchant, R.E. (2011) 'Design properties of hydrogel tissue-engineering scaffolds', *Expert Review of Medical Devices*, 8(5), pp. 607–626. Available at: https://doi.org/10.1586/erd.11.27.

Annexes

1. List of publications

- Bioprinting: Enhancing cell survival in 3D printing of organoids using innovative bioinks loaded with pre-cellularized porous microscaffolds. BPRINT_e00247

2. Participation in international conferences

- GDR B2I 21-22 in Toulouse France, September 2021. Oral presentation: “Bottoms-up bioprinting of cellularized porous microscaffolds to enhance cell proliferation, viability and migration.”

- Termis, EU-Chapter Krakow of the Tissue Engineering and Regenerative Medicine International Society, 28 to 01 June to July 2022. Oral presentation: “Bottoms-up bioprinting of cellularized porous microscaffolds to enhance cell proliferation, viability and migration.”

- ESB 2022, 32nd Conference of the European Society for Biomaterials, in Bordeaux France, 04 to 08 September 2022. Oral presentation: “Bottoms-up bioprinting of cellularized porous microscaffolds to enhance cell proliferation, viability and migration.”

3. Awards

- Best oral presentation at GDR B2I 2021
- Mature your PhD 2022

4. List of teaching modules

- 85 hours of transversal formation
- 55 hours of disciplinary formation

5. List of student supervision

- Supervision of Martin Blanck, third year student in biomedical engineering school, 2 months
- Supervision of Maxence Gouin, last year student in biomedical engineering school, 6 months
- Supervision of Mélissa Langlois, second year Master degree at Strasbourg University, 6 months

- Teaching mission in bio-chemical in second year bachelor at Strasbourg University during 1 year

Adrien ROUSSELLE

Bioimpression de tissu biologiques à base de microparticules poreuses

Résumé Francais

L'impression 3D appliqué aux cellules et particulièrement la bioimpression par extrusion, est une technologie émergente permettant d'imprimer des systèmes biologiques complexes pouvant reproduire des modèles similaires aux tissus natifs. Mais cette technologie possède des limitations importantes telles qu'une densité cellulaire faible et la viabilité cellulaire après impression diminuée dû aux forces de cisaillement exercées sur les cellules lors de l'extrusion.

Dans ce travail de thèse, nous avons élaboré de nouvelles particules poreuses de PLGA afin de servir de plateforme de prolifération aux cellules avant l'impression et de structure protectrice lors de l'impression. Ainsi, la prolifération cellulaire est augmenté jusqu'à cinq fois avec les particules et la survie cellulaire est augmenté, au minimum, de dix pourcent pour tous les types cellulaires. Nous avons ensuite utilisé ces particules pour imprimer un modèle de diaphragme avec des cellules musculaires sur des membranes de BSA. La prolifération avant et après impression est augmenté jusqu'à cinq fois avec les microparticules et la survie cellulaires est augmenté jusqu'à trente pourcent.

Mot clés : Bioimpression, extrusion, PLGA, micoscaffolds, survie cellulaire, densité cellulaire, diaphragme

English summary

3D printing applied to cells, particularly extrusion bioprinting, is an emerging technology for printing complex biological systems that can reproduce models similar to native tissues. But this technology has significant limitations such as low cell density and reduced cell viability after printing due to shear stress forces exerted on the cells during extrusion damaging the cellular membrane.

In this thesis work, we have developed new porous PLGA microscaffolds to serve as a proliferation platform for cells before printing and as a protective structure during printing. Thus, cell proliferation is increased up to five times with the microscaffolds and cell survival is increased by at least ten percent for all cell types.We then used these particles to print a diaphragm model with muscle cells on BSA membranes. Proliferation before printing is increased up to two times and after printing is increased up to five times with microscaffolds. Cell survival is increased up to thirty percent with the microscaffolds when printing in well plates and reaches up to 85% when printing on BSA membranes.

Key words: Bioprinting, extrusion, PLGA, microscaffolds, survival rate, proliferation rate, diaphragm